Carbon and Nitrogen Isotopes in Lichen as a Geothermal Exploration Tool

A thesis submitted in partial fulfillment of the requirements for the degree of

Master of Science in Geology

at the

Department of Geological Sciences,
University of Canterbury

by

Cameron Michael Asher

2014

Frontispiece

If one more person asks me if I'm lichen my thesis…

Table of Contents

List of Figures

List of Tables

Acknowledgements

Many people deserve praise for assisting me in writing this thesis:

- To my supervisors, Travis Horton, Darren Gravely, Chris Oze, and Tom Powell. Regardless of how much input you had, you all helped to make this thesis the fantastic product that it is. Travis, for your countless hours running the IRMS, proofing chapters, and teaching me about the world of isotopes. Darren for always having a nice word and helping with the final review of chapters. Tom Powell for constantly organizing new induction meetings for fieldwork at Ngatamariki, even though I kept bailing. Also to Jim Cole for always having kind words about my progress.
- To Matt Hanson, for his assistance in the field and extreme patience for a car that broke every other day. Also for handing in earlier than me, so that I had access to his results.
- To MRP, the Source to Surface (S2S) program, the Mason Trust, and UC Scholarships for the assistance and funding for this project; there is no way Studylink could have got me through.
- To all of the Technical Staff for their assistance in making my field work and writing that much easier, especially: Rob Spiers, Sascha Baldwin-Cunningham, Kerry Swanson, John Southward, and Matt Cockroft.
- To all of the land owners allowing me to collect samples from your property, and trusting me not to scare your livestock or do doughnuts on your fields. Diarmid Somerville for access to the Somerville Farm and to the Orakonui Springs. Riccarton Bush Ranger, John Moore, and Riccarton Bush Trustee, Dr Molloy, for allowing me access and sample collection in Riccarton Bush reserve. Catherine Boseley (MRP) sorting us out during field work in the North Island, and Darryn (MRP), Jo (MRP), and Maui (Ngatamariki Security) at Ngatamariki for being (incredibly) patient and keeping us safe in the field.
- To my parents for their support (and funding), not just in the past 2 years, but for the past 18 consecutive years of education.
- To all of the people around uni and at home that have kept me sane for the last few years: Gina Vettoretti, Clem Gibbens, Millie Gibbens, Ash McGill, the Kahu Manor Crew, PCAS 2013/14, and many more.

Abstract

Lichen have been used as indicators of atmospheric pollutants since Grindon (1859) observed lichen populations declining in a polluted Southern Lancashire in the mid-1800s. Since then lichen have been used in a number of atmospheric studies. A study by Tozer *et al.* (2005) attempted to use nitrogen isotopes of lichen and free-living algae as indicators of geothermal 'pollution' near Rotorua and the Te Kopia Geothermal Area, but was unable to show a correlation with distance to geothermal features. This thesis aims to build from Tozer *et al.* (2005) and use both carbon and nitrogen isotopes in lichen as an exploration tool in geothermal areas.

Three transects were completed: one across the South Island from Christchurch to Greymouth (non-geothermally influenced area), and two along (north-south) and across (east-west) the Taupo Volcanic Zone (TVZ) in the North Island (geothermally influenced area). In addition to these three transects, sampling at higher spatial resolution was conducted in the immediate vicinity of the Orakonui Stream geothermal springs at the Ngatamariki Geothermal Area. The three transects showed large variation, largely due to the type of land use from which the sample was collected. The highest nitrogen contents (1.62 ± 0.39%) and less negative nitrogen isotopic compositions (-9.44 ± 0.39‰) were found over farmland, while both exotic and native forests had low nitrogen (1.08 ± 0.35% and 1.03 ± 0.44‰, respectively) and highly negative isotopic compositions (-12.94 ± 0.26‰ and -12.09 ± 0.45‰, respectively). The statistical difference between land use classes is hypothetically explained by variations in nitrogen sources, with intensive farmland volatilizing NH_3 with $\delta^{15}N$ values of -6 to -10‰ (Tozer *et al.*, 2005), while forest areas are expected to produce biogenic nitrogen from decomposition with more negative $\delta^{15}N$.

At Ngatamariki, $\delta^{13}C$ and $\delta^{15}N$ isoscapes were produced, with both showing a large isotopic anomaly (>-23.5 and >-8‰, respectively) to the north and north-west of the study area, correlating with areas of farmland, although in some places the $\delta^{15}N$ values exceed 0‰, which is unexplained. A study by Hanson (2014) identified diffuse soil flux using $\delta^{13}C$ in the vicinity of the Orakonui South Main Crater to have a geothermal signature, the same location in which a small relatively less-negative $\delta^{13}C$ anomaly (>-23.5‰) is seen in lichen isotopes. While this could be attributed to a geothermal influence, it could also be due to the effect of substrate the lichen lives on and a reduction in carbon sourced from biogenic respiration.

Ultimately, there is the potential for isotopes in lichen to be used as a geothermal exploration tool, although this method needs to be investigated in a higher flux geothermal area, such as Rotokawa, 7km to the south of Ngatamariki.

1 Introduction

Lichen, a symbiosis between a fungus and an alga, receive the vast majority of their nutrients from the atmosphere, making them ideal candidates for atmospheric studies (Conti & Cecchetti, 2001). As lichen lack cuticle or stoma they are open to nutrient (or pollutant) intake across the whole body (thallus) at all times of the day and night, and when exposed to atmospheric pollution, lichen are known to accumulate sulphur (González *et al.*, 1996; Proemse & Mayer, 2012; Vingiani *et al.*, 2004; Wadleigh & Blake, 1999), heavy metals (Bennett & Wetmore, 1999; Poblet *et al.*, 1997; Scerbo *et al.*, 1999; van Dobben *et al.*, 2001), and radionuclides (Loppi *et al.*, 1997; Matthews, 1981). Worldwide, lichen have been used to investigate atmospheric impacts of traffic density (Angold, 1997; Frati *et al.*, 2006; Gombert, Asta, & Seaward, 2003), industrial areas (González *et al.*, 1996; González & Pignata, 1999), anthropogenic derived pollutants in remote areas (Blasco, Domeño, & Nerín, 2006; Boonpragob & Nash, 1990; Lim *et al.*, 2009; Liu *et al.*, 2008; Osyczka, Dutkiewicz, & Olech, 2007), and outputs from geothermal production (Di Lella *et al.*, 2003; Loppi & Nascimbene, 2010; Loppi, 1996; Paoli & Loppi, 2008), along with atmospheric impacts from natural systems (Grenon, 2012; Loppi & Nascimbene, 1998; Mulligan, 2009; Skinner *et al.*, 2006).

The demand for 'clean' forms of electricity generation is rising and is projected to only climb further (Bertani, 2010). The utilization of geothermal energy, a clean form of energy relative to the combustion of fossil fuels, has been rapidly increasing since the 1970's (Figure 1.1), and a recent report states that geothermal energy is now used for electricity generation in 24 countries (Turkenburg *et al.*, 2012). With an estimated electricity production potential (worldwide) of 1200GW and a currently installed capacity of <20GW, geothermal energy production has huge potential for growth. For this to happen, increasingly effective and low costing exploration and investigation techniques are required, especially for blind geothermal systems (those without surficial expressions). Currently, a number of surficial and subsurface exploration techniques exist, such as gravity, magnetic, and conductivity surveys, thermal-infrared imagery, sampling of geothermal features, and gas flux surveys.

The latter, gas flux surveys, take advantage of both the flux and composition of gases emanating from geothermal systems to identify areas of higher up-flow, and therefore increased permeability. While the most commonly investigated gas is CO_2 (Bloomberg *et al.*, 2012; Hanson, 2014; Klusman, Moore, & Leroy, 2000), geothermal features release a number of gases, referred to as 'non-condensable' gases. The majority of these are CO_2, NH_3, and H_2S, but also includes N_2, H_2, CH_4 (Barbier, 2002). A gas flux survey of the Ngatamariki Geothermal Area in New Zealand, a semi-blind

geothermal area and the focus of this study, was recently conducted by Hanson (2014), after the success of Bloomberg (2012) at a nearby high-flux geothermal area (Rotokawa). The end member isotopic composition of carbon in the geothermal CO_2 ($\delta^{13}CO_2$) was found to be slightly less depleted (-6.8‰) than atmospheric CO_2 (-8.2‰), and much less depleted than that of biogenically derived CO_2 (-27‰), and was distinguished by the CO_2 concentration within the gas flux.

It is assumed that once this geothermal flux leaves the pedosphere and enters the atmosphere it becomes available to the biosphere. **This study aims to couple the effectiveness of lichen as atmospheric monitors with the gas flux of geothermal areas to develop an effective and low cost geothermal exploration technique to identify areas of high heat and mass up-flow. We hypothesise that the carbon and nitrogen elemental and isotopic compositions of lichen near geothermal resources will be statistically different to lichen further from geothermal resources**. This is tested by comparing transects across geothermal and non-geothermal influenced regions (regional scale), before examining the impact that the proximity to geothermal features within a geothermal field (field scale) has on nitrogen and carbon isotopic compositions. This study leads on from a smaller scale study by Tozer *et al.* (2005), in which a low density sampling pattern found that distance from geothermally active features (local scale) and areas (regional scale) had no influence on either nitrogen concentrations or isotopic composition of lichen and free-living alga.

Chapter 2 of this thesis ("Background") introduces the relevant knowledge required to test this hypothesis, investigating: lichen, isotopes, geothermal areas, the Taupo Volcanic Zone (TVZ), and the Ngatamariki Geothermal Area. Chapter 3 ("Lichen Isotopes Spatially") covers the methods used (and any attempts on method optimization) and presents the results of analyses from the four study areas investigated. One transect crossed the South Island of New Zealand (regionally non-geothermally influenced), two transects ran parallel and perpendicular to the Taupo Volcanic Zone (regionally geothermally influenced area), while the fourth study area is the Ngatamariki Geothermal Area (locally geothermally influenced). Chapter 4 ("Interpreting Controls on Lichen Isotopes") compares the data of this study with that of Tozer *et al.* (2005) before discussing the controls of land use classes on lichen isotopic composition and isoscapes of the Ngatamariki Geothermal Area.

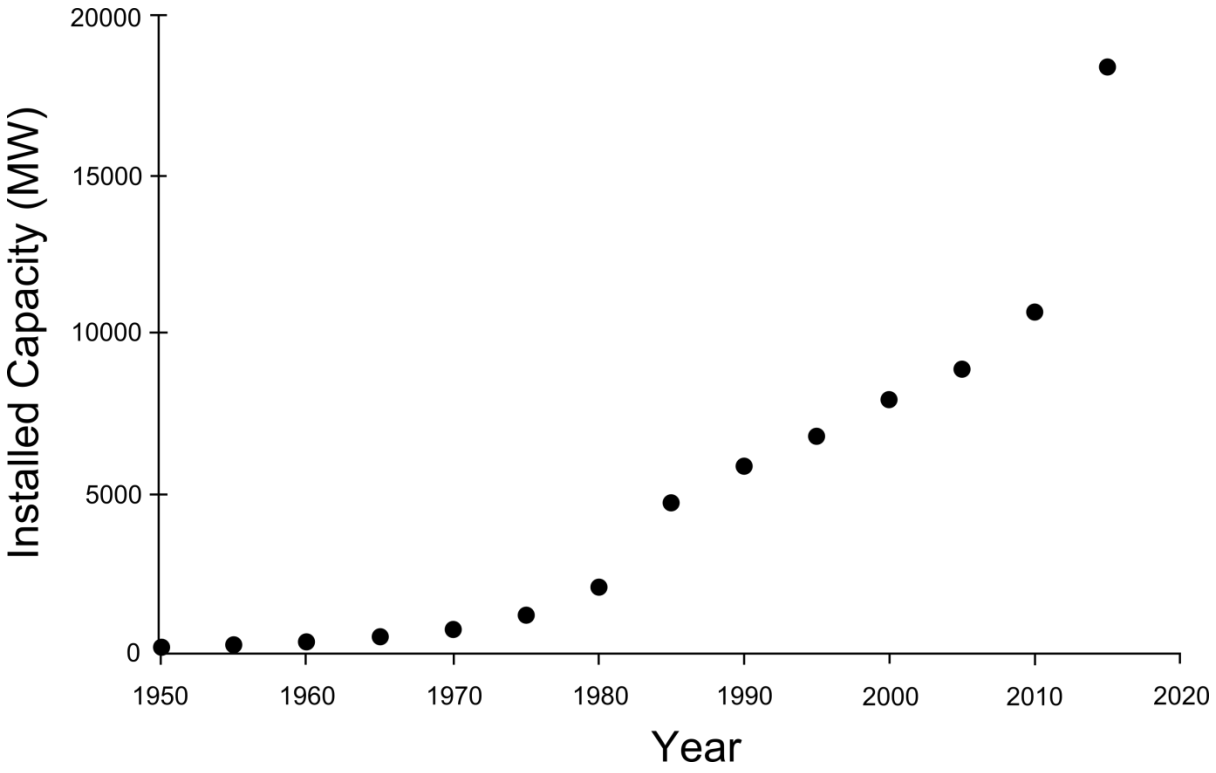

Figure 1.1: Worldwide geothermal electricity production for the period of 1950-2010, with a projected increase to 2015. Modified from Bertani (2010).

2 Background

This chapter introduces the subjects presented and discussed in Chapter 3 and 4 of this study. These subjects include: Lichen, isotopes, geothermal systems, the Taupo Volcanic Zone (TVZ), and the Ngatamariki Geothermal Area.

2.1 Lichen

Lichen exists as a symbiotic relationship between a fungal partner, the mycobiont, and a photosynthesizing partner, generally referred to as the photobiont. The photobiont may be further classified as a phycobiont if it is an algal partner, and the lichen as a whole is termed a chlorolichen (a member of the *Chlorophyceae*), or a cyanobiont if the partner is a cyanobacteria, and the lichen as a whole is termed a cyanolichen (Fahselt, 2008; Ulloa & Hanlin, 2000). Algal symbionts are by far the most common, with around 85% of mycobionts being compatible, while only around 10% of lichen contains a cyanobacterial partner. On rare occasions the lichen symbiosis may contain the fungal mycobiont and both a phycobiont and a cyanobiont in a tripartite relationship, with the third partner living in cephalodia within the lichen thallus. These lichen are known as cephalodiate species, and occupy the final 3-4% of all lichen (Honegger, 2008).

Despite containing multiple organisms from up to three separate biological kingdoms, lichen exhibit a discrete thalli and are considered as a single species, with the fungus determining the association. Lichen are found in almost all terrestrial environments on earth, in hot and cold extremes, dry deserts to tropical rain forests, and natural and anthropogenic environments (Nash, 2008a). This proves the symbiosis is successful, as certain lichen may exist in the same environment that the same fungus or alga in a non-lichenized state would be rare or non-existent.

Most flowering plants and conifers have developed the ability to maintain the water content of their extremities using stomata in the plant's cells to control influx and loss of water, and are examples of homiohydric organisms. Lichen lack stoma and are poikilohydric organisms, meaning their moisture content varies with surrounding environmental conditions (Nash, 2008a). Due to this, they become desiccated rapidly during drier periods. For most lichen, life-saving water comes in the form of rain, although lichen can receive water from fog and dew, and are also extremely well suited to extract water from non-saturated air (under certain conditions).

2.1.1 Morphology

The whole body of lichen, except for the ascocarps, is known as a thallus (plural: thalli). The morphology of lichen thalli is heavily influenced primarily by the mycobiont, however the influence

of the photobiont is not to be overlooked, and in a few cases is shown to determine the morphology of the whole thallus (Büdel & Scheidegger, 2008). The morphology is of great importance, as structures such as conglutinated cortical layers influence CO_2 diffusion resistance, therefore altering photosynthetic ability (Cristina Máguas, Pinho, Branquinho, Hartard, & Lakatos, 2013). While the internal structure of lichen is generally the same across most lichen, variations occur dependant on morphology.

External Morphology

Three general morphologies are recognised – crustose, foliose, and fruticose – as follows.

Crustose

Lichens with a crustose morphology are by far the most numerous, and as the name suggests, lie as a crust over or within the surface of the host substrate (Figure 2.1A). While other morphologies attach to the substrate using the lower cortex, rhizines, isidia, or soredia, crustose lichens lack all of these, and are instead attached by the medullary hyphae (Martin & Child, 1972). Due to the close attachment of lichen to the host surface, water loss only occurs on the uppermost surface (Büdel & Scheidegger, 2008). While this morphology is the most common, separating the whole thallus of the lichen from the substrate is a difficult and painstaking process, resulting in destruction of the thallus (Büdel & Scheidegger, 2008; Jahns, 1988). Isotope contamination occurs easily, and for this reason, crustose lichen are not used in this study.

Foliose

Foliose lichen exhibit a flat dorsiventral morphology, partially attached to the host substrate by rhizines or a central holdfast (Figure 2.1B). It may also be round, lobed, dissected and is often, but not always, pitted, folded or crumpled, however it is always leafy in character (Martin & Child, 1972). Unlike the crustose or fruticose morphology, foliose lichen exhibit both an upper and lower cortex (Büdel & Scheidegger, 2008). The genera *Xanthoria*, used in this study, is of foliose morphology. While easier to collect than lichen of a crustose morphology, care is needed to remove any attached material, such a bark, seeds, spider webs and canopy soils from the underside of the sample.

Fruticose

Fruticose lichen attach to the host substrate by a central holdfast, and exhibit an erect or pendulous bushy form (Figure 2.1C; Martin & Child, 1972). While some fruticose lichen are dorsiventral, the majority possess radially symmetric thalli. The thallus may have the terete stems of *Usnea*, or the flattened stems of *Ramalina*, both of which are used in this study. The high surface-to-volume ratio allows for more rapid wetting and drying than in other morphologies, and may act as a 'comb' to condense and collect dew and fog (Büdel & Scheidegger, 2008). Lichen with this morphology are the

easiest to collect without contamination from the substrate, and hence are the primary morphology used in this study.

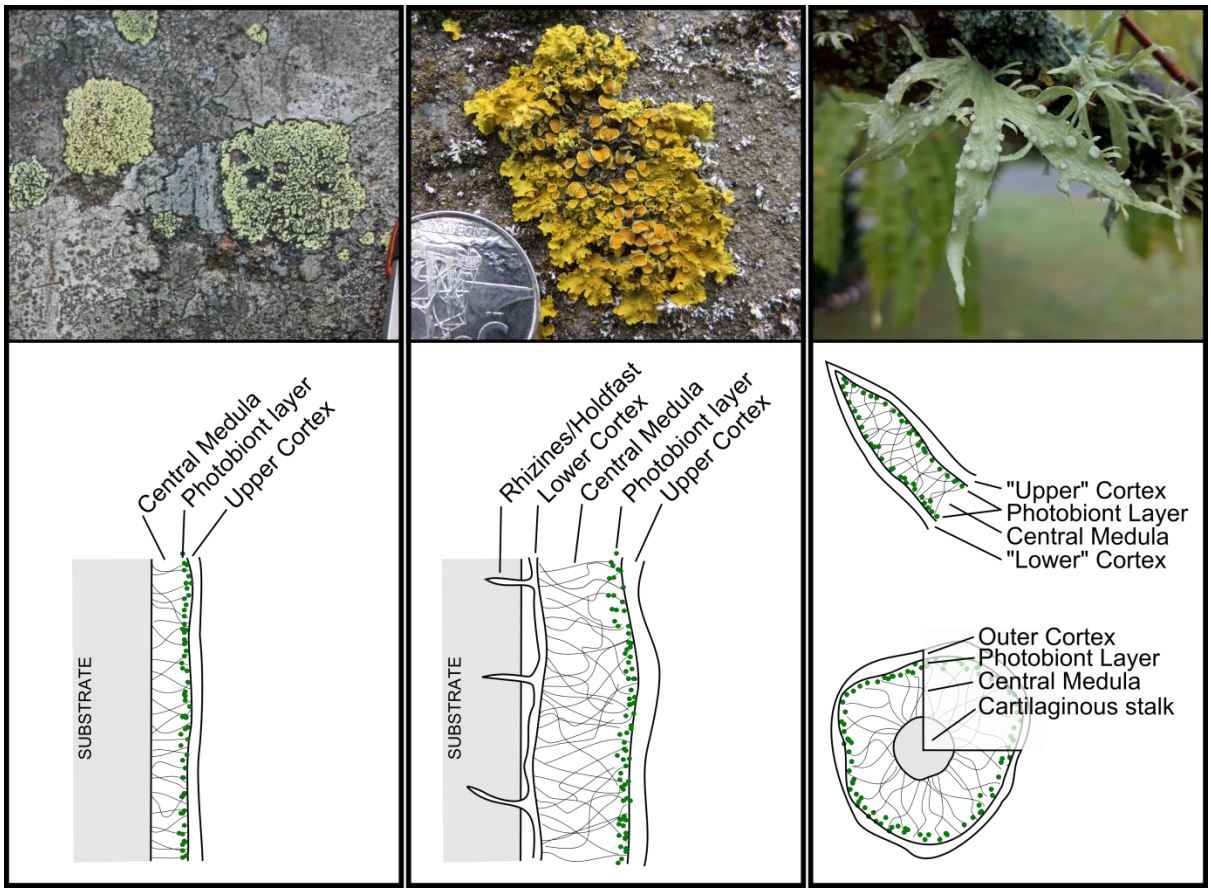

Figure 2.1: The three main lichen morphologies. A) Crustose morphology, B) Foliose morphology (*Xanthoria sp*. pictured), and C) Fruticose morphology (*Ramalina sp*. pictured). The three species used in this study are foliose (*Xanthoria sp*.) and fruticose (*Usnea sp*. and *Ramalina sp*.). Sketches of internal lichen morphology were drafted by the author from samples under the microscope (4-7x magnification).

Internal Morphology

The majority of lichen are heteromerous, having an internally stratified thallus, with a heterogeneous distribution of both the mycobiont and photobiont. This structure can typically be divided into four simplified parts: the upper cortex, photobiont layer, central medulla, and lower cortex, as summarised by three main morphologies in Figure 2.1.

Non-lichenised algae are generally restricted to moist terrestrial or aquatic environments where the intensity of the sun's rays are reduced; if the algae where exposed above water it would soon dehydrate and die. One of the greatest benefits to the photobiont to live with the fungal mycobiont is the protection from the sun's radiation due to the **upper cortex**, which provides further mechanical protection and modification of energy budgets (Kappen, Meyer, & Bolter, 1988; MacFarlane & Kershaw, 1985). Thalli in direct sunlight also have thicker cortical layers than a thallus of the same species in a low light or shaded environment (Jahns, 1988). The **lower cortex**, which

generally only occurs in lichen of foliose morphology may have a different structure to that of the upper cortex to allow the attachment of the lichen thallus to the substrate on which it lives (Jahns, 1988).

Between the upper and lower cortex is the **central medulla**, an area of loosely packed, interwoven fungal hyphae which make up the majority of the structure of foliose and fruticose lichen (Büdel & Scheidegger, 2008). The low density of the fungal hyphae facilitates gas exchange between parts of the thallus and between partners (Jahns, 1988). Just below the upper cortex, at the top of the central medulla, there exists a **photobiont layer**. In this section, algal cells, which can be seen under even a low powered microscope as green balls, are suspended on and around the hyphae.

The supporting tissues of fruticose lichen, and to a lesser degree in other lichens, are formed in the medulla, as thick walled, conglutinated hyphae, and as irregularly arranged strands, a central cylinder, or as a central, thread like elastic strand, as seen in *Usnea*.

Magnified images of the three lichen genera used in this study can be seen in Figure 3.4 (fruticose), Figure 3.5 (fruticose), and Figure 3.6 (foliose).

2.1.2 Growth

Mature lichen exhibit “growth zones” at the apical ends of the thallus or lobes within the thallus, where the cortex is pierced by pores to facilitate the elongation process. Fungal hyphae grow ahead into the surrounding atmosphere and host substrate, forming a peripheral zone void of algae, known as the prothallus. Some lichen develop hyphae within the main thallus that push algae out into the prothallus, while others detach part of the lichenised thallus which then become enmeshed by the hyphae of the prothallus. It is also believed that free-living algae might just as easily be incorporated by the advancing hyphal strands (Jahns, 1988).

2.1.3 Nutrition

Generally the relationship between mycobiont and photobiont is considered to be mutualistic, in which all parties receive benefits from the symbiosis, while some authors consider the relationship to be an example of controlled parasitism, as the fungal partner receives the majority of the benefits, and the growth rate of the photobiont may be reduced (Crittenden, 1988; Nash, 2008a).

In the lichen symbiosis, the alga is the partner concerned with the formation of nutrients, while the fungus supplies the alga with water, minerals, and protection (Conti & Cecchetti, 2001). The majority of nutrients taken up by the lichen partnership originate from the atmosphere, however minor influence is exerted by the substrate on which the lichen grows, as shown by lichen living on

calcareous substrates amassing calcium, or lichen on metal-rich ground accumulating elements such as iron, copper, zinc, and cadmium (Crittenden, 1988; Nash, 2008a). This influence may be in part due to atmospheric processes transporting particles from the substrate to become trapped in the thallus.

Strong correlations between element concentrations in the lichen thallus and atmospheric deposition rates have been shown by many studies (Crittenden, 1988; Grenon, 2012; Johansson, 2011; Poblet *et al.*, 1997; Skinner *et al.*, 2006). Also, as lichen lack cuticle or stoma, they are open to nutrient intake over the entire surface of the thallus during both the day and night (Blanco, Suárez, & Vicente, 1984; Conti & Cecchetti, 2001). When exposed to atmospheric pollution, lichen are known to accumulate sulphur (González *et al.*, 1996; Proemse & Mayer, 2012; Vingiani *et al.*, 2004; Wadleigh & Blake, 1999), heavy metals (Bennett & Wetmore, 1999; Poblet *et al.*, 1997; Scerbo *et al.*, 1999; van Dobben *et al.*, 2001), and radionuclides (Loppi *et al.*, 1997; Matthews, 1981).

Of upmost importance in this study is the metabolism of carbon and nitrogen. Carbon is assimilated through photosynthetic processes carried out by the alga, while nitrogen is integrated from dry and wet deposition as well as fixing atmospheric nitrogen (N_2)

Metabolism of Carbon by Lichen

Carbon is assimilated by the photobiont - which contains chlorophyll - through the process of photosynthesis (Cuna, Balas, & Hauer, 2007), according to the following equation:

$$6CO_2 + 6H_2O + \text{photons} \rightarrow C_6H_{12}O_6 + O_2$$

Photosynthesis converts light energy into chemical energy, to be used by lichen for maintenance, growth, and reproduction. In terms of photosynthesis, the lichen symbiosis can be looked at as a partnership between an autotroph, the photobiont, and a heterotroph, the mycobiont. On average, 40-50% of the dry weight of lichen is carbon (this study: 43.3 ± 2.8%), fixed almost exclusively by the photobiont (Green, Nash, & Lange, 2008). The photosynthesis by the photobiont produces carbohydrates which are 'shared' between both partners; a high proportion of the carbon that is fixed by the photobiont is transferred to the mycobiont (MacFarlane & Kershaw, 1985). The carbohydrate is transferred from the donor, the photobiont, to the mycobiont as a simple, single molecule, which the mycobiont rapidly converts to a carbohydrate that is unable to return to the photobiont (Galun, 1988a). Different photobionts vary in photosynthetic efficiency, while cyanobionts (and one phycobiont) possess a carbon concentration mechanism that increases this efficiency (Cuna *et al.*, 2007; Cristina Máguas & Brugnoli, 1996).

While the photobiont controls to a large degree the creation and transfer of carbohydrates to the mycobiont, other factors also play a part in the carbon metabolism in lichen.

The **thallus structure** affects the ease through which gas is exchanged from the atmosphere into the thallus. Conglutinated cortical layers reduce permeability, while soralium fissures and thinner apical regions may aid gas exchange (Jahns, 1988). Lower CO_2 diffusion resistances, such as in the apical regions, lead to lower ^{13}C discrimination, and a more depleted $\delta^{13}C$ value (Cristina Máguas *et al.*, 2013).

Phycobionts are able to initiate photosynthesis at low moisture contents relative to cyanobionts, and therefore **thallus water content** plays a part in carbon metabolism (Lange, 1980). In particular with phycobionts, photosynthetic ability increases with moisture content, until it reaches a compensation point and rapidly decreases to zero at thallus saturation, in the process decreasing carbon fractionation (Lange & Tenhunen, 1981; Smith & Griffiths, 1998). **Temperature** reduces the moisture content required to achieve photosynthesis, however it also increases respiration (Lange, 1980; Palmqvist, 2000).

Metabolism of Nitrogen by Lichen

Nitrogen is an essential macronutrient for life, however, as nitrogen is not part of earth's crustal material, its limited availability often constrains the growth and development of lichen (Nash, 2008b). Nitrogen sources are highly varied for lichen, making the subject of nitrogen metabolism much more complicated than that of carbon assimilation.

Typical nitrogen contents in lichen thalli range from 1-45 mg/gDW (dry weight). Chlorolichens on average have the lowest concentrations, between 1-30mg/gDW (Palmqvist *et al.*, 2002), replicated almost identically by data from this study (Figure 2.2). Cyanolichen exhibit the highest nitrogen contents out of any lichen symbiosis, and cephalodiate lichen (tripartite symbiosis of both phycobiont and cyanobiont partners) have contents in between these two (Rai, 1988). While nitrogen concentrations vary extensively, concentrations between groups overlap to the point where concentrations of the three different groups are not statistically different (Palmqvist *et al.*, 2002).

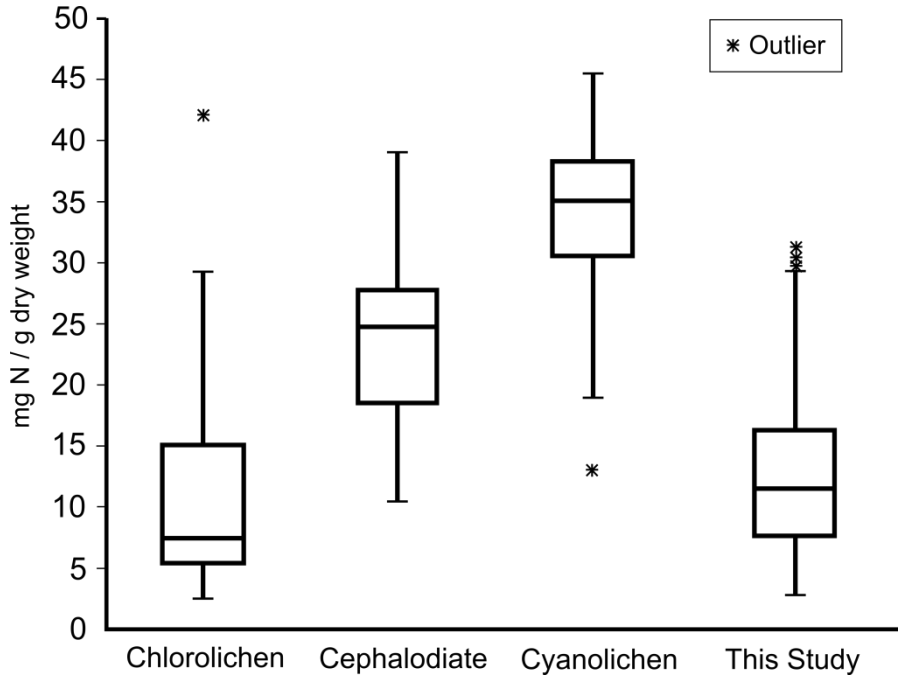

Figure 2.2: Thallus nitrogen content of the three types of lichen partnerships, compared to values obtained in this study. Other than for this study, data is from the median of ranges presented by Palmqvist *et al.*, (2002). Results from this study are from 690 samples across the South and North Island.

Lichen assimilates nitrogen in three main ways:

1) **nitrogen can be fixed** from atmospheric nitrogen (N_2),
2) aerosols can be deposited on the thallus, known as **dry deposition**,
3) nutrients can be deposited on the samples through rain water and runoff, known as **wet deposition**.

Nitrogen fixation only occurs in lichen with a cyanobacterial partner, and as atmospheric nitrogen is the standard for $\delta^{15}N$ (see Section: 'Isotopes', Page 15), this results in cyanolichen having $\delta^{15}N$ values approaching 0‰. Cyanolichens are not considered in this study, and as such fixation of atmospheric nitrogen is not considered further.

Nitrate (NO_3^-), ammonia (NH_3) and ammonium (NH_4^+) are inorganic forms of nitrogen, universally available to organisms, and are found in the atmosphere at significantly lower concentrations than N_2. Nitrate and ammonium are also found in the soil from decomposition and microbial mineralisation of organic material, however, as lichen lack root systems and acquire minimal nutrition from the host substrate this nitrogen pool is unavailable to lichen, other than through soil respiration. Under natural conditions, Hauck (2010) showed that lichen can efficiently take up both nitrate and ammonia simultaneously.

Lichen are incredibly efficient at removing nitrogen from rain water and assimilating it into the thallus. A study by Crittenden (1988) in which water with nutrient concentrations similar to that of natural rainfall were sprayed on to lichen thalli showed that on average >80% of inorganic nitrogen was retained by the thallus of the species studied, including during periods of high rainfall intensities. Nitrogen concentrations in lichen thalli often related to rates of atmospheric deposition (Hyvärinen & Crittenden, 1998; Nash, 2008c).

Excessive accumulation of ammonium leads to cytotoxicity (as does NO_2^- accumulation), therefore any ammonium assimilated from atmospheric deposition or converted from nitrate is further converted to amino acids (Hauck, 2010; Neuhäuser, Dynowski, Mayer, & Ludewig, 2007). Ammonium assimilation, and the intake and conversion of nitrate to ammonium requires carbon skeletons, produced by the photobiont, to bind the nitrogen, avoiding a toxic accumulation of free intracellular ammonium (Hauck, 2010).

Lichen have proven to be just as efficient in the uptake of inorganic nitrogen (NO_3^-, NH_3, NH_4^+) as with organic forms of nitrogen, such as amino acids (Dahlman *et al.*, 2004). Rainwater, when filtered through a forest canopy, has long been shown to be enriched in amino acids (Carlisle, Brown, & White, 1966; Heaton, Spiro, & Robertson, 1997), and as such this source of nitrogen is available to lichen under forest canopies.

Note

This above section only considers the extreme basics of carbon and nitrogen metabolism relevant to this study. The complexity and full explanation of these concepts requires a much greater space allowance than is available in this study. For a more in-depth focus on these topics the reader is referred to:

- "Assimilation of Mineral Nutrients" (Chapter 12) of Taiz & Zeiger (2002),
- "Carbon Metabolism" (Chapter VI.A) and "Nitrogen Metabolism" (Chapter VI.B) of Galun (1988b),
- "Nitrogen, its Metabolism and Potential Contribution to Ecosystems" (Chapter 11) of Nash (2008a).

2.1.4 Lichen as Atmospheric Indicators

As far back as 1859, Grindon observed the disappearance of lichen from the area around South Lancashire, England, and hypothesised that this was due to increases in air pollution. Since then, negative correlations between atmospheric pollutants and lichen biodiversity have been recorded in countries around the world, both in the laboratory and in the field including transplant studies.

Lichen depend directly on atmospheric conditions for the majority of their nutrition, and have been shown to be influenced by many natural and anthropogenic environmental factors, making them excellent atmospheric indicators (Cristina Máguas *et al.*, 2013). They have been noted by many authors as important 'early warning systems' due to their sensitivity and abundance, exhibiting changes well before other parts of the surrounding ecosystem (Cristina Máguas *et al.*, 2013).

Lichen and other biological entities that are used as atmospheric indicators are known as bioaccumulators, which are further classified as either bioindicators and biomonitors as defined by Conti & Cecchetti (2001) are as follows:

> "*Bioindicators are organisms that can be used for the identification and* ***qualitative*** *determination of human generated environmental factors, while biomonitors are organisms mainly used for the* ***quantitative*** *determination of contaminants and can be classified as being sensitive or accumulative*"

While most studies look into the accumulation of toxic contaminants from anthropogenic sources, this study differs slightly. The nitrogen measured in this study is intended to come from natural geothermal sources, although there is likely to be an impact from anthropogenic sources (such as land use) of unknown magnitude.

Conti & Cecchetti (2001) provide a valuable definition of a bioaccumulator, and by using this we can prove that lichen are an effective atmospheric indicator.

1. **Bioaccumulators must accumulate the pollutant without, however, being killed by the levels with which it comes into contact.**

The nitrogen species in the atmosphere (NH_x, NO_x) with which the lichen acquires nearly all of its nitrogen nutrition, is diluted to the point where it will no longer be of toxic concentration. As at least one of the species in this study is a nitrophytic species (ie. *Xanthoria parietina*), lack of the 'pollutant' is likely to be of more concern. It is however, possible that intensive farming practices will introduce excessive nitrogen quantities on a scale that will reduce affinity of a lichen species for that area.

2. **Bioaccumulators must have a wide geographical distribution.**

Lichen grow in almost every environment on earth, from polar caps to hot desserts, from coastal dunes to mountain tops. Generally this applies to lichen as a whole, as each species occupy its own specific environmental niche. The species selected in this study are easy to identify at genus level, and are abundant across the length and width of New Zealand.

3. **Bioaccumulators must be abundant, sedentary, or of scarce mobility, as well as being representative of the collection area**.

The lichen used in this study are highly abundant across New Zealand, and similar to other lichen, moss, liverworts, and vascular plants, have very limited or no mobility whatsoever. Lichen are open to receiving nutrients at all times of the day or night (assuming sufficient moisture content), and receive almost all of their nutrients from the atmosphere, making them representative of the long term atmospheric composition of the area in which they were collected.

4. **Bioaccumulators must be available all year round and allow for the collection of sufficient tissues for analysis.**

As the lichen genera used in this study are so abundant, there is a large amount of collectable samples that are easily identifiable (to genus level in the field). While some lichen are ephemerals, almost all lichen are perennials, with some species living up to 1000 years, and are therefore not restricted to collection during preferential weather and seasonal conditions.

5. **Bioaccumulators must be easy to collect and resistant to laboratory conditions.**

As mentioned previously, lichen are easily recognisable and identifiable, and are therefore easy to collect. With correct collection and handling procedures (see Section 3.1: Methods), lichen can be stored for extended periods of time without degradation (Dahlman *et al.*, (2003), Gauslaa & Solhaug, (1996); also see Section: 3.1.5 'Time in Storage', page 41).

6. **Bioaccumulators must have a high concentration factor for the contaminant under study, and thus allow direct analysis with no prior increase in concentrations.**

This is the premise behind the study, to determine if the nitrogen from geothermal sources produce a large enough concentration to significantly alter the nitrogen isotopic composition of lichen close to geothermal source. Lichen are approximately 40-50% carbon and 0.1-5% nitrogen (Green *et al.*, 2008; Palmqvist *et al.*, 2002), making even a small sample well over the detection limit of IRMS used for analysis (see Chapter 3, Section 1: Methodology).

7. **Bioaccumulators must have a simple correlation between the quantity of contaminant contained in the organism and the average contaminant concentration in the surrounding environment.**

As mentioned previously, strong correlations between element concentrations in the lichen thallus and atmospheric deposition rates have been shown by many studies (Crittenden, 1988; Grenon,

2012; Johansson, 2011; Poblet *et al.*, 1997; Skinner *et al.*, 2006). Also, as lichen lack cuticle or stoma, they are open to nutrient intake over the entire surface of the thallus during both the day and night (Blanco *et al.*, 1984; Conti & Cecchetti, 2001).

8. **Have the same contaminant content level correlation with the surrounding environment in every site studied and under any condition.**

This is assumed to be true.

The above points illustrate that lichen are suitable atmospheric indicators for this study.

2.2 Isotopes

Isotopes are atoms of an element whose nuclei contain the same number of protons but a different number of neutrons (eg. ^{14}N = seven neutrons, seven protons; ^{15}N = eight neutrons, seven protons). Isotopes are either stable or unstable, relative to detection limits of radioactive decay times. Only 21 elements are considered pure elements, with only one stable isotope, and therefore the remaining elements will have a number of stable isotopes that can be expressed in terms of abundance relative to the other isotopes of the same element. The abundances can be evenly distributed such as between the isotopes of ^{63}Cu and ^{65}Cu which have an average abundance of 69 and 31% respectively. Generally, however, isotope abundances are dominated by one isotope with one of more less frequent isotopes, such as with nitrogen which has two stable isotopes, ^{14}N and ^{15}N which have abundances of 99.6337 and 0.3663% respectively (Hoefs, 2004; West *et al.*, 2010). These abundances can be simplified into ratios between of the heavier atom to the lighter, known as **molar ratios**. In the case of nitrogen, the ratio of ^{15}N/^{14}N would be 0.0036765 (Fry, 2006; Robinson, 2001).

Stable isotope abundances are expressed as a ratio relative to an internationally accepted reference standard. Delta (δ) notation is used to indicate a difference relative to the rare to common isotope ratio of a standard:

$$\delta^{xx}E = \left(\frac{R_{sample} - R_{standard}}{R_{standard}}\right).1000 \quad (1)$$

Where E is the element of interest, xx is the mass of the heavy (rare) isotope, R is the molar ratio of the heavy (rare) to light (common) isotope of the sample and standard (eg. the ratio of ^{15}N to ^{14}N, or ^{13}C to ^{12}C). Delta values are quite small, so are generally multiplied by 1000 and reported in units of parts per thousand (per mil, ‰). The final δ value is expressed as the amount of the rarest to most common isotope in the sample. **Positive values indicate greater amounts of the heavier isotope (more enriched in minor isotope) than the standard, while negative values indicate less (less enriched in minor isotope)**. There are generally two levels of standards used to determine isotopic ratios. The first level is an easily accessible non-specific standard that is used regularly to ensure consistency between samples. This first level standard is then calibrated to a less available international standard (ie. the Vienna Pee Dee Belemnite Standard, PDB, for carbon isotopic ratios). By definition, these standards have a δ value of 0‰ (Dawson, Mambelli, Plamboeck, Templer, & Tu, 2002; West *et al.*, 2010).

The isotopic value of a given element in a system is controlled by two processes, fractionation and mixing. Fractionation acts to separate isotopes, whereas mixing acts to reunite isotopes (Fry, 2006).

2.2.1 Fractionation

The process in which a samples isotopic composition alters from the standard is called **isotopic fractionation**. This may occur through a simple process (eg. evaporation), or may be the result of a series of complex steps (eg. cellulose formation). The 'amount' of fractionation that occurs for a certain process can be expressed by a fractionation factor, α, as shown:

$$\alpha_{A/B} = \frac{R_A}{R_B} \tag{2}$$

where R_a and R_b are the molar ratios of the two substances after and before, respectively[1]. If the source and the sink maintain the same molar ratio, this implies that no fractionation has occurred, and α=1; when α≠1, fractionation has occurred. This ratio generally provides values less than one, due to the lighter isotopes reacting slightly faster, and becoming slightly enriched in the product (R_A). For α values to be expressed on the δ scale, α values are transformed using the following equation:

$$\varepsilon_{A-B} = 1000(\alpha_{A-B} - 1) \tag{3}$$

where ε is the difference in isotopic value between the source and sink[1], referring to the fractionation in terms of per mil (Robinson, 2001). For small values of ε, $\varepsilon_{A\text{-}B} \approx \delta_A - \delta_B$ (Kendall & Caldwell, 2006). For each process or reaction ε is not constant, rather it varies depending on external conditions, such as temperature (Robinson, 2001). This variation can be seen in Figure 2.3, in which the ε of nitrogen isotopes is shown to range considerably for several important nitrogen cycle reactions.

During a given reaction, the isotopic value of the remaining source (δ_{So}) changes according to:

$$\delta_{so} = \delta_0 + \varepsilon \ln(1 - f) \tag{4}$$

where δ_0 is the initial isotopic value of the source and f is the fraction of the source that has been consumed at a given time (f=1 referring to no conversion, f=0 referring to complete conversion from source to sink; Robinson, 2001). Equation 4 requires that the source is of limited quantity in a closed system. As the fraction of the residual source approaches zero (ie. lim[f→0]) the isotopic values of the residual source approaches +∞. The isotopic value of the accumulating sink (δ_{si}) follows this reaction:

[1] It should be noted here that the notation for the above equations may vary in biological or ecological isotopic studies. α may be derived from $^{L}K/^{H}K$ (rather than R_A/R_B in our case) referring to heavy (^{H}K) and light (^{L}K) isotope substitution rates, giving a value generally >1. ε may be referred to as Δ, giving a positive fractionation value (rather than a negative one in our case). For a more detailed explaination, see pg.27-8 of Fry, (2006).

$$\delta_{si} = \frac{\varepsilon(1-f)[\ln(1-f)]}{f} \quad (5)$$

As the source approaches complete conversion (ie lim[f→0]) $\delta_{si}=\delta_0$, and the sink takes on the same isotopic value as the initial source (δ_0).

Fractionation Processes

The major fractionation processes are controlled by isotope exchange, kinetic effects, and diffusion, as well as pressure, chemical composition, and crystal structure (Hoefs, 2004). It is only when the element in question leaves the system can the isotopic values of said system change, and even then, only if the isotopes leaving the system are isotopically distinct from the system will the isotopic value of the system change (Robinson, 2001).

Fractionation through **isotope exchange** occurs when there is no net reaction, but the isotope distribution changes between different chemical substances, phases, or molecules; heavier isotopes concentrate where bonds are the strongest (Fry, 2006). Evaporation-condensation processes are of special interest in stable isotope applications, as the differences in vapour pressures of isotopic compounds lead to significant isotopic fractionations. As condensation or evaporation proceeds the residual vapour or liquid will become progressively depleted or enriched with respect to the heavier isotope.

Kinetic isotope effects are associated with incomplete or unidirectional processes and also occur when the rate of a chemical reaction is sensitive to atomic mass at a particular position in one of the reacting species (Hoefs, 2004). Simply put, the lighter isotopes usually react easier or faster than the heavier isotopes of the same element (Fry, 2006). This can include evaporation, dissociation reactions, almost all biological reactions, and diffusion.

Light isotopes are generally more mobile than heavier isotopes; therefore **diffusion** can lead to a separation of light from heavy isotopes, leaving the reservoir enriched in the heavy isotope. Using evaporation as an example, the velocities of lighter molecules allows them to break through the liquid surface preferentially. ^{13}C is preferentially incorporated into organic tissues during photosynthetic reactions, giving distinctly low $^{13}C/^{14}C$ ratios (Sharp, 2007).

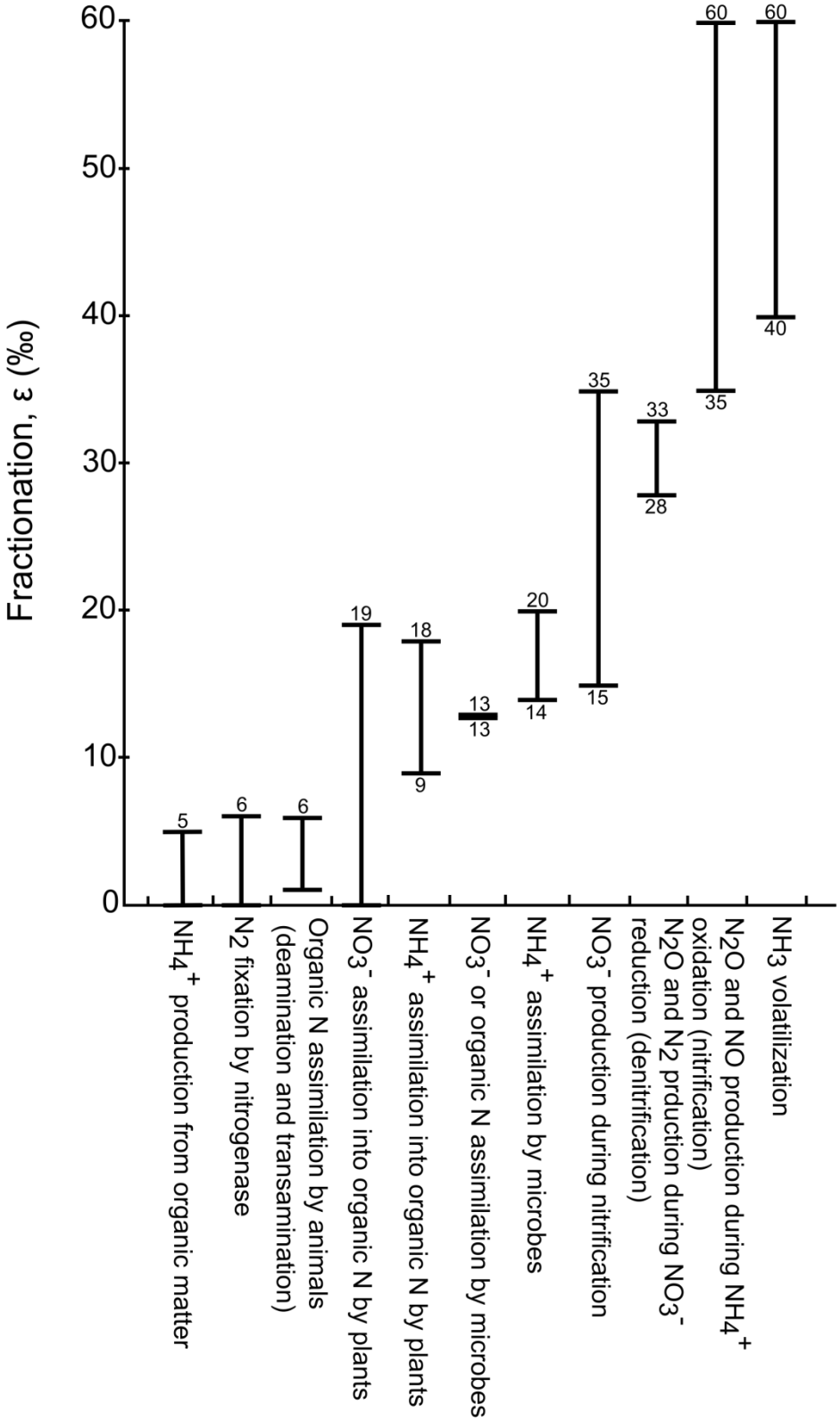

Figure 2.3: A comparison of fractionation values (ε) through various nitrogen cycle processes. From data presented in Robinson (2001).

2.3 Geothermal Systems

Geothermal systems are areas of the earth's crust in which convecting fluids transfer heat from a deep heat source to the surface or a shallow horizon. A geothermal system requires three main components: a heat source, a reservoir, and a fluid. Permeable reservoir rocks also aid fluid convection and heat transfer.

As illustrated in Figure 2.4, a convective or conductive heat source causes geothermal waters to rise through permeable conduits (faults and fractures) to either a permeable horizon or the surface. The system is recharged through meteoric waters or groundwater.

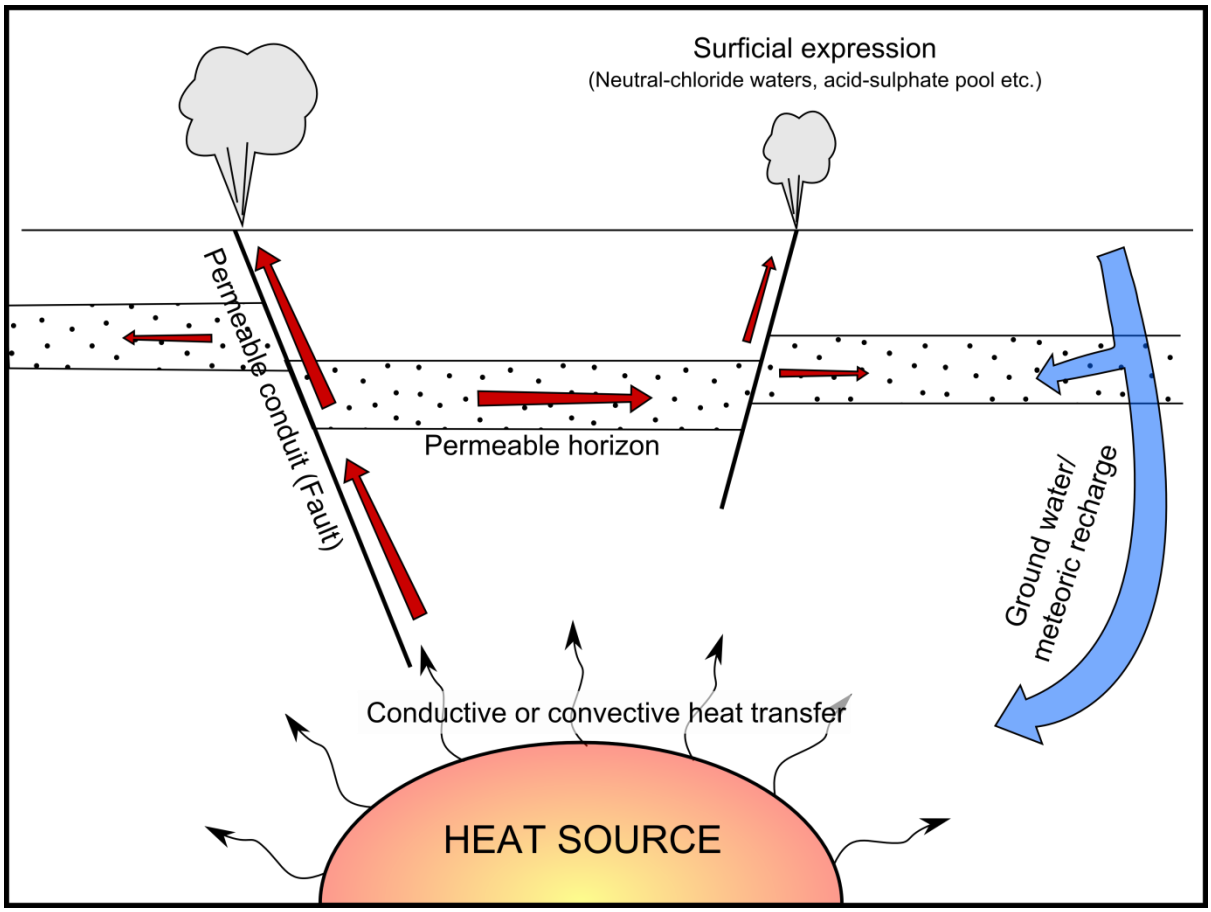

Figure 2.4: A highly generalised theoretical geothermal system, exhibiting a convective or conductive heat source and geothermal waters rising along permeable conduits to either a permeable horizon or the surface. The system is recharged by cool meteoric waters or ground water. Simplified based on Henley & Ellis (1983).

The temperature (or enthalpy) of geothermal reservoirs is an important component in terms of fluid chemistry and potential resource usage. Systems are most commonly divided loosely into low-enthalpy (<150 ˚C) or high enthalpy (>150˚C) systems (Chandrasekharam & Bundschuh, 2008), although some authors make a further classification of intermediate systems (120-180˚C).

2.3.1 Controls on Geothermal Distribution

As the typical thermal gradient in any given area is usually between 5-70˚C/km, water at temperatures approaching and exceeding 100˚C between 1-2km is common in many areas, however, it takes specific geological settings for this temperature to increase above 150˚C at similar depths (Ellis & Mahon, 1977). The major geothermal systems (high enthalpy) occur in areas of high heat flow, often associated with zones of volcanism or mountain building near the edge of converging or diverging crustal plates, such as the Taupo Volcanic Zone in New Zealand (converging) or Iceland, which straddles the Mid-Atlantic Ridge (divergent), while lower enthalpy systems are widespread, such as Australia, China, Germany, and Alaska, U.S.A., and may occur in close proximity or far from high-enthalpy systems (Chandrasekharam & Bundschuh, 2008). The main sources of geothermal heat in high-enthalpy systems is uprising magma, or deep seated intrusives, although in low-enthalpy systems the natural radioactivity (which varies dependant on rock-type) and the conduction of heat from the mantle to more shallow levels provide heat.

Geothermal systems are split into a broad classification based on the geological and tectonic association, from Chandrasekharam & Bundschuh (2008):

1. Associated with **active volcanism and tectonism**, which is often controlled by subduction (eg. New Zealand, Indonesia, South America)
2. **Continental collision zones** (eg. Himalayan geothermal belt between the Eurasian and Indian plate)
3. **Continental rift systems associated with volcanism** (eg. Ehtiopia, Kenya)
4. **Continental rift systems not associated with volcanism** (eg. West and Central India, Larderello, Italy)

Geothermal systems in settings other than these exist, occuring in large sedimentary basins and are known as ‘geopressured reservoirs’. They form when sedimentation occurs rapidly (over geological time) without expulsion of the fluids within the pores of the sediments, resulting in abnormally high pore pressures, approaching those of lithostatic pressures. The geothermal gradient is around 75˚C/km, and with burial of 2-3km the temperature of the pore fluids approaches those of high-enthalpy geothermal systems. These settings are commonly associated with oil and gas reservoirs.

2.3.2 Geothermal Fluids and Gases

The convection of heat in geothermal areas occurs through transport of geothermal fluids and their associated geothermal gases.

Geothermal Fluids

The chemistry of geothermal fluids varies greatly, depending on temperature, gas content, heat source, rock type, permeability, age of the geothermal system, fluid source and degree of mixing (Barbier, 2002). At depth, the primary type of fluid is a sodium-chloride brine containing gas (mostly CO_2) formed by the absorption of magmatic volatiles (HCl, CO_2, SO_2, H_2S) into deeply circulating meteoric waters.

Geothermal fluids are then characterised based on composition, with most fluids falling into one five categories, from Chandrasekharam & Bundschuh (2008), Nicholson (1993), Barbier (2002), and Ellis & Mahon (1977) unless otherwise stated:

- **Chloride** (also known as Alkali Chloride, Neutral Chloride, or Na-Cl type)

  Chloride waters are found in volcanic areas where the fluid has ascended to the surface with minimum conductive heat loss. They have a near neutral pH, high Cl, Si, Na, and K content, and have magmatic CO_2 and H_2S as the major gas phases within the fluid. Chloride waters are a distinctive clear blue-green in colour (eg. Ngatamariki's Main Crater)
- **Acid Sulphate** (also known as Sulphate)

  These form when geothermal gases condense into near-surface, oxygenated waters, where H_2S is oxidised to sulphate (SO_2^{-4}). The gases originate from deeper fluid, but due to boiling, have separated from the chloride waters. Acid sulphate waters are more likely found at the fringes of geothermal fields or high upflow areas above boiling zones, topographically above the water table. These pools are distinctive and may be found as boiling mud pools, steaming ground, turbid pools and occasionally springs (eg. Ngatamariki's Main Crater Side Spring)
- **Bicarbonate**

  These waters occur when steam containing CO_2 and H_2S condense into poorly oxygenated groundwater, and under stagnant condition and fluid/rock reactions produce neutral pH bicarbonate and sulphate-bicarbonate fluids.
- **Dilute Chloride-(bicarbonate)**

  These waters form through dilution of chloride waters by groundwater or bicarbonate waters during lateral flow. The pH is generally near neutral (6-8) with chloride as the major anion. Surficial expressions appear to be restricted to the margins of major upflow areas in high enthalpy systems, and often discharge as springs in low enthalpy systems.
- **Sulphate-Chloride**

  These waters form through large amounts of H_2S of volcanic origin contained within chloride waters forming bisulphate ions (HSO_4^-). Bisulphate formation increases with a decrease in

temperature; as the fluid approaches the surface the pH decreases, and Cl^- content increases.

Geothermal Gases

Along with steam, six 'non-condensable' gases are commonly present within geothermal fluids, both at the surface all the way down to the reservoir. These are CO_2, H_2S, NH_3, N_2, H_2, and CH_4, from Barbier (2002):

- **Carbon Dioxide (CO_2)**

  CO_2 is the most abundant gas, often making up 85% of the total gas content.
- **Hydrogen Sulphide (H_2S)**

  H_2S originates from either the alteration of host rocks or is sourced from magmatic volatiles.
- **Ammonia (NH3)**

  Ammonia is highly soluble, especially at lower temperatures, although it travels as a gas in steam. It may be the result of the alteration of organic matter during the ascent of the fluids.
- **Hydrogen (H)**

  Hydrogen is often removed from geothermal fluids during reactions with host rock.
- **Methane (CH_4)**

  Methane is most likely produced from alteration of organic rich host rock, and is the most common geothermal hydrocarbon.
- **Nitrogen (N_2)**

  Most N_2 is mostly derived from atmospheric gases present in meteoric water prior to heating, and high concentrations may indicate mixing of geothermal waters with shallower aquifers, although a magmatic origin is possible.

The concentrations of gas species in the steam is inversely related to the percentage of steam flashed from the water (Ellis & Mahon, 1977). The vapour phase can migrate vertically, unlike the fluid phase which often migrates laterally, resulting in the potential for fluids and gases to become significantly separated.

2.4 Taupo Volcanic Zone (TVZ)

The **Taupo Volcanic Zone (TVZ)** is a 300km long, 60km wide back-arc system running SW-NE through the North Island of New Zealand (Figure 2.5), and is the southern end of the Taupo-Hikurangi subduction system resulting from the subduction of the Pacific Plate beneath the Australian plate (Hochstein, 1995). The boundary of the TVZ is defined by the area of active volcanism in the past 2.0Ma using vent positions and caldera margins, but does not include faulting parallel to but outside of the envelope of the vents (Wilson *et al.*, 1995). Andesitic activity began as early as this, with rhyolitic and some basaltic and dacitic activity from 1.6Ma (Cole & Lewis, 1981; Wilson *et al.*, 1995). The TVZ developed in Mesozoic metasedimentary rocks, in crust which has been highly thinned, with studies showing the upper mantle at a depth of 15km depth (Bibby, Caldwell, Davey, & Webb, 1995). Running along the strike of the TVZ is a series of north-east trending faults known as the **Taupo Fault Belt**, resulting from extensive rifting and is related to the emplacement of hot magma into the thinned crust (Figure 2.5; Kissling & Weir, 2005; Wilson *et al.*, 1995).

The TVZ is divided into three areas based on volcanic activity: the southern and northern sections exhibit andesitic activity, while the middle section shows caldera forming eruptions. The central rhyolite dominated section of the TVZ contains many calderas, with the majority of erupted material sourced from eight main calderas. These are Rotorua, Okataina, Kapenga, Reporoa, Ohakuri, Mangakino, Whakamaru, and Taupo calderas (Wilson *et al.*, 1995).

2.4.1 Geothermal Activity in the TVZ

Bibby *et al.* (1995) identified 23 geothermal fields in the TVZ; 17 fields with heat outputs of >20MW, along with six lower output fields (Figure 2.6). The thermal outputs of the fields range from <1MW (Motuoapa) up to 540MW (Waiotapu) (Kissling & Weir, 2005). On average they are spaced 10-15km from each another implying a heat source at a depth of 8km, with surveys showing high resistivity in the regions between the geothermal areas also implying that these areas have undergone hydrothermal alteration, and therefore the systems must be spatially stable over longer time periods (Bibby *et al.*, 1995; Kissling & Weir, 2005) The 23 fields together produce a total output of 4200 ± 500MW, with the four largest fields producing 40% of this thermal output (Bibby *et al.*, 1995; Kissling & Weir, 2005). In the TVZ as a whole, greater heat output is grouped towards the eastern margin (Kissling & Weir, 2005). Groundwater convection is crucial for the transportation of heat to surficial geothermal sites with the upwelling of warm fluids is complimented by the downwelling of colder meteoric waters through the Taupo Fault Belt (Kissling & Weir, 2005). Of these 23 geothermal fields, only seven have been developed for energy generation at the time of publication (Figure 2.6). The lack of exploitation from some of the larger fields is due to their protection status.

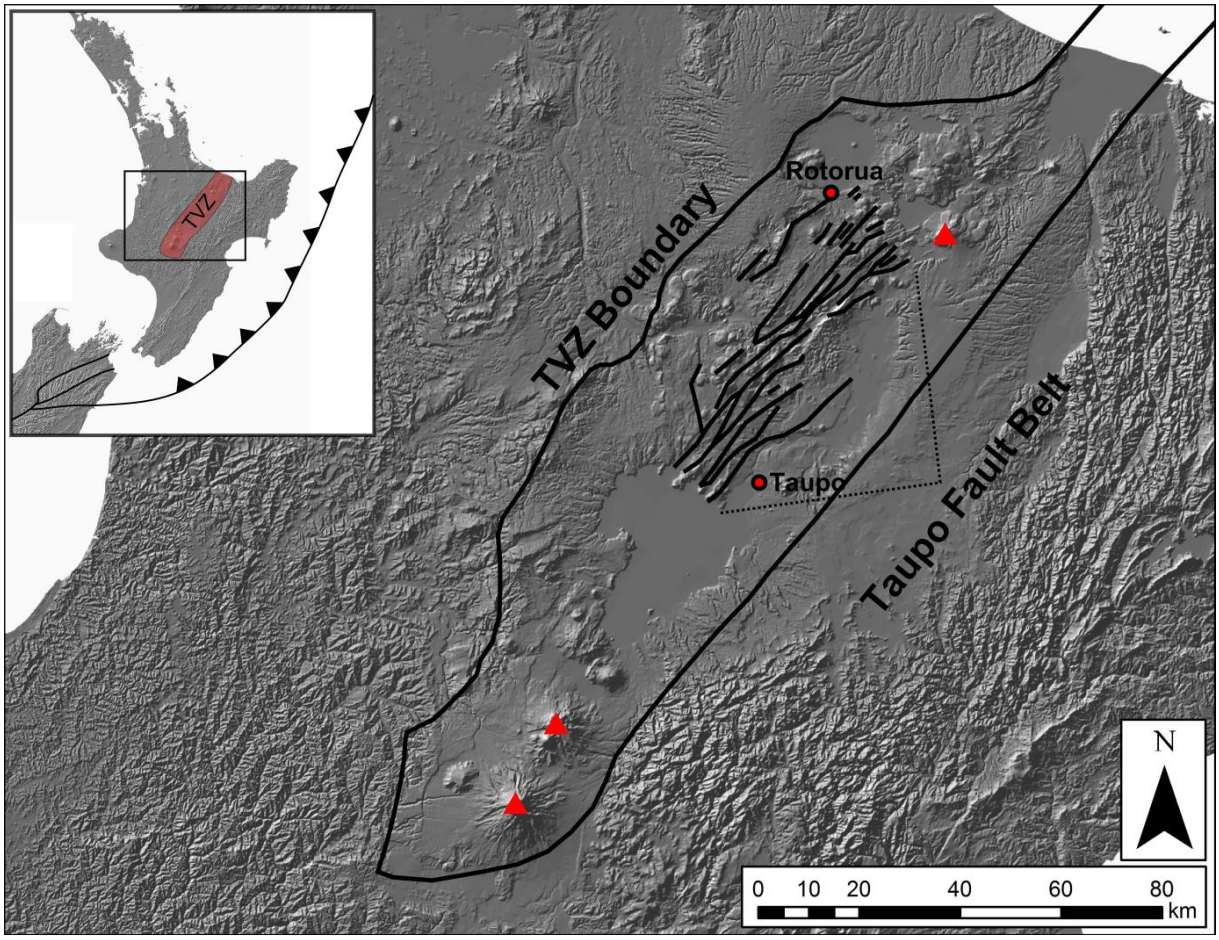

Figure 2.5: The extent of the Taupo Volcanic Zone (TVZ). The inset indicates the location of the TVZ within New Zealand. The main picture indicates the extent of the TVZ, the Taupo Fault Belt and major volcanoes (red triangles). Modified from data from Cole (1990) and Kissling & Weir (2005). For GIS data sources see section 0 'GIS Data Sources'.

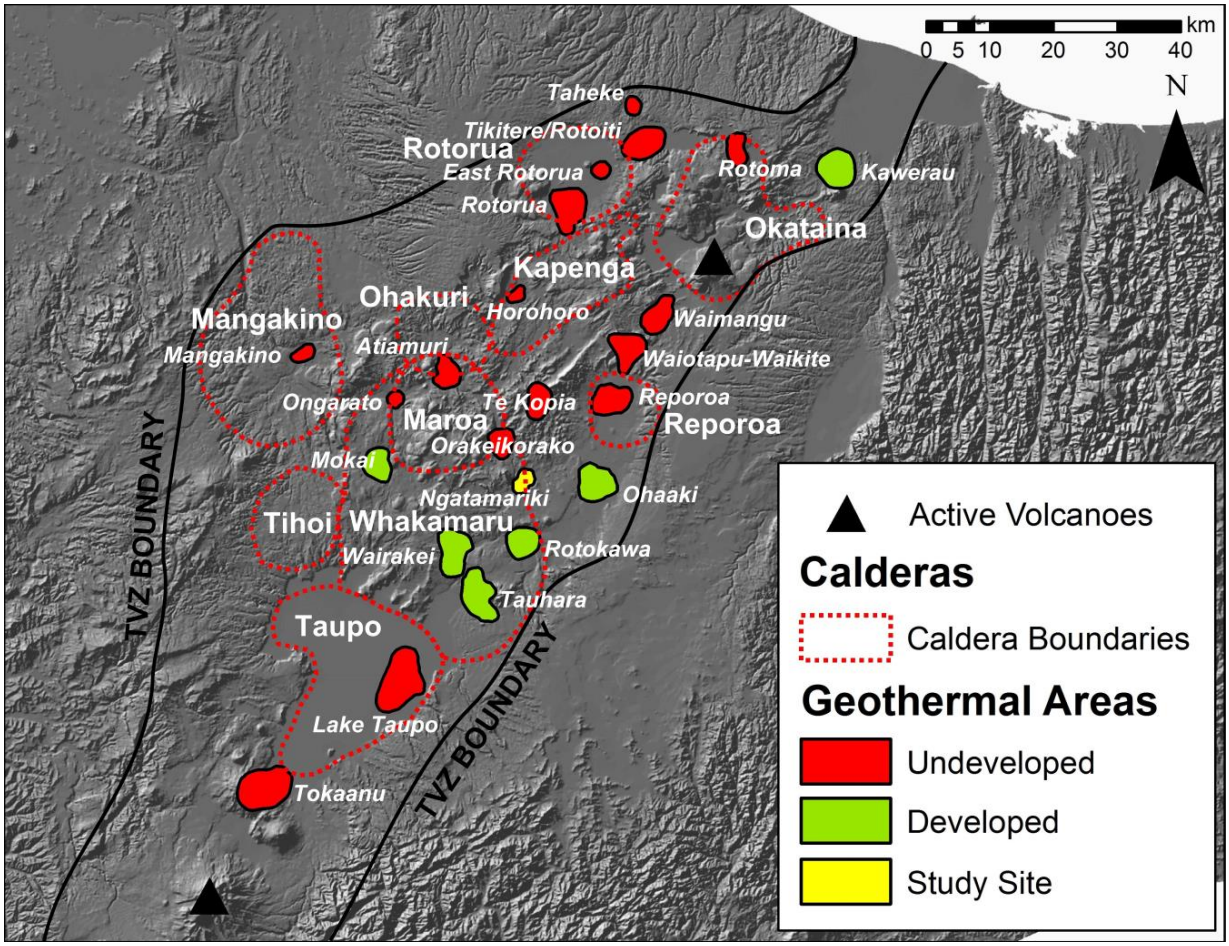

Figure 2.6: The calderas (dashed polygons) and geothermal systems (coloured polygons) of the TVZ. Geothermal systems are colour-coded based on development status. Caldera names are bold type, while geothermal area names are smaller italicised type. Locations are approximate, based on Kissling & Weir, 2005 and O'Brien, 2010. For GIS data sources see section 0 'GIS Data Sources'.

2.5 Ngatamariki

The Ngatamariki geothermal area is located 20km north-east from Taupo in the central TVZ, North Island (Figure 2.6). It sits on the edge of the Whakamaru caldera as inferred by Wilson (1986 and 1995), and is approximately 8km from the eastern edges of the Maroa Volcanic Centre (MVC) (O'Brien, 2010). The geothermal 'boundary' is roughly bound to the north by the Waikato River, the west by Orakonui stream, and to the south by State Highway 5. MT surveys by Urzua (2008) determined that the field covers an area of 12km^2 (Figure 2.7)

Construction of an 82MW power station at Ngatamariki began in June 2011, and was completed in September 2013, slightly under the budget of NZD$475m, annually producing 700GWh of electricity (Mighty River Power, 2013). The station is located to the south-east of the Orakonui Springs, and significant infrastructure was required to transport geothermal fluids to and from injection and production wells, and to transport generated electricity to the substation 7.5km to the south, at the Nga Awa Purua substation.

There exists 11 deep wells to depths of >3000m, and 21 sentinel or monitoring wells to depths of 1500m (Figure 2.7). The original 4 wells (NM1-4, 1308 to 2400m deep) were commissioned and sunk by the Crown in 1985-6 (Wood, 1985a, 1985b, 1986a, 1986b). The Rotokawa Joint Venture (Mighty River Power and the Tauhara North #2 Trust) undertook further drilling in 2008-9 (Boseley *et al.*, 2010), with another three deep wells (NM5-, 2997 to 3398m deep; Rae, Ramirez, & Bardsley, 2009; Rae, Ramirez, & Boseley, 2009; Ramirez & Rae, 2009). Further drilling was also undertaken by MRP in 2012, with an additional four deep wells (NM8-NM11, 3028 to 3551m deep; (Lewis, Chambefort, Rae, Sanders, & Massiot, 2013; Lewis, Chambefort, Rae, & Sanders, 2013, 2012; Lewis, Chambefort, & Rae, 2012).

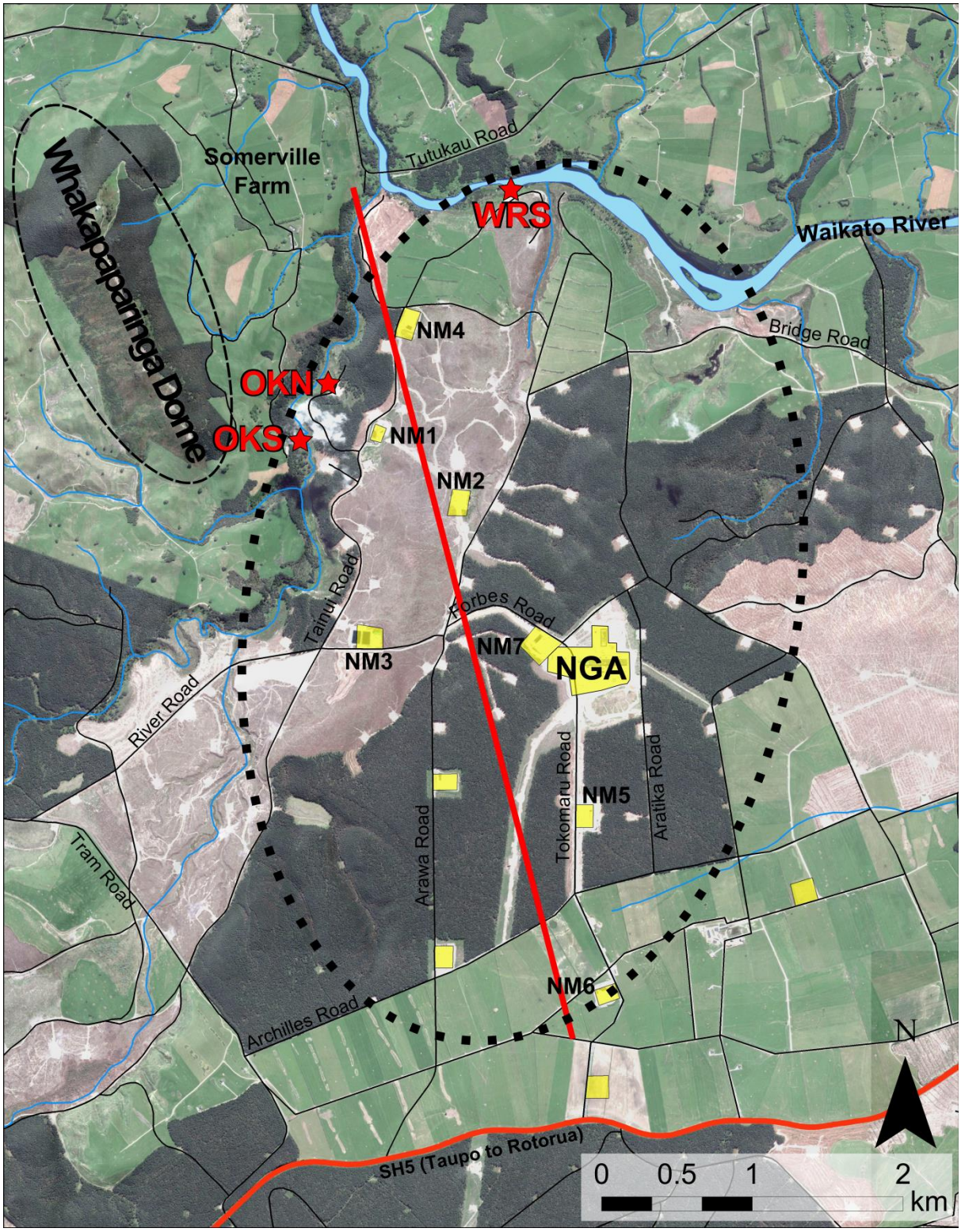

Figure 2.7: Geography of the Ngatamariki Area, showing the subsurface geothermal 'boundary' (black dashed line), geothermal features (red stars), well pads (yellow polygons), major well-heads (bold text next to well pads), geothermal power plant (yellow polygon labelled NGA), major roads, and important land marks. For GIS data sources see section 0 'GIS Data Sources'.

2.5.1 Geology of the Ngatamariki Area

The majority of the surficial geology at Ngatamariki is rhyolite or rhyolitic eruptive products (Figure 2.8). These can be divided into seven groups/formations, originally mapped by Grindley (1960) and Lloyd (1972) and described by Brotheridge (1995). These were then updated by Urzúa-Monsalve (2008) and to a lesser degree O'Brien (2010).

- **Hydrothermal eruption breccias**: These are most noticeable at the Orakonui South main pool, which was the location of the 1948 and 2005 Ngatamariki hydrothermal eruptions. In the 2005 event, mud and ash was erupted in a 70-100m radius, up to 2m thick. The eruption breccias consist of fresh-hydrothermally altered tuffs, pumices, and lithics, and sit on top of Taupo pumice alluvium (Brotheridge, 1995; O'Brien, 2010).
- **Taupo pumice alluvium**: is attributed to the 186AD Taupo eruption and outcrops in the streams and valleys, and most likely mantles the entire area (Brotheridge, 1995). Large cliff sections are seen along the Orakonui stream, and a small quarry is located on the Somerville Farm above the Orakonui South main pool, where charcoaled wood pieces typical of this deposit are seen.
- **Hinuera Formation**: (by Healy, 1946) is a sedimentary deposit derived from older volcanic deposits and the Huka Falls group. The formation ranges from bedded gravels to bedded sands and is lithologically very similar to the Taupo pumice alluvium. It covers a large lateral area (Schofield, 1965), although outcrops are mostly restricted to the north-east and north-west of the area (Brotheridge, 1995).
- **Orakonui Formation**: (by Beck and Robertson, 1955) comprises soft ignimbrites and pumice breccias from pyroclastic flows from the Maroa Volcanic Centre, and is the predominant formation making up the upper surficial geology in the Ngatamariki area.
- **Parekauau Andesite**: (by Grindley, 1961) is an andesite dike seen in a road cutting to the north of the study area, near where the Tutukau road (which runs E-W along the north of the Waikato River) crosses the Waikato River, 100m downstream of the Orakonui-Waikato confluence.
- **Huka Falls Formation**: contains a series of tuffaceous sandstones, mudstones, and siltstones of a fluvial or lacustrine facies (Wood, 1986b). They are derived from the sedimentation of local ignimbrites and other volcanics. The Huka Falls formation and the Waiora formation are collectively known as the Huka Group, and act as an aquifer/aquitard (respectively) for the Wairakei Geothermal Field (Brotheridge, 1995; O'Brien, 2010). The predominant outcropping area is to the north and north-west of the Ngatamariki area (Brotheridge, 1995).

- **Haparangi Rhyolite**: are Pleistocene rhyolite flows and domes, named by Grange (1937). The major landform in the Ngatamariki area is a rhyolitic dome to the west of the field, known as the **Whakapapataringa Dome** (680m.a.s.l.) which belongs to the Haparangi Rhyolite group. The dome extends along north-west fractures, parallel to the edge of the Whakamaru caldera boundary, which was based on the alignment of domes in the area, including Whakapapataringa (Urzúa-Monsalve, 2008; Wilson *et al.*, 1995; Wilson, Houghton, & Lloyd, 1986).

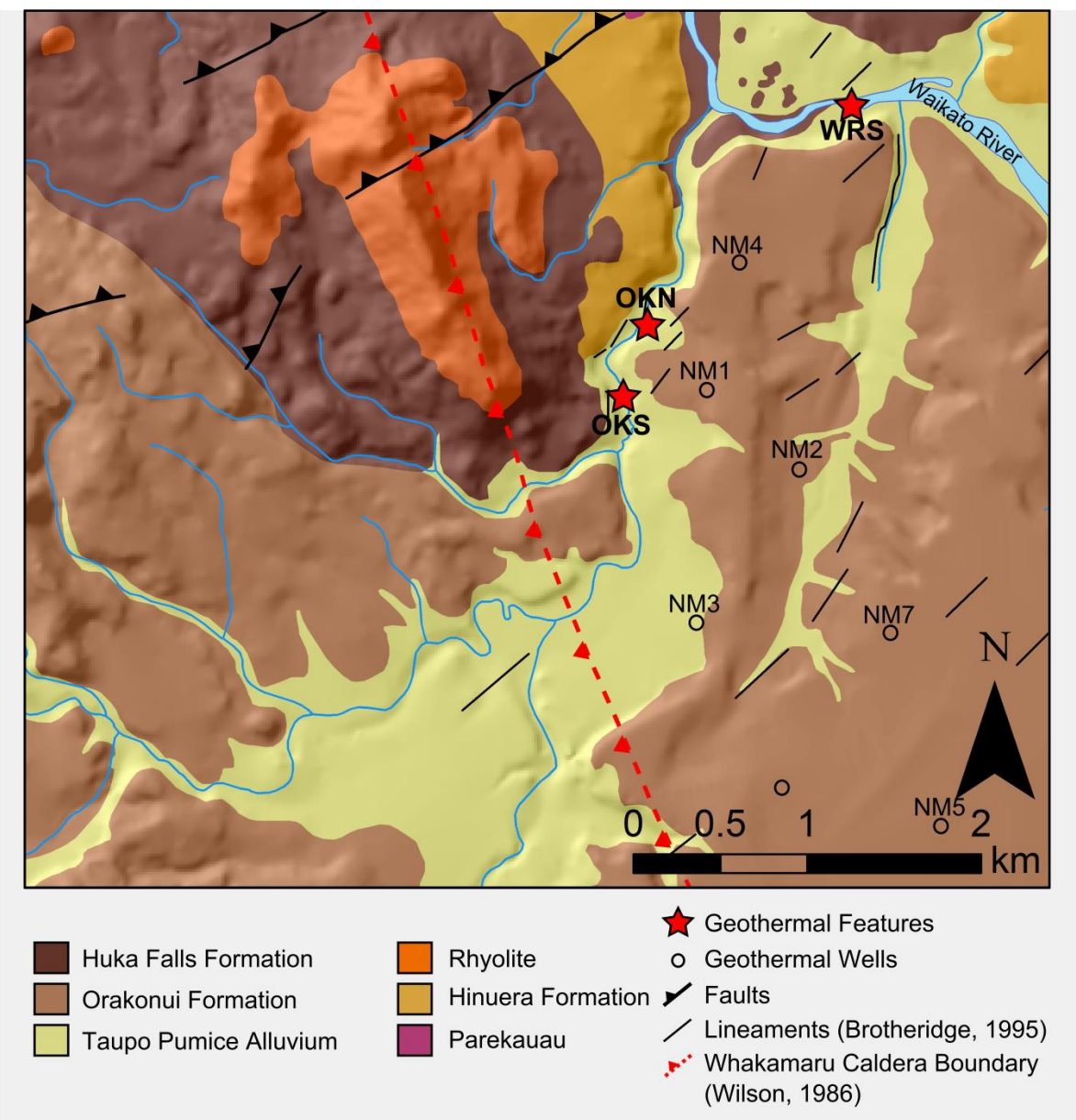

Figure 2.8: The geology of the Orakonui Springs in the Ngatamariki Geothermal Area, modified from Urzúa-Monsalve (2008) and including data from Brotheridge (1995) and Wilson *et al.* (1986).

2.5.2 Geothermal Features of Ngatamariki

Relative to the geothermal 'boundary' generated by MT surveys and proposed by Urzúa-Monsalve (2008), the majority of geothermal expressions are located along the western and northern boundaries. These surface expressions can be divided into three main areas; two of these areas occur on the Orakonui Stream and are known as Orakonui South (OKS) and Orakonui North (OKN), and the third and much smaller area is located on the banks of the Waikato River and is known as the Waikato River springs (WRS; Figure 2.7). A number of low temperature minor springs and seeps along the Mangamingi Stream have also been shown by Bennie (1983), and numerous unmapped springs and seeps were measured by Brotheridge (1995), all of which were very minor (<0.1 l/s), but some of which had high temperatures (up to 76˚C). Bennie also calculated the total heat loss from springs at Ngatamariki, and attributed 80% to the Orakonui Stream springs, while 10% went to both of the Waikato and Mangamingi springs.

Field work was carried out in March 2013, during a period of intense and widespread drought conditions, and it is likely that springs temperatures and conditions may be affected by the level of the reduced water table. Generally only visual observations of the thermal features were recorded, although in some occasions temperatures were taken to compare to those of pre-eruption publications such as Bennie (1983) and Brotheridge (1995), and post-eruption publications such as O'Brien (2010). A study by Brotheridge, Browne, & Hochstein (1995) showed that significant changes had occurred within less than 50 years, a point agreed on upon by observations and measurements made in this study.

For a more in-depth look at the geothermal expressions and characteristics of the Ngatamariki Geothermal Area refer to Brotheridge (1995) for information prior to the 2005 eruption, and O'Brien (2010) for post-eruption.

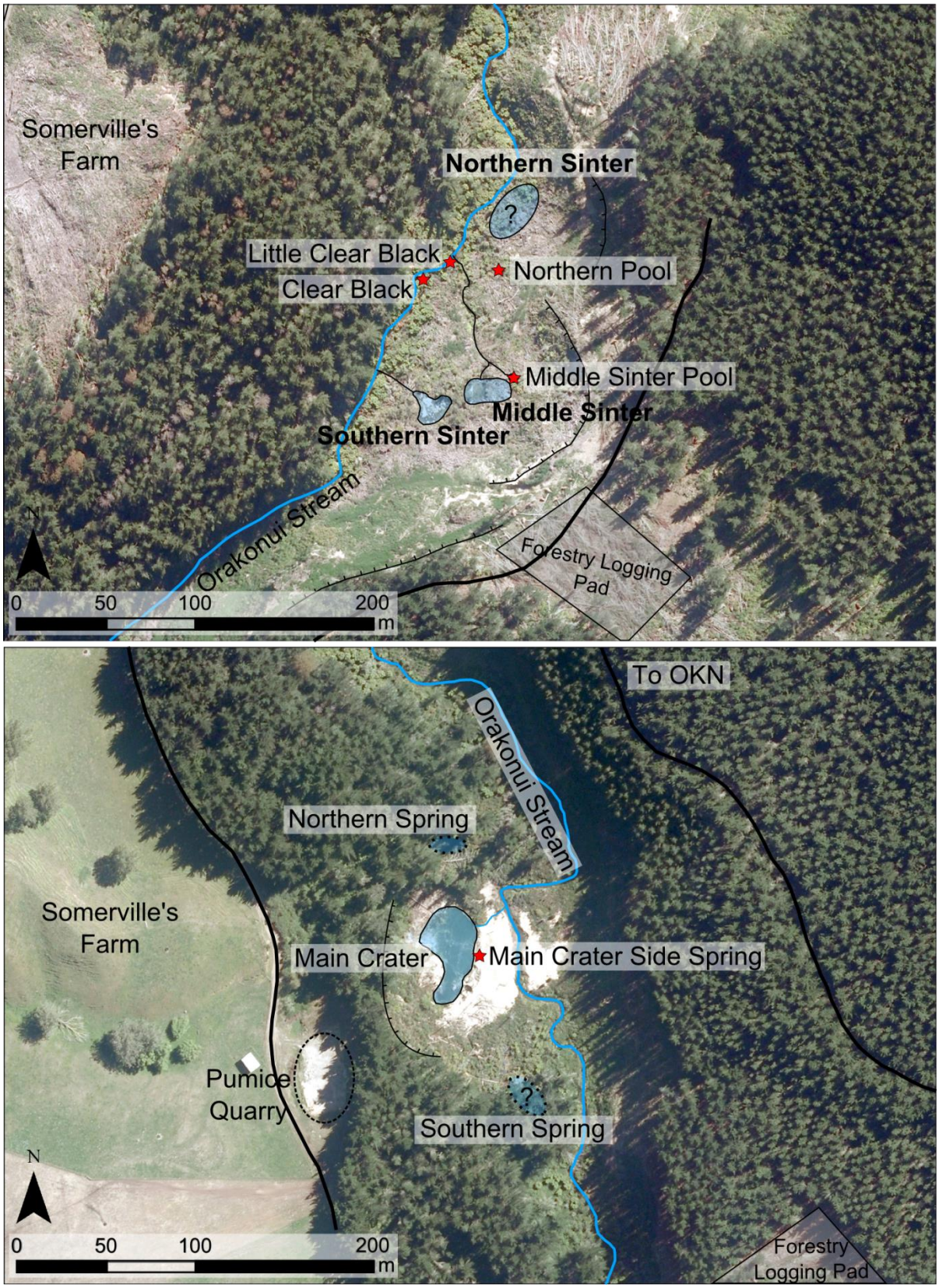

Figure 2.9: Distribution of geothermal features in and around: a) Orakonui North (OKN), and b) Orakonui South (OKS) spring areas. For GIS data sources see section 0 'GIS Data Sources'.

Orakonui South (OKS)

Orakonui South is around 1.8km up-stream from the Waikato-Orakonui confluence and consists of three major pools. There are numerous smaller springs around the largest and most active pool, known as Main Crater (Figure 2.9B).

Main Crater

The Main Crater is the largest (50x30m) and most active geothermal feature in the Ngatamariki Geothermal area (Figure 2.10A). The majority of geothermal activity (upwelling and steaming surface) occurs in the north-west section of the Main Crater pool, although the entire surface appears to bubble. This major upwelling appears to have moved around 5-10m to the north when compared to photographs from O'Brien (2010). The outlet for this pool is a small channel on the north-eastern side of the pool, discharging directly into the Orakonui Stream. A large bank exists in the south-eastern section of the pool, a result of the 2005 eruption that occurred here. The hydrothermal eruption breccia can be seen scattered to the east on the far bank of the Orakonui Stream. When investigated by O'Brien (2010), the pool had a temperature of 54˚C and a pH of 8 (February, 2008). When visited for this study (March, 2013) the temperature was consistent at 56˚C (no other recordings other than temperature were taken).

There are many smaller springs around the banks of this pool, the most notable of which is a roughly circular acid-sulphate pool 1m wide, simply named 'Main Crater Side Spring' by O'Brien (2010).

Other OKS Features

There are two other major pools near Main Crater, one of which is 50m to the south, while the other is 30m to the north. Both are around 10x5m in size (O'Brien, 2010).

The southern feature, named Southern Spring, was not accessible due to time constraints and the large degree of overgrowth. Brotheridge (1995) and O'Brien (2010) found Southern Spring to be the warmest of the OKS features at the time, at 78 and 72.3˚C (respectively) with a pH of 7.5. The springs here follow a curved shape, with the majority of upflow in the eastern end, and cover an area of 12x6m.

The northern pool appears to be currently inactive, as duckweed (*Lemnoideae*) has formed a thick continuous layer across the pool (Figure 2.10B), although this has not always been the case. It is believed to occupy an old explosion crater similar to that of Main Crater. In 1981 when Bennie (1983) surveyed the Ngatamariki area, the pool was a deep blue in colour, with a temperature of 88˚C at the outlet with a discharge rate of 8.5l/s. Prior to the 2005 eruption at Main Crater, Brotheridge (1995) recorded the pool to be 8m deep in places, with a surface temperature of 61˚C

(79 ˚C at deepest point) and deep-blue-green, although the pool was 1.5m below the rim where normal outflow would have occurred. When O'Brien (2010) studied the area in 2008, well after the 2005 hydrothermal eruption to the south, the pool had a temperature of 30˚C and a pH of 7.2, however there was no duckweed at that time and the pool was a deep blue colour. During field work for this study (March 2013), the pool was not a deep blue, nor did it have a surface discharge (water level was 1.5-2m below crater rim).

Orakonui North (OKN)

Activity at Orakonui North is much more subdued than Orakonui South. The area is pronounced in that it has three areas of sinter, with many small springs and seeps (Figure 2.9A). Other than the areas of sinter, the area is heavily overgrown and with a large portion covered by forestry debris that has been tipped down the escarpment. The thermal activity is mostly confined to the eastern side of the Orakonui Stream; the closest features to the river are two springs at river level on the eastern bank. The three sinters are known as Southern Sinter, Middle Sinter, and Northern Sinter.

Southern Sinter

Southern Sinter is the largest of the three, The sinter is exactly the same as shown by (O'Brien, 2010), rock for rock, other than the vegetation is slightly more overgrown (Figure 2.11A). There is a small spring in the centre of the sinter, with a very low discharge (~1l/min estimate) at a temperature of 68.2˚C. The waters from this spring flow west down the sinter fan to the Orakonui Stream. Mid-way between the spring and the Orakonui stream, on the sinter terraces, is another even smaller spring. Even in the drought conditions in which the field work was carried out, the sinter maintained a constant surface water covering. A few meters to the north-west of South Sinter is a large hot spring and mud-pot known as Father and Son. The spring when measured by O'Brien (2010) was found to be 94.4˚C, while the mud-pot was 75.8˚C. The discharge from the Father spring cascades down to the Orakonui Stream following a different path to the South Sinter discharge.

Middle Sinter

Middle Sinter contains numerous small springs and seeps (Figure 2.11B), and on the northern edge contains one of the larger springs of the OKN hidden underneath bushes, named Middle Sinter Pool spring by O'Brien (2010). The temperature of which was measured to be 63˚C, and by O'Brien to be 64˚C. Another spring exists to the north-east of the Middle Sinter known as Devils Mouth Spring. At the time of field work this spring was covered in forestry debris (logs/branches etc.) and was not visible, although and area of thin sinter could be seen originating from within the debris. When measured by O'Brien (2010) the pool into which the spring flowed was larger but shallower than Middle Sinter Spring Pool, at a temperature of 83˚C. The drainage path for the Middle Sinter and

associated springs can be seen in Figure 2.9A running at in north-west direction towards the Orakonui Stream.

Northern Sinter

The Northern Sinter was largely overgrown, even more so than as described by O'Brien (2010). No significant discharge was noted, although a 3x1.5m, a <1m deep pool with a thin floating sinter crust was located to south-east. The Northern Sinter was difficult to map due to the overgrowth, as shown in Figure 2.9A.

Other Springs

Between the points in which the Southern Sinter and the Middle Sinter join the Orakonui Stream there are two springs, known as Clear Black and Little Clear Black (O'Brien, 2010). Clear Black was on the eastern bank, while Little Clear Black was not located at all. Clear black was located at stream-level at the base of a small bank (Figure 2.11D). It was the warmest of all springs measured, at 96˚C, similar to measurements by O'Brien of 94˚C. The seeping aquifer to the south of Clear Black as presented by O'Brien was also not located.

A large pool was located roughly halfway between Middle Sinter and Northern Sinter (Figure 2.11C). The pool was 3x1.5m with a thick layer of floating sinter. The pool was not mentioned by O'Brien but was likely shown by Bennie (1983).

Waikato River Springs

Investigations by Bennie (1983) indicated that there were numerous springs occurring on the banks of the Waikato river near the end of Tainui road, around 800m upstream of the Tutukau bridge (Figure 2.7). The highest temperature recorded from these springs was 76˚C, while the largest spring here had built up a sinter platform roughly 200m^2 in size, discharging at 4l/s and with a temperature of 74˚C. Bennie's calculations determined ~10% of the total heat loss at Ngatamariki was from these springs. Construction of the Ohakuri dam and the subsequent filling of Lake Ohakuri in 1961 flooded the majority of these springs, and those remaining are regularly flooded by changes in river level. Observations by Brotheridge (1995) agreed with observations from Bennie (1983) of a 200m^2 sinter area, with a spring discharging 3l/s at 74˚C. However, during fieldwork of 2009, O'Brien (2010) located numerous seeps of between 60-80˚C, but failed to mention a large sinter area, which has potentially overgrown. O'Brien also located a small spring on the Orakonui Stream around 50m upstream of the confluence, although this is not noted in any other literature.

Figure 2.10: The main features of the OKS springs area. A) Main Crater, showing the area of greatest upwelling (dashed circle) and the outflow (red arrow). Person for scale indicated by yellow arrow. View is roughly to the north. B) Northern Spring, showing the lack of blue colour as it is covered by a mat of duckweed. View is roughly to the south-west.

Figure 2.11: The main features of the OKN springs area. A) Southern Sinter, which is identical almost rock to rock to that of O'Brien (2010). View to the south. B) Middle Sinter. View to the north. C) (bottom left) pool in the vicinity of Northern Sinter. View to the east. D) (bottom right) Clear Black pool. View to the east.

2.5.3 Hydrological Model

The Ngatamariki geothermal resource consists of a high temperature (260-300˚C) permeable reservoir surrounded by a low resistivity, low permeability smectite cap. Along with another smectite-rich layer, these two aquicludes separate three permeable zones (Figure 2.12), from Boseley *et al.* (2010):

1. A 15˚C meteoric aquifer,
2. A 160˚C intermediate aquifer near wells NM1-4, found in all wells at roughly sea-level.
3. A deep 260-300˚C geothermal reservoir that extends 3km to the south of NM1-4.

Geochemistry of the springs along the Orakonui Stream show that the fluids being expelled here are not directly from the reservoir, but from the 160˚C intermediate aquifer (Boseley *et al.*, 2010; O'Brien, 2010). Chemistry and temperature of the intermediate aquifer show that there is limited permeability between this and the reservoir.

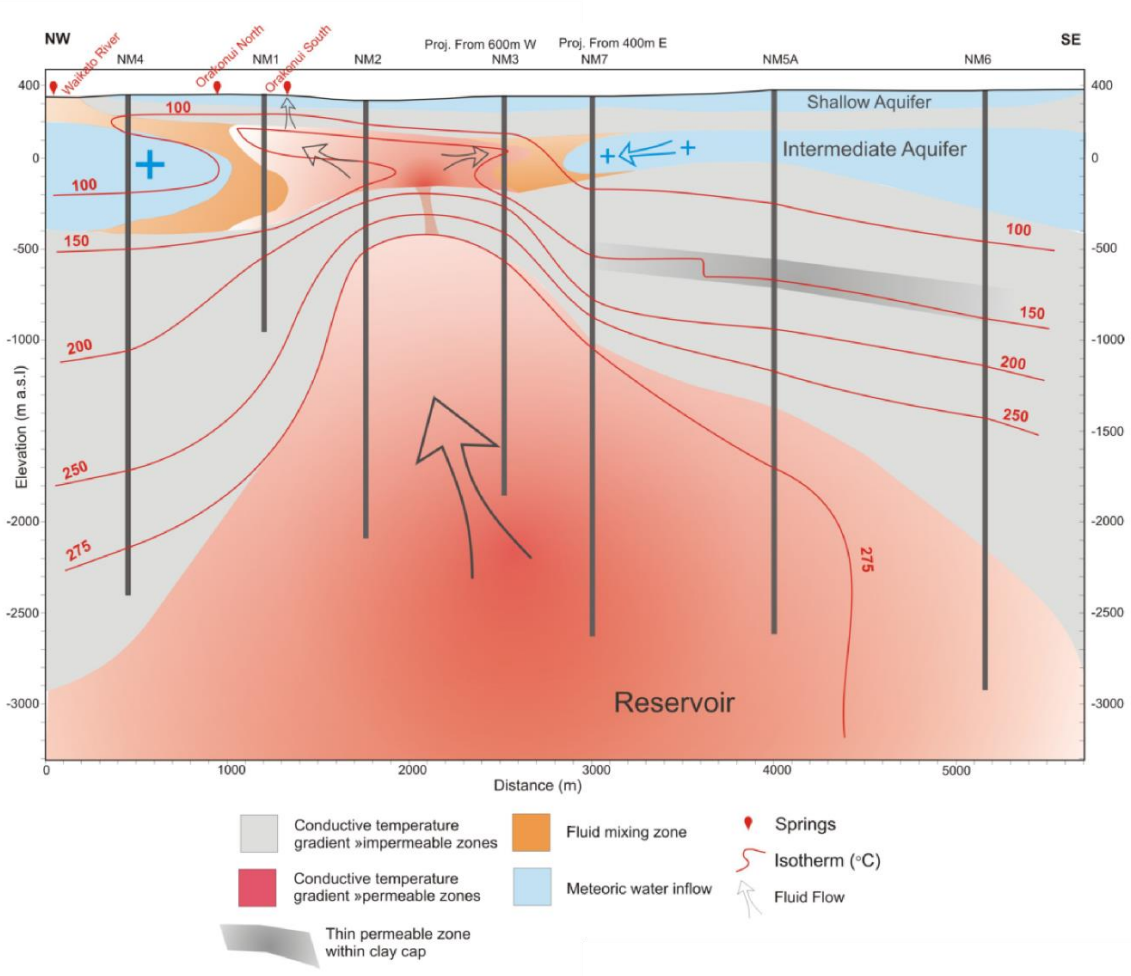

Figure 2.12: Hydrological zonation of the Ngatamariki Geothermal Reservoir, from Boseley *et al.* (2010). Red lines indicate isotherms, while grey areas indicate impermeable clay caps. The Orakonui Stream springs and Waikato River springs are in the NW of the transect (left). For well locations and transect orientation/location see Figure 2.7.

3 Lichen Isotopes Spatially

This chapter outlines the methodology used for sample collection and analysis, including attempts at method optimization, followed by the results from the analysis of isotopes in lichen along the three transects and at the Ngatamariki Geothermal Area.

3.1 Methods

3.1.1 Lichen Selection

For this study to be viable, a lichen genus, or multiple lichen genera was needed that satisfied the desirable attributes of bioaccumulators outlined by Conti & Cecchetti (2001) in the previous chapter. A pilot study examining the South Island Transect area and the Ngatamariki area revealed three suitable genera – *Usnea*, *Ramalina*, and *Xanthoria* – as described in a later section (see Section: 3.2.1 'Pilot Study'). These genera exhibited favourable features, including: wide distribution, generally abundant, and easily identifiable.

3.1.2 Site Selection

Site selection was specific to the study area, with the size of the study area controlling the number of possible sites, and the features within the study area (such as geothermal pools) controlling the distribution. For the three transects (see Section: 3.2 'Transects'), sites were evenly distributed, with a spacing of ~5km (SIT and REW) or ~15km (TNS). The focus at the Ngatamariki Geothermal area was the Orakonui Stream springs (see Section: 3.3 'Ngatamariki'), therefore sites are centred on these, along the perimeters of circles with increasing radii (Figure 3.1). This allowed a higher site density near the springs with decreasing density as distance from the springs increases. These Ngatamariki sites were further relocated up to 100m on a case-by-case basis if they were placed in a location unlikely to support a suitable lichen population (ie. middle of pasture area).

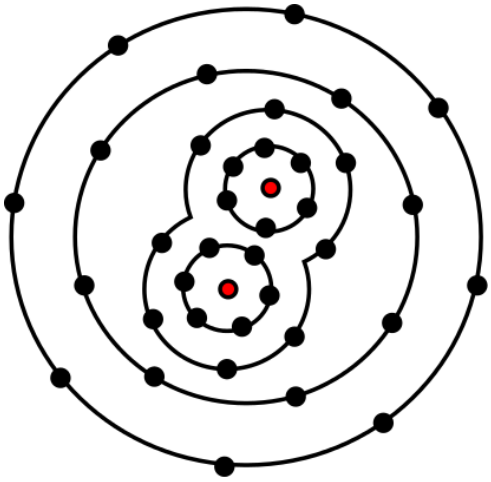

Figure 3.1: An example of the sampling plan used at Ngatamariki. The red circles are the Orakonui Springs, the focus of sampling in this area. Black dots are sites, evenly distributed along the perimeters of circles with increasing

3.1.3 Sample Collection

At sample collection sites, potential samples were first checked to ensure as minimal thallus damage as possible and larger extraneous debris was removed, before samples were placed into small labelled snap-lock bags in chilled polystyrene containers for storage.

Where possible, samples were collected on as similar substrate to each other as possible, as Beck & Mayr (2012) showed that differing substrates can influence not only the nitrogen and carbon content, but also the isotopic compositions. Thus, samples were collected from the most frequently inhabited substrate: organic substrates such as tree trunks and branches. On a few occasions for the South Island Transect (SIT) and the North Island Transects (NIT), and on rare occasions for the Ngatamariki (NGA) samples, collection was from fence posts, but never from rock surfaces.

Some studies have found that a variety of local factors, which were not controllable in this study, may affect elemental concentrations and isotopic composition. This included factors such as slope dip, slope aspect, sample orientation, exposure, and collection height (Batts *et al.*, 2004; Hietz *et al.*, 2002; Wania *et al.*, 2002). Samples were also not always able to be collected as far from roads as desired, due to property access issues. The impact of the distance to roadways on the measured parameters is discussed in the next chapter (see Section: 4.3 'Distance to Road').

3.1.4 Sample Storage

During sample collection, each sample was stored in separate snap-lock bags, within chilled polystyrene boxes. Upon return to the lab, these polystyrene boxes were moved into refrigerators (4˚C) to maintain reduced metabolic rates. The samples were not removed from the bags except during the sample preparation stage, after which any remaining sample material was returned to the refrigerator.

3.1.5 Sample Preparation

After refrigerated storage of between 1-5 months, samples were inspected for any damage, such as further fungal growth or decay during storage, which, along with any remaining extraneous debris or host material included during sample collection was removed from the sample. For the South Island transect, the majority of lichen samples were unwashed, with only a small portion (n=25) washed for later comparison (see Section: 'Effect of Washing', page 40). Upon inspecting the results from this transect, it was determined that washing does not significantly alter the measured elemental concentrations or isotopic compositions (α=0.05, paired t-test, H_o: $\mu_{(washed\ sample)} = \mu_{(unwashed\ Sample)}$), contrary to that suggested by Gombert *et al.* (2003). However, samples from the North Island were washed to aid in the removal of extraneous debris and to more closely follow accepted methodology in the literature (Batts *et al.*, 2004; Cuna *et al.*, 2007).

All lichen samples were dried at 60˚C for ≥24 hours to remove excess water. While drying, weights rapidly decreased in the first 3-4 hours, before reaching a constant weight at >8 hours. This drying

regime reduced the weight of lichen samples by between 10-15%, which agrees with weight reductions from water loss during drying as seen in the literature (Lange *et al.*, 1993).

Initial results showed a heterogeneous distribution of isotopic composition and elemental concentrations (see Section: 'Same-sample Variability', page 57), and in an effort to reduce the impact on further results, samples were homogenised by crushing samples immersed in liquid nitrogen in a mortar and pestle, which follows the literature more closely (Di Lella *et al.*, 2003; Riera, 2005; Skinner *et al.*, 2006, and others). The mortar and pestle were cleaned between each sample using KimWipes and distilled water to ensure minimal contamination between samples.

During all stages of preparation, sterile nitrile gloves were used to avoid contamination of the samples through skin contact.

Effect of Washing

It is important to understand the effects that various preparation steps have on the determined isotopic δ-values. Washing lichen samples prior to analysis may remove external nitrogen and carbon sources that are yet to be assimilated, thus influencing the measured value in an unknown way. For example, Gombert *et al.* (2003) showed washed samples to have significantly lower concentrations of nitrogen than their unwashed equivalents, hypothesising this to be result of the loss of fine particles adsorbed to the thallus surface and gaseous compounds such as HNO_3. Bettinelli *et al.* (1996) similarly found that washing can unpredictably alter the elemental composition of lichen. The undersides of the samples collected for this study show extensive amounts of pollen, unknown minerals, soil particles, and insects with associated debris. A typical unwashed sample is shown in Figure 3.2.

To test this hypothesis, duplicate samples were analysed, with one sample being thoroughly rinsed with distilled water, while the other was untreated to determine if there was a significant difference in isotopic compositions or elemental concentrations (H_o: $\mu_{(\text{washed sample})} = \mu_{(\text{unwashed Sample})}$). The results, in Table 3.1, show that there was no significant difference in washed samples compared to unwashed samples (paired t-test, $\alpha = 0.005$) in $\delta^{13}C$, $\delta^{15}N$, carbon or nitrogen content.

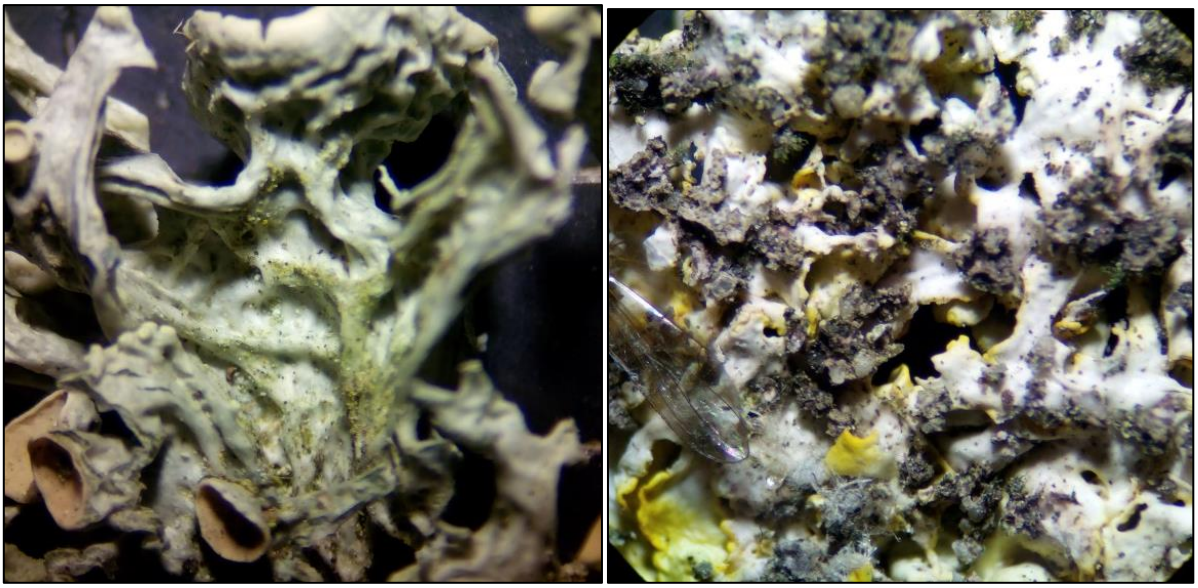

Figure 3.2: The underside of an unwashed A) *Ramalina* thallus showing large amounts of pollen, and b) *Xanthoria* thallus, showing the degree of attached detritus. Note the insect wing to the centre-left. The wrinkled nature in both samples is due to desiccation. Field of view is approximately 10mm in both images.

Table 3.1: T-test matrix comparing the effect of washing or not washing on measured parameters (paired t-test, α = 0.005, H_o: $\mu_{(washed\ Sample)} = \mu_{(unwashed\ Sample)}$). The lack of significance indicates no significant difference between washed and unwashed samples.

	$\delta^{13}C$	$\delta^{15}N$	N%	C%	C:N
p value	0.901	0.276	0.442	0.125	0.851
df	23	24	22	22	22

Time in Storage

Sample analysis was conducted over an extended period due to limited analytical capacity in the UC Stable Isotope Laboratory. Samples that were run in the first analysis (March 2013) were reanalysed in further analyses (August 2013) to determine if storage has a detrimental impact on isotope or elemental concentrations within the lichen sample (H_o: $\mu_{(Fresh\ Sample)} = \mu_{(Old\ Sample)}$). The results, in Table 3.2, summarises these tests (paired t-test, α = 0.005), and shows that there was no significant difference between the values of samples run in March (fresh) to the same samples reanalysed in August (old).

3.1.6 Analysis

For analysis, 400-3000µg of uncrushed (SIT) or 1000-3000µg of homogenised (NIT and NGA) lichen samples were placed into silver/tin capsules, before the capsules were placed into 96-well NUNC trays. Following a short second drying period in the ovens (≥24 hours @ 60˚C), the capsules were folded shut using tweezers to prevent and further contact with the atmosphere.

Table 3.2: T-test matrix comparing the effect of storage time on measured parameters (paired t-test, $\alpha = 0.005$, H_o: $\mu_{(Fresh\ Sample)} = \mu_{(Old\ Sample)}$). The high p-values indicate no significant difference in isotope of elemental concentrations in fresh samples and those being refrigerated for five months

	$\delta^{13}C$	$\delta^{15}N$	N%	C%
P Value	0.979	0.521	0.792	0.255
df (n/2 -1)	34	34	30	30

All stable isotopic analyses were performed in the University of Canterbury Stable Isotope Analytical Facility housed in the Department of Geological Sciences. Stable carbon and nitrogen isotope ratios were determined using a Costech ECS 4010 elemental analyser connected under continuous flow conditions to a ThermoFinnigan Delta V Plus Isotope Ratio Mass Spectrometer. Ultra-high purity helium (99.9999%) served as the carrier gas with a flow rate of ~100 ml/minute at the ECS outlet. The ECS combustion reactor was set at 900°C and the reduction reactor at 650°C while the GC column was operated at 40°C. Nitrogen to Carbon Dioxide peak jump calibrations, standard on-off zero-enrichment tests, and linearity tests were performed prior to the start of each analytical sequence . All data reported in this thesis were normalised to the Air (for N_2) and V-PDB (for CO_2) scales based on replicate analysis of certified reference materials IAEA-N-1, IAEA-N-2, IAEA-CH-3, NBS22 using a 2-point (i.e. stretch-and-shift) normalisation. Certified reference materials were analysed at both the start and end of every analytical sequence. Internal lab standards of acetanilide and collagen, as well as additional certified reference materials including USGS24, NBS19, NBS18 were used for quality control purposes. Internal precision of all analyses was better than 0.05‰ for both $\delta^{15}N$ and $\delta^{13}C$ based on zero-enrichment tests, and external precision was better than 0.2‰ for both $\delta^{15}N$ and $\delta^{13}C$ based on replicate analysis of the reference materials.

3.1.7 Methodology Summary

The methodology is summarised as follows:

- Three **lichen genera were chosen based on favourable attributes**: wide distribution, generally abundant, and easily identifiable.
- Lichen **samples were collected, placed into individual snap-lock bags, and chilled** until the next stage of preparation.
- While there is no statistical difference between isotopic compositions and elemental concentrations of samples before or after washing (α=0.05, paired t-test), **samples were washed** to aid in the removal of extraneous debris, and for the methodology to more closely match that in the literature.
- **Samples were oven dried** for ≥24 hours at 60˚C.
- Due to the heterogeneous distribution of isotopic compositions and elemental concentrations within the lichen thallus, **samples were homogenised** in a mortar and pestle while being submerged in liquid nitrogen.
- Homogenised **samples were placed into silver/tin capsules** (of known weight) and weighed to determine sample weight.
- A **second round of oven drying** (≥24 hours at 60˚C) removed any remaining moisture.
- The silver/tin **capsules were folded shut** to prevent interaction between the sample and the atmosphere.
- The **capsules were then loaded into the IRMS-EA** in the Stable Isotope Laboratory at the University of Canterbury **for analysis.**

3.2 Transects

In order to be able to determine whether carbon and nitrogen isotopes in lichen are suitable as a geothermal exploration technique, we need to examine the expected values outside of the geothermal area. Therefore, three transects, shown in Figure 3.3, were considered:

- A transect well outside of the geothermally active Taupo Volcanic Zone (TVZ). This transect is known as the **South Island Transect (SIT)** and runs east-west through the centre of the South Island.
- Two transects outside of the Ngatamariki Geothermal Area, but still within the TVZ. The **Rotorua East-West Transect** (REW) runs across the strike of the TVZ, while the **Taupo North-South Transect** (TNS) runs parallel to the structural axis of the TVZ.

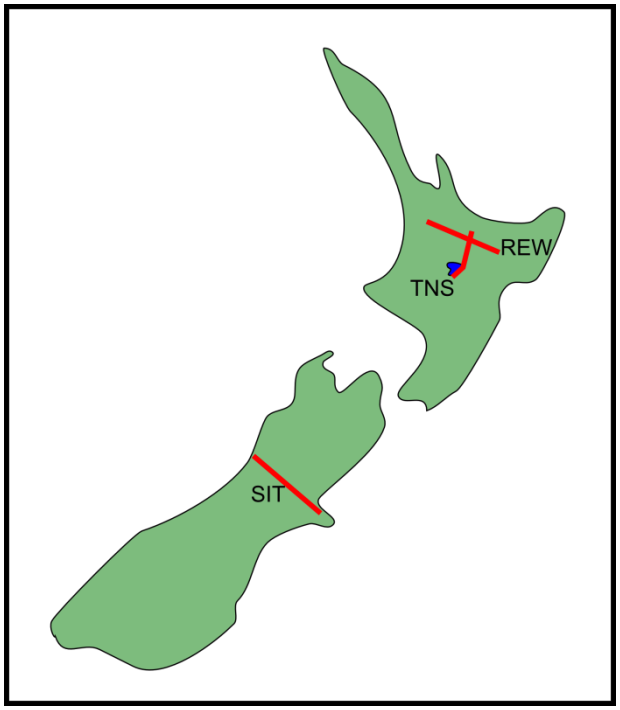

Figure 3.3: Simplified map of the location of the three transect in New Zealand. SIT = South Island Transect, TNS = Taupo North-South, REW = Rotorua East-West.

The South Island Transect was also used as a pilot study to test the biogeographical distribution of potentially useful genera.

3.2.1 Pilot Study

The pilot study involved locating and identifying the types and abundance of various lichen genera across the South Island to determine suitable species to use for the majority of this study. Three species were identified that were widely distributed, abundant and were easily identifiable, as discussed below.

Usnea

Of all of the lichen species identified across the either the South Island or North Island, none were as abundant or as widely distributed as *Usnea*. This genus is easily recognised, even from a distance, with the thalli of *Usnea* at some sites in the eastern REW transect reaching half a meter in length. It is often referred to as “Old Man’s Beard” or “Beard Moss”; however this name may refer to multiple types of moss and plants, a completely separate biological kingdom, as well as four different genera of lichen. While it is easy to identify to genus level, it is regarded as one of the hardest genera to

classify to species level (Martin & Child, 1972). The number of species is estimated to be between 350-600, however only 86 species appear on the PLANTS database (Kirk, Cannon, David, & Stalpers, 2008; Thell *et al.*, 2012; Truong, Divakar, Yahr, Crespo, & Clerc, 2013; United States Department of Agriculture, 2013; Wirtz, Printzen, Sancho, & Lumbsch, 2006), with between 28-50 identified in New Zealand alone (de Lange *et al.*, 2012; Martin & Child, 1972). *Usnea* is part of a monophyletic lineage belonging to the family *Parmeliaceae*, of which 10% of all lichen belong to (Hibbett *et al.*, 2007; Thell *et al.*, 2012; Truong *et al.*, 2013)

Usnea Identification

Usnea is typified by an erect or pendulous fruticose thallus, with cylindrical branches that extend from a cartilaginous stalk (Figure 3.4A). They may hold sexual (apothecia) or vegetative (soralia) reproductive structures (Truong *et al.*, 2013), however these were rarely observed in the samples collected in this study. The stalk and branches of this genus are composed of three sections: a central cartilaginous strand, a middle area of loose to compact hyphae and an outer cortical layer, as shown in Figure 3.4B. This final layer contains usnic acid, which gives *Usnea* its distinctive yellow-green colour (Truong *et al.*, 2013).

Usnea are most commonly seen on organic substrates such as bark (corticolous), dead wood (lignicolous), wooden posts/fences, although there few species of *Usnea* are known to occupy rocky substrates (saxicolous).

Ramalina

Ramalina is a common and easily identifiable genus, and as such it satisfies the criteria required for this study. *Ramalina* is similar to *Usnea*, sharing a close phyletic relationship, divided at the order level “Lecanorales”. *Ramalina* is different in that it has flat stems, with apothecia positioned across the upper side of these stems (Figure 3.5A), rather than the cylindrical cartilaginous stems and terminal apothecia of *Usnea*.

Ramalina Identification

As mentioned, *Ramalina* differ to *Usnea* in that they have flat leaves, often lanceolate shaped, compared to the cylindrical structure of *Usnea* branches (Figure 3.5A). The internal structure of *Ramalina* is similar also, having an outer cortex surrounding the medullary layer of hyphae which support the algal partner. The centre of the lichen contains woven hyphae that support the structure of the lichen (Figure 3.5B); there is no central cartilaginous as seen in *Usnea* (Figure 3.4B). The apothecia of *Ramalina* are generally more bulbous than the cup-like apothecium typical in *Xanthoria*.

The predominant *Ramalina* species used in this study is identified as most likely being the species *R. ecklonii*, which is distinctive in that it is non-sorediate, with large, flat, lanceolate lobes, and numerous surficial apothecia (Figure 3.5A). Colour ranges from a dull grey to grey-green when dry to a darker green when wet.

Xanthoria

Xanthoria, like *Ramalina* and *Usnea* is an easily identifiable genus, having a dull yellow colour when dry ranging up to bright sulphur yellow when hydrated (Figure 3.6A). It has a foliose habit, setting it apart from the two other genera used in this study. This also presents contamination issues, as it is common for dirt and dust to become trapped in the spaces beneath the thallus, as well as being used as shelter for spiders and other small insects. While *Usnea* and *Ramalina* are both part of the Lecanorales order, *Xanthoria* is part of Teloschistales.

Identification

The distinctive yellow sulphur colour along with the prominent darker yellow/orange apothecia on the upper surface are the key distinctive features when identifying this genus, however the colour may range from shades of yellow and orange up to dull greens. The structure of *Xanthoria* is typical of foliose lichens, exhibiting a medulla of loose hyphal strands which host the algal partner, encompassed between an upper and lower cortex (Figure 3.6B). The lower cortex exhibits rhizinae that attach the thallus to the substrate and is white.

It is predominantly discovered near the coast on rocks (saxicolous) and walls, but is also commonly found inland on rock, walls, and bark (corticolous).

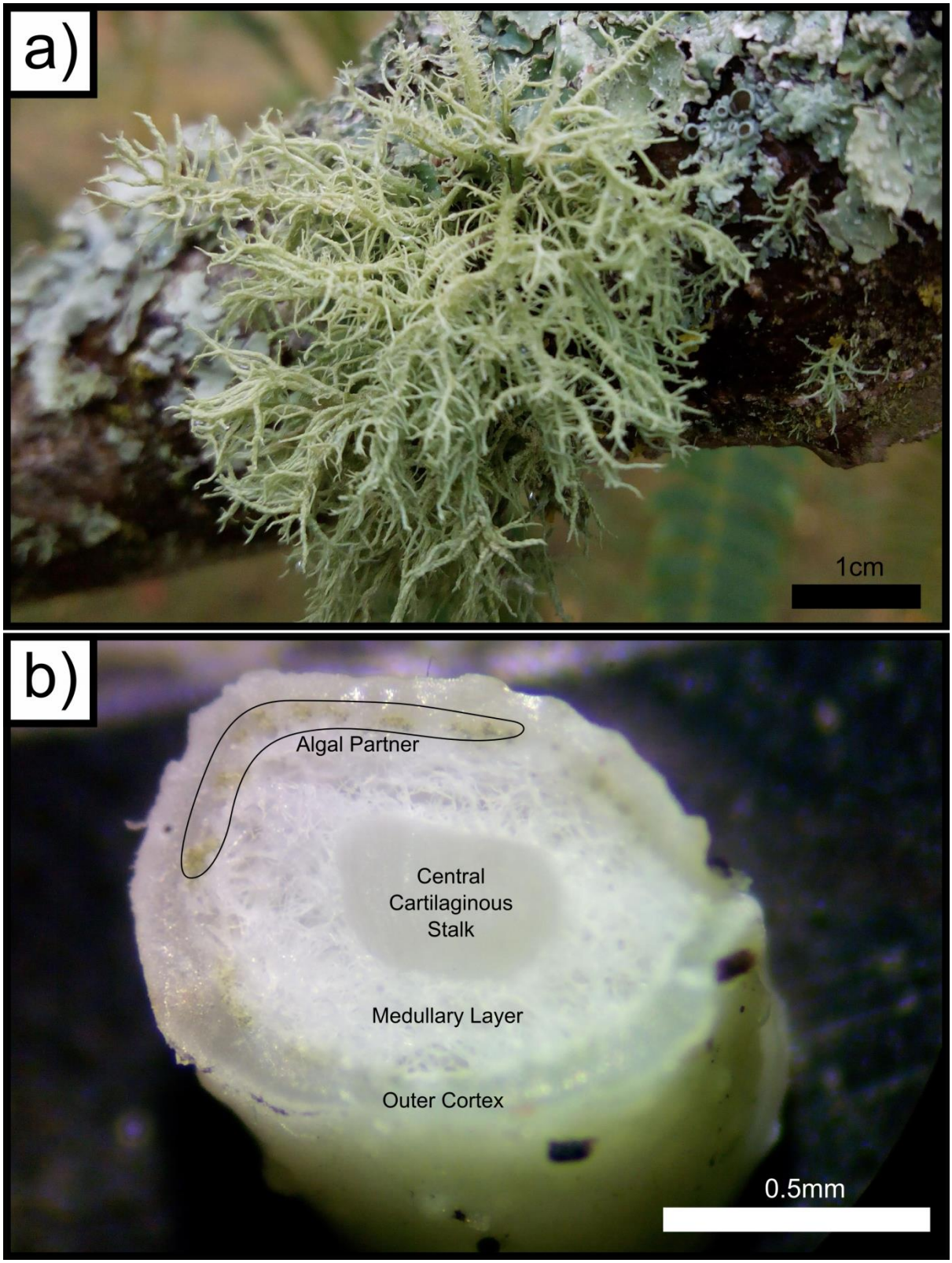

Figure 3.4: Examples of the genera *Usnea*. A) *Usnea* on a branch in Motueka, April 2014. Note the thin, roughly cylindrical branches that split at regular intervals, and the lack of visible reproductive structures. Other species of *Usnea* may have fewer branches. B) *Usnea* under the microscope, showing the major sections of the cylindrical branches.

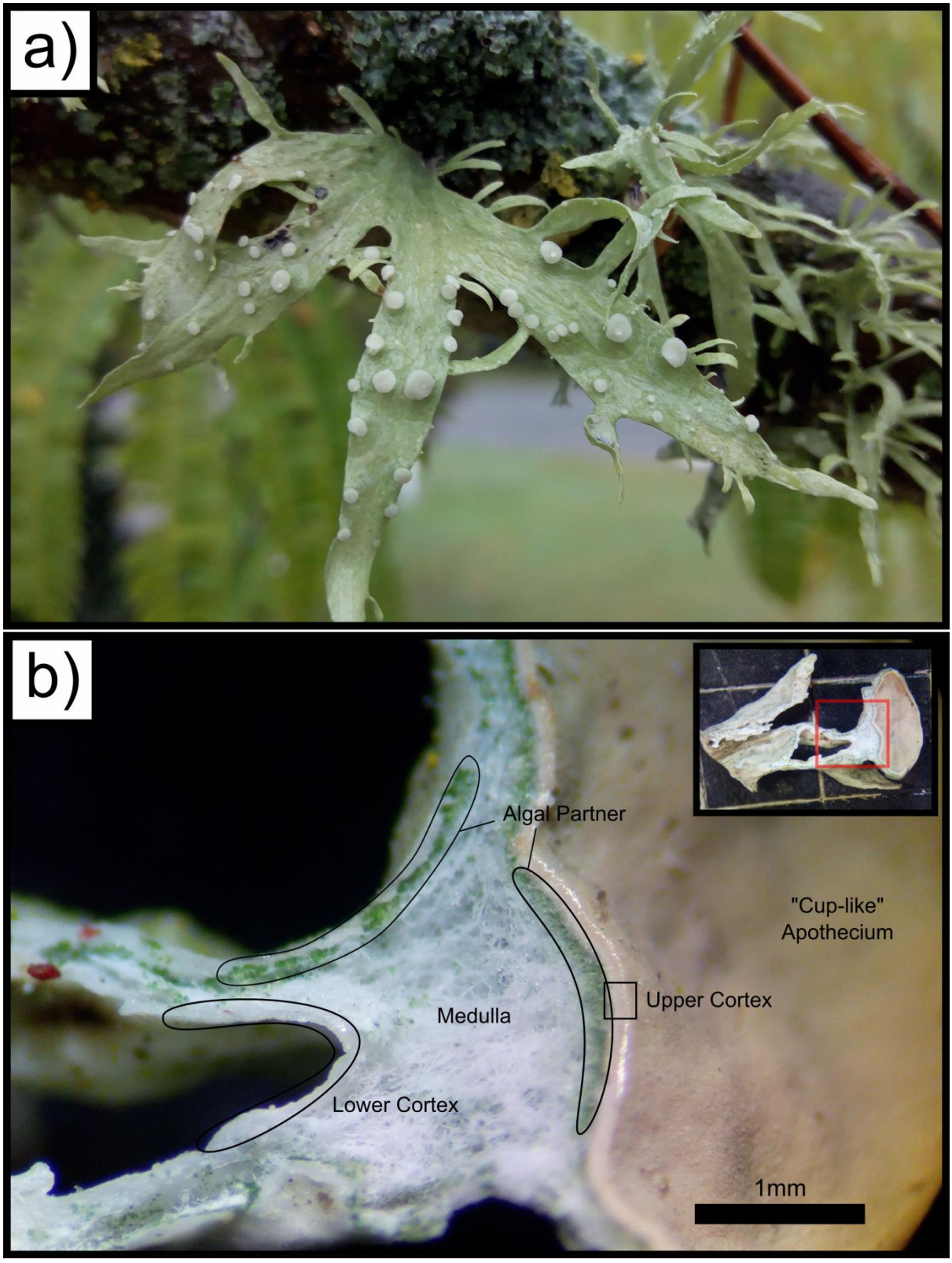

Figure 3.5: Examples of the genera *Ramalina*. A) *Ramalina sp.* on a branch in Motueka, April 2014. Note the broad, flat 'branches' with many bulbous apotheica sticking up from the upper surfaces. Sample roughly 4cm wide. The blackened area in the top left of the thallus is damage. B) *Ramalina* under the microscope, showing the major sections of the thallus. The image centres on the surface of a halved apothecium.

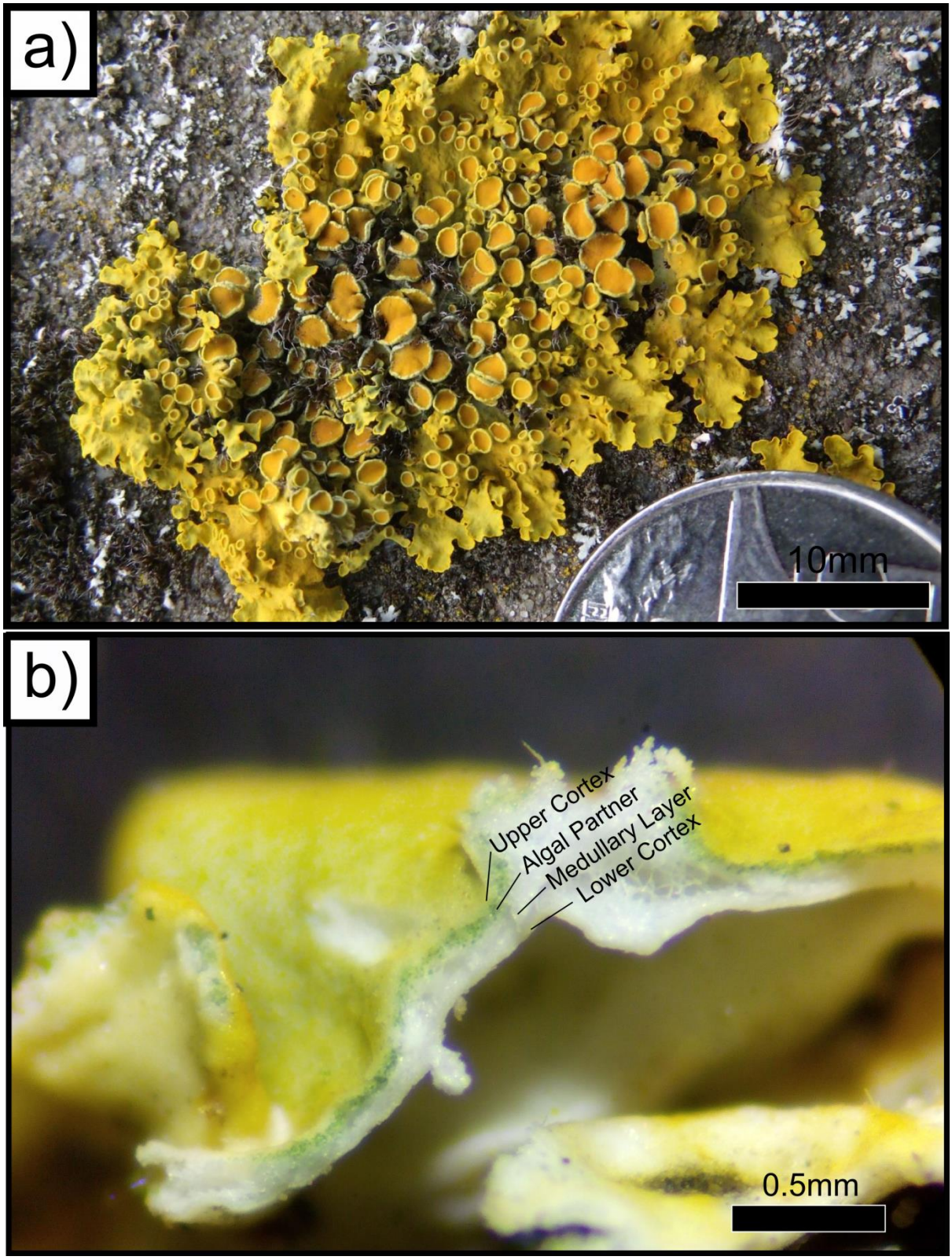

Figure 3.6: Examples of the genera *Xanthoria*. A) *Xanthoria*, South Island (exact location unknown), December 2012. The centre of the thallus shows a high density of apothecia; both mature and dead, while new apothecia can be seen forming near the margins. B) *Xanthoria* thallus under a microscope, showing the major sections. As the thallus is desiccated, the thickness is severely reduced.

3.2.2 South Island Transect (SIT)

A transect of the South Island is used to determine 'background' isotope ratios well outside of any geothermally active area. The SIT also allows the analysis of multiple isotope controls that may not be able to test in the North Island, such as elevation and the distance of sample sites from major roadways (discussed in the next chapter).

SIT Sites

A total of 37 sites were used over a distance of 160km with an average euclidian distance of 4.4km between sites (Figure 3.8). The transect predominantly follows State Highway 73, bar a small segment near Christchurch where it diverts but still follows parallel along Old West Coast Road with similar traffic densities (sites 007-010). Figure 3.8, which shows significant landmarks through which the transect follows (bold capitalised text), also traverses a range of land types, geological types, and climates. It reaches a maximum elevation of 947m as it passes through Porters Pass and 918m as it passes through Arthur's Pass, and starts and ends at roughly sea level (Figure 3.7).

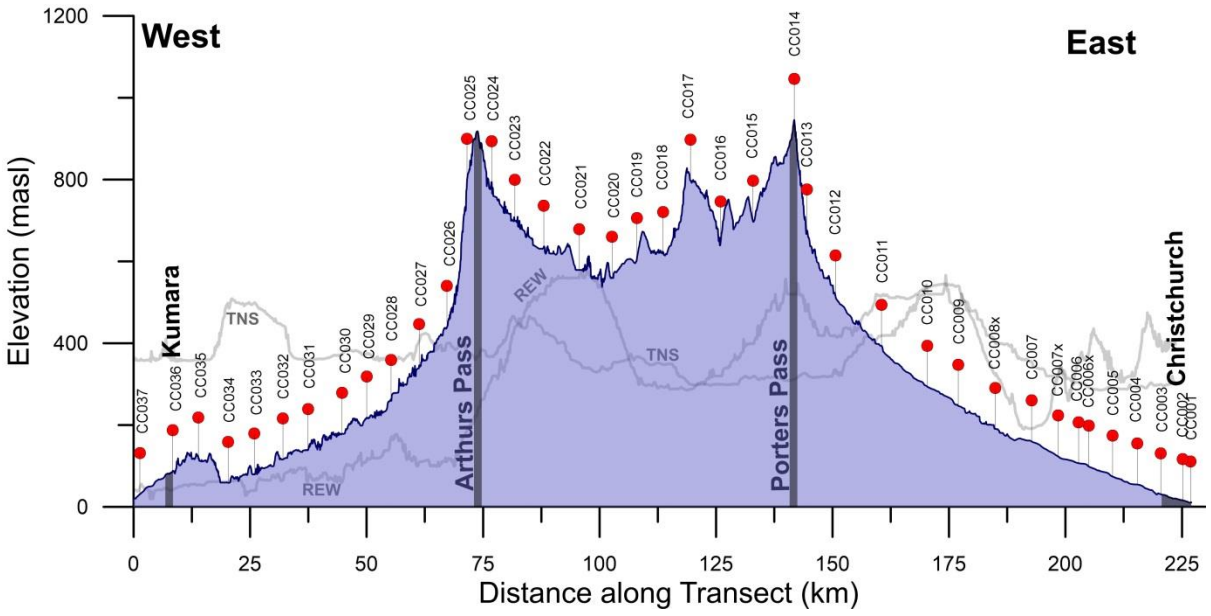

Figure 3.7: Elevation Profile of the SIT Transect. Red circles refer to sample sites as labelled, while blue-grey shaded areas show areas of significant landmarks. Pale grey lines in the background show the TNS and REW transect profiles in comparison, as labelled, with distances normalised to the length of the SIT. The length of the x axis is longer than the Euclidean distance as the elevation profile follows the road. For GIS data sources see section 0 'GIS Data Sources'.

Sample Collection

Table 3.3 summarises the number of samples that were collected and analysed at sites on the South Island transect. Generally five samples of *Usnea* were collected at each site, although some of the sites warranted bigger collections to allow for testing of variance between genera, and variance within one sample site. Collections of the other two genera, *Ramalina* and *Xanthoria*, were dependant on availability.

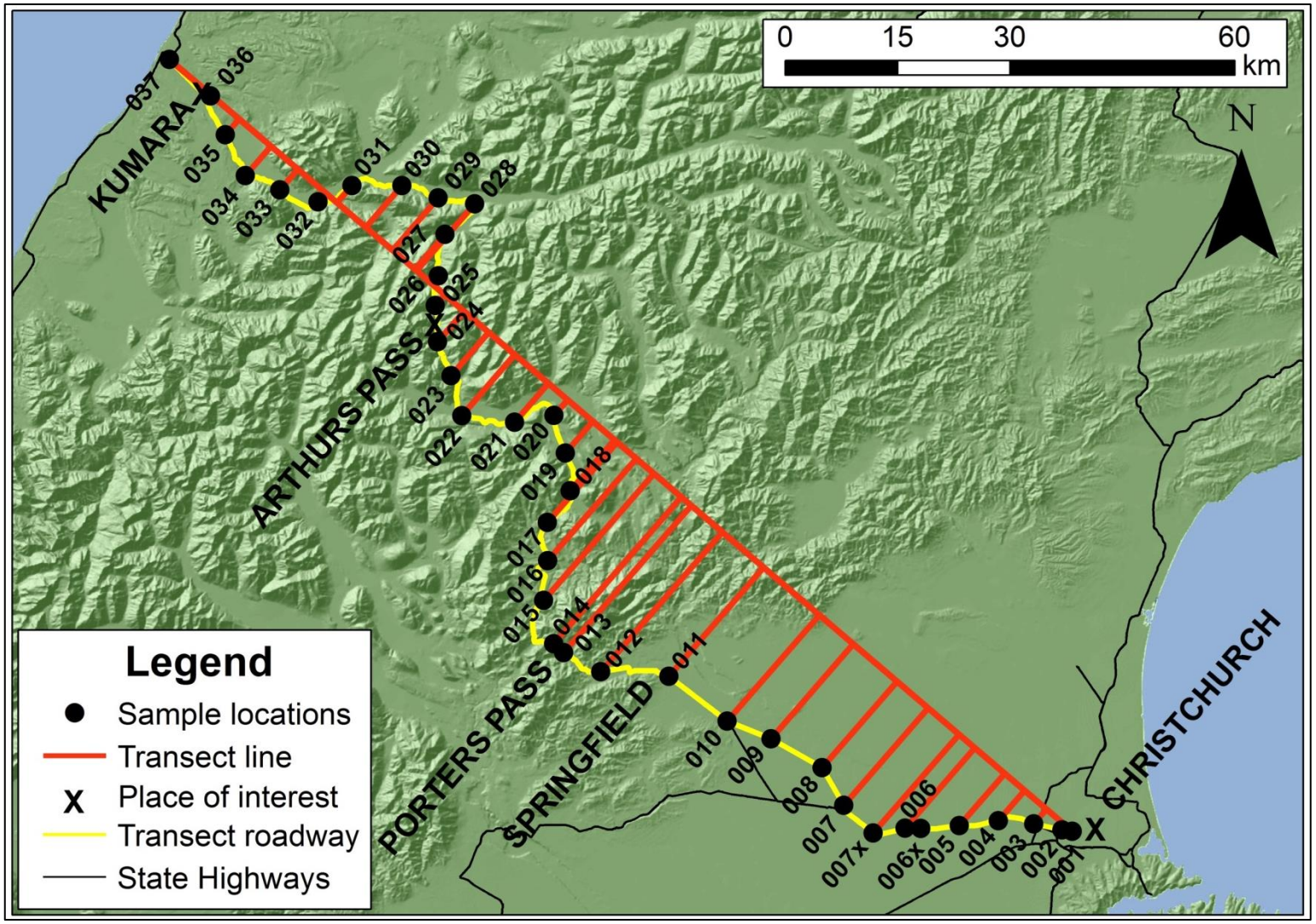

Figure 3.8: A detailed South Island Transect (SIT) map, indicating sample sites, sample site numbers, major landmarks (bold black text), and the true transect line used (bold red line). For GIS data sources see section 0 'GIS Data Sources'.

Table 3.3: Summary of collected and analysed samples along the South Island Transect in reference to sample site. Some sites indicate that more samples were analysed than we collected, this is due to duplicates being analysed to test variance and the impact of preparation techniques.

Site	Collected			Analysed		
	Usnea	*Ramalina*	*Xanthoria*	*Usnea*	*Ramalina*	*Xanthoria*
CC001	8	17	10	17	8	
CC002	5			7		
CC003	5			5		
CC004	5			6		
CC005	5	4	4	6	2	
CC006	5	5		6		
CC007	5	3	3	6	3	3
CC008x	5	6	3	8	1	2
CC009	5	3	3	13	4	
CC010	5			7		
CC011	5	5	5	7	2	4
CC012	5	3	3	9	3	3
CC013	5			6		
CC014	5			5		
CC015	7	7		8		
CC016	5			5		
CC017	5			12		
CC018	5			5		
CC019	5			5		
CC020	5			6		
CC021	5			6		
CC022	5			6		
CC023	5			8		
CC024	5			5		
CC025	5			6		
CC026	5			5		
CC027	5			6		
CC028	5	2		7	2	
CC029	5			7		
CC030	5	5		12	7	
CC031	5			4		
CC032	5	3		7	3	
CC033	5			9		
CC034	5			9		
CC035	5			10		
CC036	5			10		
CC037	7	6		12	8	

Variation between Genera

The South Island transect allowed the testing of the correlation between the isotope and elemental values of one genera of lichen with another. If a strong correlation existed, this would allow the substitution of lichen genera in habitats where the other may not exist, expanding the geographical range through which this technique may be applicable.

As mentioned earlier, three lichen genera where used (*Usnea* sp., *Ramalina* sp., and *Xanthoria* sp.), selected due to a number of favourable characteristics. Based on the P values summarised in Table 3.4, and the visual representation of the differences in means in Figure 3.9 (ANOVA with multiple comparisons: Tukey Contrasts with Sandwich estimator, H_o: $\mu_{(Genera\ A)} \neq \mu_{(Genera\ B)}$, $\alpha = 0.05$), we can draw a number of conclusions:

- $\delta^{13}C$ values are significantly different when comparing *Usnea*/*Ramalina*, and *Usnea*/*Xanthoria*, indicating that **different lichen genera may not be suited to substitute for others in terms of $\delta^{13}C$**. This agrees with the literature in which variation in $\delta^{13}C$ of lichen from the same substrate is attributed to species-specific differences in resistances to inwards CO_2 flux and the CO_2-fixation mechanism of the photobiont (Cristina Máguas & Brugnoli, 1996; Cristina Máguas *et al.*, 2013; Smith & Griffiths, 1998)
- All comparisons showed high p values (ie. no significant difference) when comparing $\delta^{15}N$ values, indicating that **substitution between differing lichen genera may be suitable in terms of $\delta^{15}N$**.
- In terms of elemental concentrations, carbon shows no significant difference, with high P values, while nitrogen content in *Usnea* appears significantly different to the that of *Ramalina*, even at α=0.01.

Using these results, **only the $\delta^{15}N$ and C% values from *Ramalina* and *Xanthoria* will be used alongside the full data set of *Usnea***, while $\delta^{13}C$ and N% from genera other than *Usnea* will be disregarded.

Table 3.4: P values for the statistical comparison of elemental and isotope values in differing genera. Significant difference at α=0.05

	Usnea - Ramalina	*Usnea - Xanthoria*	*Ramalina - Xanthoria*
$\delta^{13}C$	<0.001**	0.018*	0.467
$\delta^{15}N$	0.942	0.966	0.908
N%	<0.001**	0.191	0.947
C%	0.746	0.958	0.841

* Significant difference at α=0.05, ** Significant difference at α=0.01

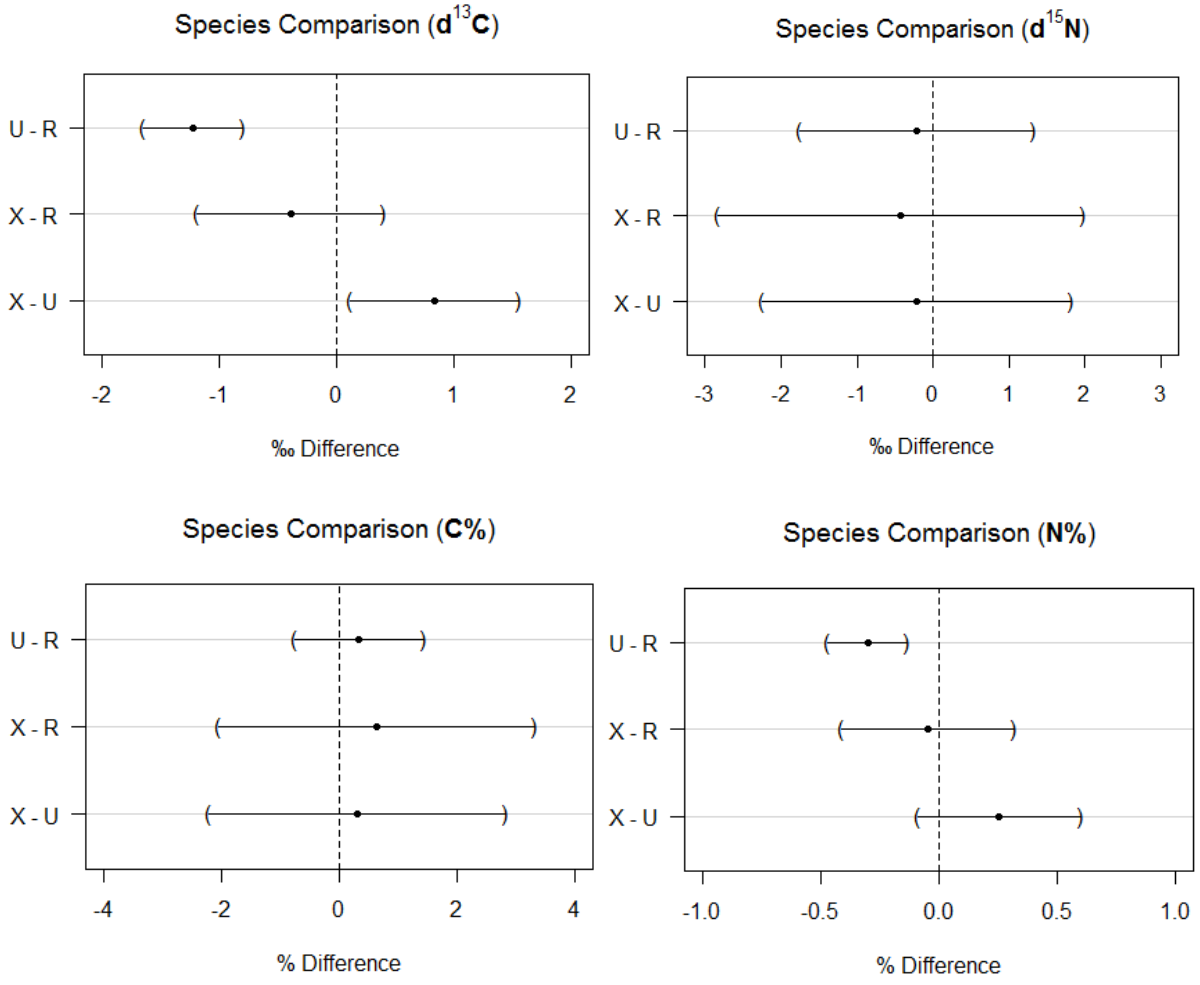

Figure 3.9: 95% Confidence intervals for the difference between means of isotope or elemental concentrations for the three genera of lichen examined in this study. "U" = *Usnea*, "R" = *Ramalina*, "X" = *Xanthoria*. For genera to be statistically similar, the differences between means must include zero within the 95% range.

Same-Site and Same-Sample Variability

While the IRMS-EA produces internal and external errors in isotope ratios of ±0.05 and ±0.2‰, much higher ranges were seen, not only between samples from the same site, but also from duplicate samples from the same thallus. This section aims to quantify this variability, and postulate as to its source.

Same-Site Variability

Of interest is the variability within a site, as a large variation in isotopic compositions and elemental concentrations may undermine the premise of this study. This is tested by comparing the ranges (widths) of the 95% confidence intervals (CI) from each sample site in both the South Island Transect

and North Island Transects (NIT, including both the "Rotorua East-West" (REW) and "Taupo North-South" (TNS) transects), as well as the sites at Ngatamariki in which two samples were analysed.

Across the South Island transect, samples from the same site had CI ranges between 0.40 and 4.67‰ for $\delta^{13}C$ (mean = 1.47‰), and between 0.98 and 6.90‰ for $\delta^{15}N$ (mean = 2.84‰). This means that for any given sample to fit into the $\delta^{15}N$ 95% confidence interval for the associated sample site, it can vary, on average, over a range of 2.84‰.

Homogenisation by crushing samples in liquid nitrogen using a mortar and pestle prior to analysis, which was a favoured preparation technique in the literature, was used in the North Island samples in an effort to reduce sample variability. The extent of CI ranges appear to decrease for all parameters except for $\delta^{15}N$ after employing this technique, as shown in the data in Table 3.5 and Figure 3.10. There is a significant decrease in the variability of $\delta^{13}C$ and C%, while no significant difference is seen in $\delta^{15}N$ or N% between sample sites from the SIT and the NIT (Student one-tailed t-test, H_o: $\mu_{(SIT\ CI\ Ranges)} = \mu_{(NIT\ CI\ Ranges)}$, $\alpha = 0.05$).

The Ngatamariki samples however, show average CI ranges equal to or greater than even those of the SIT (Table 3.5). The Ngatamariki samples were prepared identically to the NIT samples, and it would be expected that they show a similarly low variation relative to SIT sample sites. The explanation behind the increased variability is likely due to the substantial sample size decrease at each site; five samples were collected and analysed at each NIT site, while the Ngatamariki CI ranges are the result of only two samples per site. To reduce the high CI ranges at Ngatamariki to those of the NIT, more samples would be required to be analysed.

Table 3.5: Average same-site 95% CI ranges, comparing the South Island Transect (SIT), North Island Transects (NIT), ands Ngatamariki (NGA). Bracketed subscript refers to the number of sample sites used in the averaging process. The results of the t-test to determine statistical difference between CI ranges of the SIT and NIT can be seen in the fourth row. (Student t-test, one tailed, H_o: $\mu_{(SIT\ CI\ Ranges)} = \mu_{(NIT\ CI\ Ranges)}$, $\alpha = 0.05$)

	$\delta^{13}C$ (‰)	$\delta^{15}N$ (‰)	N (%)	C (%)
SIT	1.465 $_{(37)}$	2.845 $_{(37)}$	0.405 $_{(37)}$	2.727 $_{(37)}$
NIT	1.120 $_{(32)}$	3.542 $_{(34)}$	0.361 $_{(32)}$	1.288 $_{(34)}$
NGA	1.540 $_{(84)}$	3.574 $_{(84)}$	0.555 $_{(83)}$	1.785 $_{(84)}$
P (NIT < SIT)	0.016*	0.090	0.220	<0.001***

* significance at α=0.05, *** significance at α=0.001,

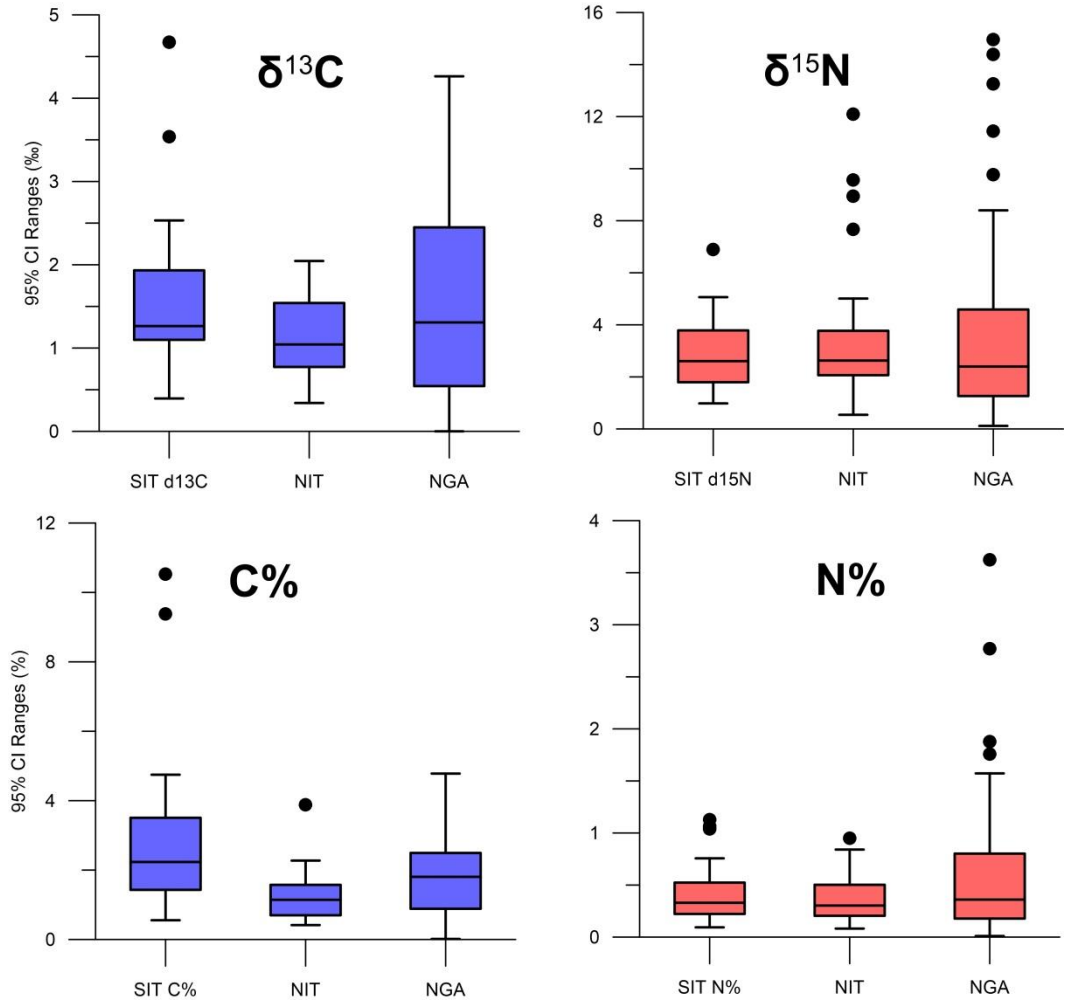

Figure 3.10: Comparison of CI ranges at the three major sample areas in this study. CI ranges are in ‰ for $\delta^{13}C$ and $\delta^{15}N$, while C% and N% ranges are in %. Black dots show outliers, outside of an IQR factor of 1.5.

The large variation in $\delta^{15}N$ values is a concern, as it is unclear whether this is natural variability, or the result of contamination from one or more of the sample collection and preparation stages. The observed average single-site variation of 2.84‰ for the SIT covers almost 25% of the total range of values seen across the SIT sites (12.30‰).

Contamination via sample collection and preparation would likely result in some form of correlation between anomalous carbon and nitrogen isotope ratios. There appears to be no, or limited correlation (linear) between large CI ranges in $\delta^{13}C$ and $\delta^{15}N$, shown in Figure 3.11 (Pearson's correlation, ρ=-0.055). In the outliers shown, larger variations in one variable result in low variations in other variables.

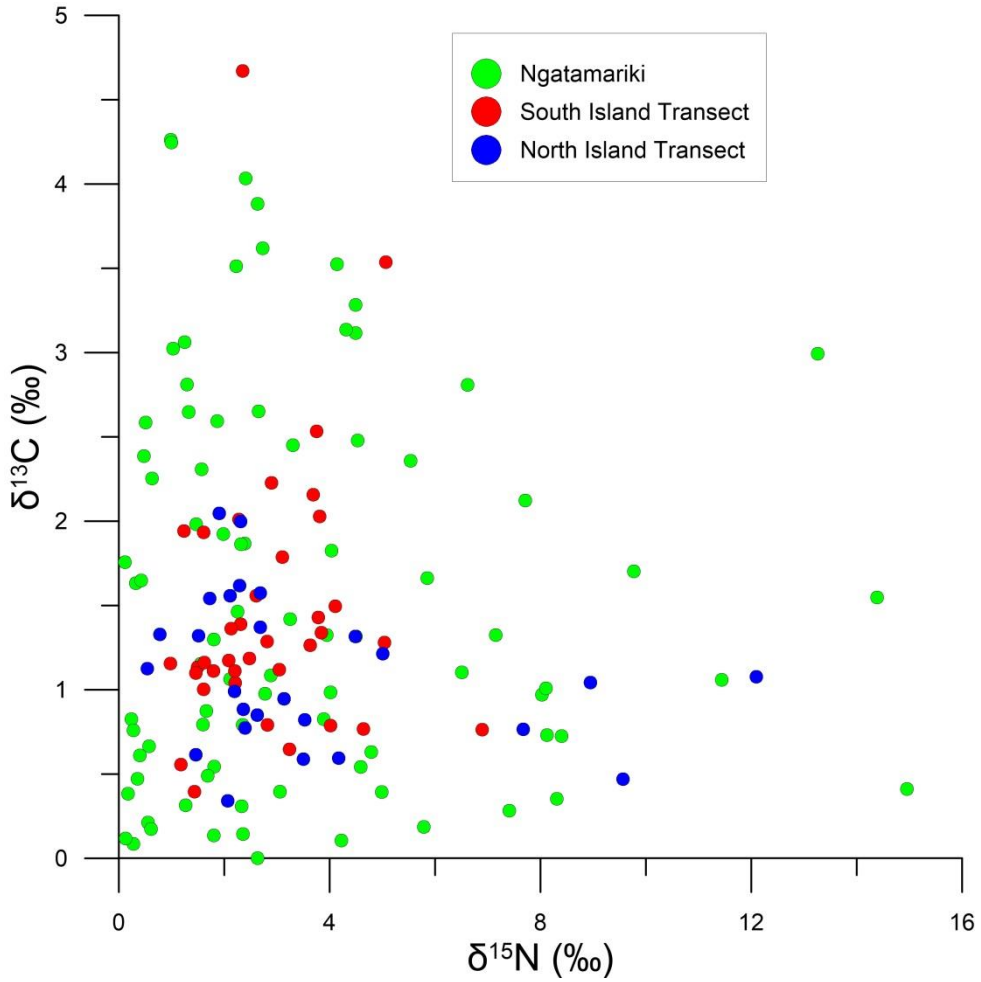

Figure 3.11: Comparison between $\delta^{13}C$ and $\delta^{15}N$ CI ranges showing the lack of correlation, as well as the outliers.

Beck & Mayr (2012) noted a greater range of $\delta^{15}N$ values in lichen on organic substrates than on minerogenic substrates. As the majority of samples collected in this study, not just in the South Island but also at Ngatamariki and the North Island transects, were collected from organic substrates (including processed wood such as fence posts), this could explain some of the large variance in $\delta^{15}N$ seen here, but this would require further analysis of minerogenic lichen to be interpreted more fully.

Same-sample Variability

It has been shown that the mycobiont (fungal partner) and the photobiont (algal partner) often have different isotopic values (Beck & Mayr, 2012). Mycobionts, at least in the case of *Xanthoria*, are more enriched in both $\delta^{13}C$ and $\delta^{15}N$ than the photobiont, while carbon/nitrogen ratios are lower, due to higher nitrogen content. A change in the proportion of mycobiont in relation to the photobiont will therefore alter the measured elemental concentrations and isotopic composition of the lichen thallus as a whole.

While determining the variation in proportions between the mycobiont and photobiont is well beyond the scope of this study, it was important to determine if isotope ratios were homogenous across the whole thallus of a single sample or if a heterogeneity exists and the value varies depending on where on the thallus the sample is taken. This would affect some of the sample preparation methods, especially of the SIT samples, in which part of the sample was taken for analysis, rather than homogenising it as was done with the NIT and NGA samples.

To test same-sample variability, an intact, defect free *Usnea* thallus from a SIT site with an excess of sample mass was dissected. Samples were required to be at least 400µg, preferably 1000-3000µg, limiting the number of samples that could be tested. The thallus from a single specimen was divided into 14 sections, each section weighing roughly 5000ug (to allow for duplicate testing).

The average absolute difference in the $\delta^{13}C$ ratio between duplicate section samples was 0.213‰, while $\delta^{15}N$ differed by 0.792‰ (Table 3.6). Samples from the same site (duplicate samples from 84 Ngatamariki sites) were found to have an absolute difference of 0.79 and 1.81‰ for $\delta^{13}C$ and $\delta^{15}N$ respectively, well over twice that seen within a single sample.

Table 3.6: Summary of Same-sample variability statistics

	$\delta^{13}C$ (‰)	**$\delta^{15}N$ (‰)**	**C%**	**N%**
Section Ranges	-22.38 to -21.93	-6.77 to -4.53	39.21 to 42.97	0.40 to 1.02
Average	-22.15	-5.46	41.42	0.72
Average difference	0.213	0.792	0.516	0.079

There existed a correlation between all investigated parameters and distance to base/stem. $\delta^{13}C$ was moderately negatively correlated (Pearson's correlation, r=-0.585), while $\delta^{15}N$ had a moderately positive correlation (Pearson's correlation, r=0.613). A stronger correlation exists between C% (Pearson's correlation, r=0.915) and N% (Pearson's correlation, r=0.865) in relation to distance from stem. These trends are shown in Figure 3.12 ($\delta^{15}N$ and $\delta^{13}C$) and Figure 3.13 (N% and C%) through the colour-coding of each section by value. The $\delta^{13}C$ values agreed with those in the literature; Máguas & Brugnoli (1996) found that the greatest fractionation (lowest $\delta^{13}C$ values) were found in the younger marginal regions of the lichen thallus.

Two possible explanations the spatial heterogeneity exist:

1) These correlations between isotopic composition/elemental concentrations and distance to stem may be explained through the mechanisms of *Usnea* growth. Growth occurs through

the outer branches (apical regions), which become thicker and longer. These younger outer branches may contain a greater proportion of essential nutrients than older branches. Some fruticose lichen have been shown to translocate nitrogen from older parts at the base to growing apical sections (Ellis *et al.*, 2005; Hyvärinen & Crittenden, 1998).

2) The proportion of mycobiont to photobiont changes as distance from stem increases, due to the age and thickness of newly grown branches, with some foliose species shown to have thinner thallus margins and therefore higher photobiont:mycobiont ratios (Dahlman, Nasholm, & Palmqvist, 2002; Nash, 2008a). The difference between the isotopic composition and elemental concentration of the two lichen partners has been shown by Beck & Mayr (2012) to be significant, which could explain the heterogeneity.

SIT Results

SIT: Isotopes

Both $\delta^{13}C$ and $\delta^{15}N$ lack obvious salient patterning, other than to gradually increase as the transect progresses from west to east (Figure 3.14A). Weak linear correlations of r=-0.3 and -0.13 for $\delta^{13}C$ and $\delta^{15}N$ respectively are present (Pearson's correlation). Site averages for $\delta^{13}C$ vary between -21.28 and -26.53‰ (range of 5.25‰), while those for $\delta^{15}N$ are between -4.34 and -16.64‰ (range of 12.3‰).

The large variability of $\delta^{13}C$ within a single site is worth noting; at some sample sites, error bars of one standard deviation either side of the average can be seen to cover most of the total range of values across the whole transect (Blue line, Figure 3.14A). For example, the error bar range of CC026 (2σ) is ±2.66‰ (a range of 5.32‰), covering more than the range of all South Island $\delta^{13}C$ data (5.25‰)

SIT: C%, N%, and C:N Ratio

Carbon contents show high variation, as seen by the error bars (Figure 3.14B), but the site averages across the SIT remain reasonably constant. The nitrogen content data however (Figure 3.14B), exhibits two distinct populations of data: the western SIT (west of Porters Pass) with low nitrogen contents averaging 0.7%, and the Canterbury Plains (east of Porters Pass), averaging 1.9% nitrogen at dry weight

Carbon:Nitrogen ratios reflect the relatively stable carbon contents and high-eastern/low-western nitrogen contents, with high C:N ratios in areas of low nitrogen, and low ratios in areas of high nitrogen (Figure 3.14C).

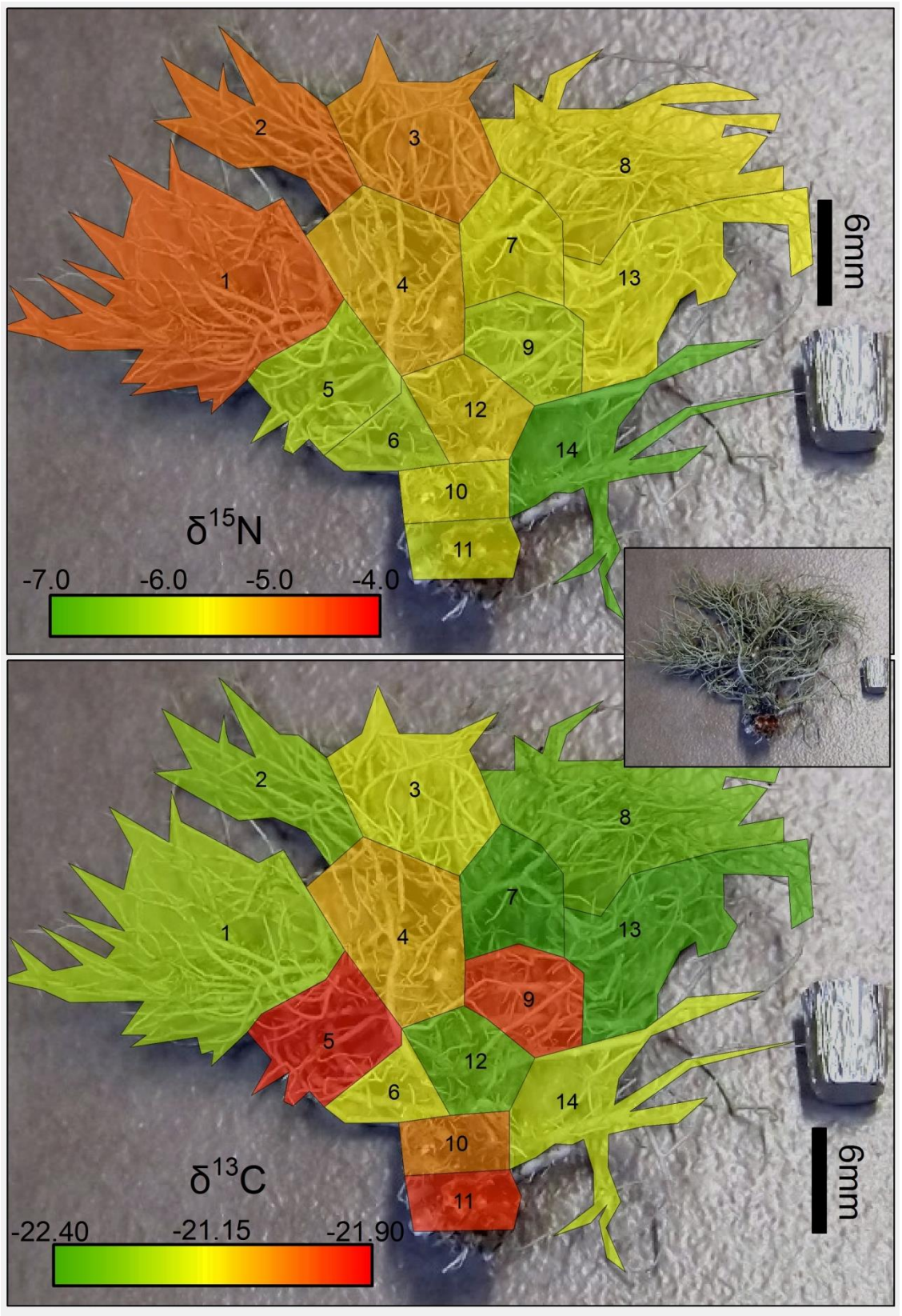

Figure 3.12: The 14 sections of the single lichen thallus analysed for same-sample variance, showing a) $\delta^{15}N$ and b) $\delta^{13}C$. The sections are colour-coded to represent the average values of duplicate samples from that section, except for section 7, which only has one $\delta^{13}C$ value. Scale used is a 6mm tall silver capsule in the right of the picture. Inset shows original sample

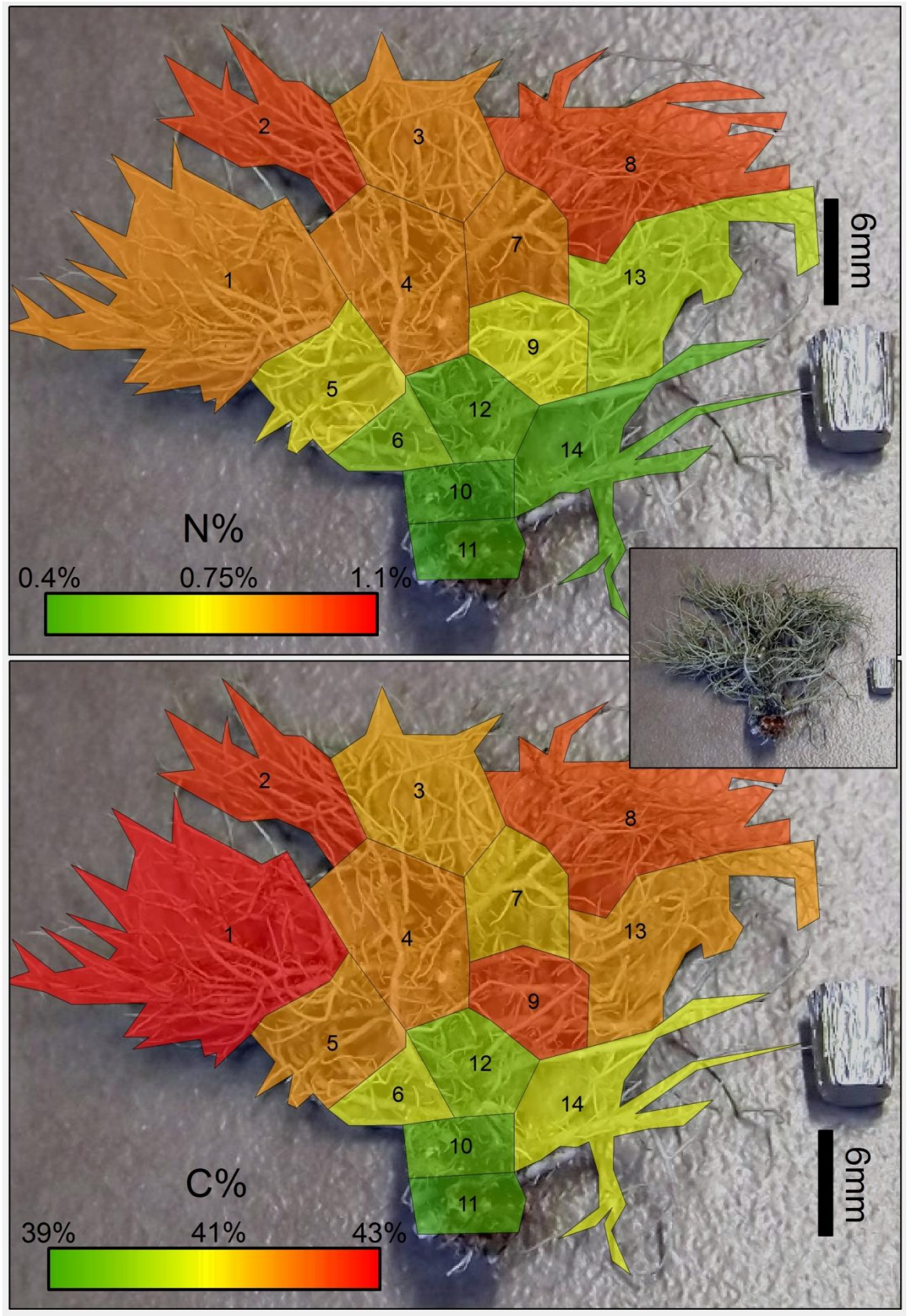

Figure 3.13: The 14 sections of the single lichen thallus analysed for same-sample variance, showing a) N% and b) C%. The sections are colour-coded to represent the average values of duplicate samples from that section, except for section 7, which only has one N% and C% value. Scale used is a 6mm tall silver capsule in the right of the picture. Inset shows original sample

Canterbury Plains vs Western SIT

For the purposes of this section, the Canterbury Plains refers to all sites east of Porter's Pass, beginning with Springfield (CC011) extending to Christchurch (CC001), while Western SIT refers to all sites from Porters Pass (CC012) to Kumara (CC037).

As seen in Figure 3.14, the ratio of carbon to nitrogen shows two populations, which correlate to: a) the Canterbury Plains, and b) everything west of the Canterbury Plains. When compared in terms of $\delta^{15}N$ vs nitrogen content (Figure 3.15B), the two populations appear to occupy separate areas, with Canterbury Plains having higher nitrogen contents, and a slightly more positive $\delta^{15}N$ value. Nitrogen contents between the two populations are highly significantly different ($\alpha = 0.01$, $p<0.001$, Students t-test, df=13), and while $\delta^{15}N$ values overlap a significant difference between the two populations exists ($\alpha = 0.05$, $p=0.019$, Students t-test, df=21).

This divide between the nitrogen contents and $\delta^{15}N$ values between the Canterbury Plains and the rest of the South Island is not replicated in the carbon data (Figure 3.15A). Both populations occupy the same area when plotted as $\delta^{13}C$ vs carbon content and are not significantly different either in terms of carbon content ($\alpha = 0.05$, $p=0.783$, Students t-test, df=23) or $\delta^{13}C$ ($\alpha = 0.05$, $p=0.990$, Students t-test, df=20).

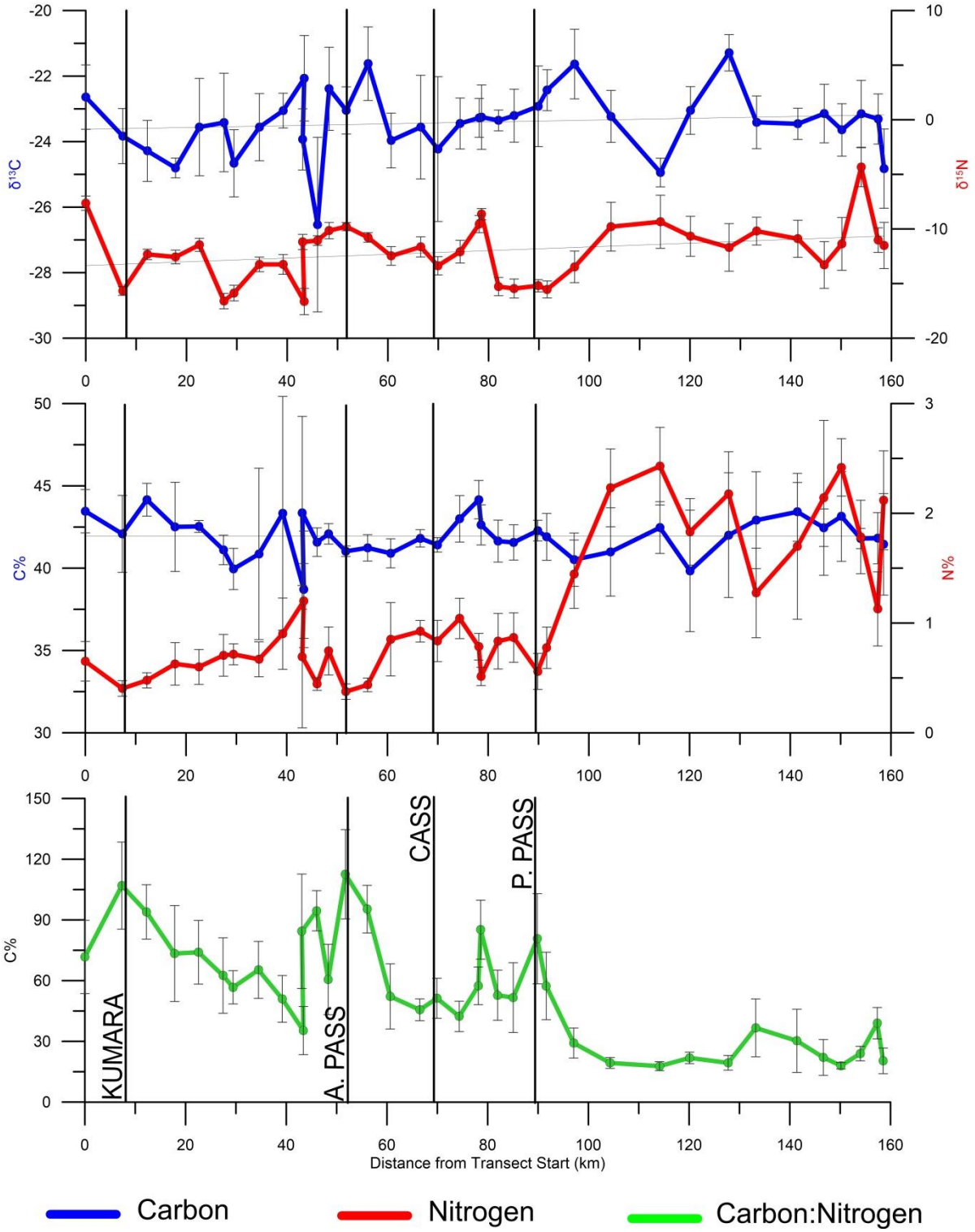

Figure 3.14: South Island Transect values for A) $\delta^{13}C$ and $\delta^{15}N$, B) C% and N%, and C) C:N ratios. The x axis ("Distance from Transect Start") starts in the west on the left (Greymouth), and finishes on the right in the east (Christchurch), almost 160km apart. For more detail on the transect and sample site placement, refer to Figure 3.8. Vertical error bars represent one standard deviation, with each site having a sample size (n) of between 5 – 25. Solid vertical lines refer to important landmarks as labelled; "A. Pass" = Arthurs Pass, "P. Pass" = Porters Pass.

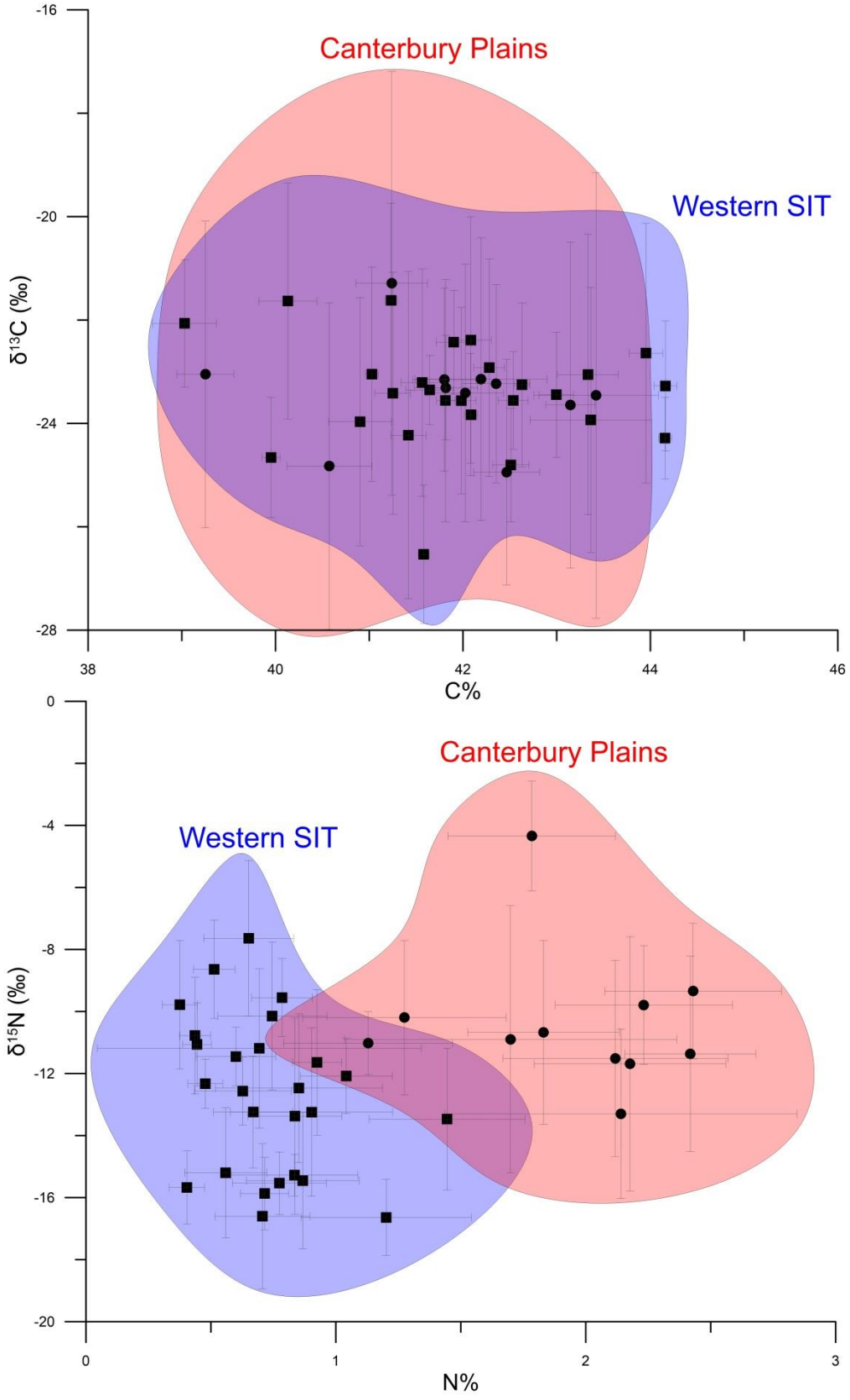

Figure 3.15. A comparison between two parts of the South Island Transect, the western SIT, characterised by low N% (~0.5%), and the Canterbury Plains, characterised by high N% (~2%), while the carbon isotope ratio of content shows no apparent difference.

3.2.3 North Island Transects (NIT)

Two transects were analysed across the North Island (Figure 3.16), in order to determine isotopic compositions and elemental concentrations within, across, and just outside of the Taupo Volcanic Zone (TVZ), but also aiming to replicate the Rotorua-Hamilton transect carried out by Tozer *et al.*, (2005). One transect cuts across the TVZ on a SE-NW trend (transect bearing: 234), known as the 'Rotorua East-West' (REW) transect, while the other was parallel to the strike of the TVZ, roughly NNE-SSW (transect bearing: 014), known as the 'Taupo North-South' (TNS) transect. As the two transects intersect near Rotorua, sample sites in this area contributed to both transects.

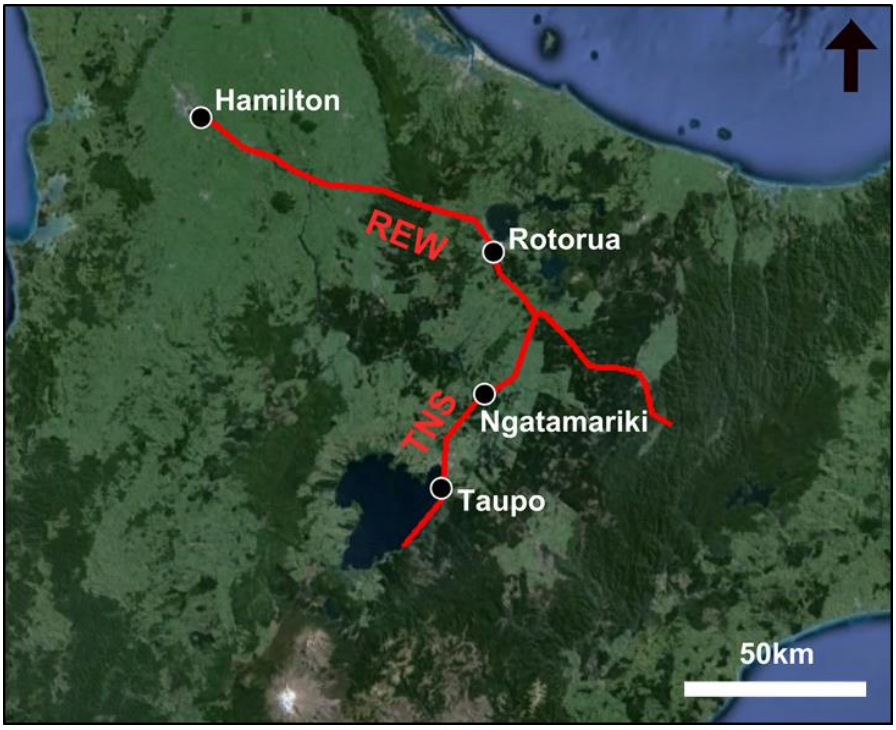

Figure 3.16: Simplified schematic of the two North Island Transects (NIT), known as 'Rotorua East-West' (REW) and 'Taupo North-South' (TNS). These transects intersect in the Rotorua area, and sites here are used for both transects. From Google Earth & Landsat (2013).

Rotorua East-West (REW)

The REW transect includes 23 sites along a 158km line, one of which was collected for the TNS transect (Figure 3.17). The eastern limit of the REW transect (REW001) sits in the Te Urewera National Park, just outside of the TVZ on Torlesse greywacke basement rock. It follows SH38 west to the junction of SH5/38 (REW008), just north of Rainbow Mountain (TNS001), after which it follows SH5 through Rotorua (REW011) to the junction of SH1/5 near Tirau (REW017). It then follows SH1 through Cambridge (REW020) to Hamilton, where the final site (REW022) is located in the Hamilton Gardens, near the south-eastern boundary of Hamilton City limits.

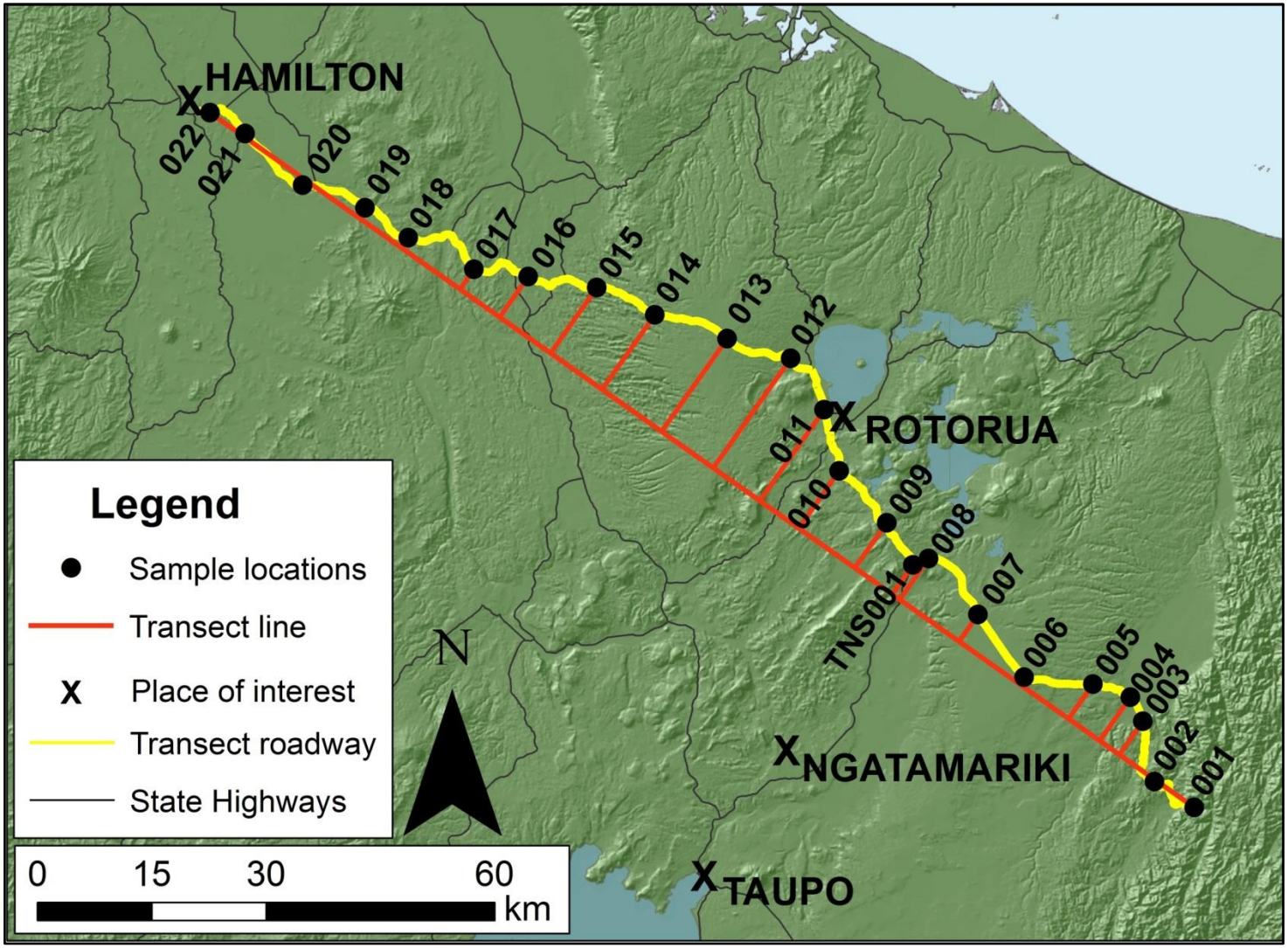

Figure 3.17: A detailed Rotorua East-West Transect (REW) map, indicating sample sites, sample site numbers, major landmarks (bold black text), and the true transect line used (bold red line). For GIS data sources see section 0 'GIS Data Sources'.

Sites were chosen based on 10km sections of roadway, having an average Euclidean distance of 7.8km, and an average true transect distance of 7.2km (straight along transect line). An elevation profile of the REW transect (Figure 3.18) shows the elevations of each sample site relative to sea level and the other two transects. Sample sites reach a maximum of up to 500m (immediately east of Rotorua), and a minimum of ~40m (Hamilton).

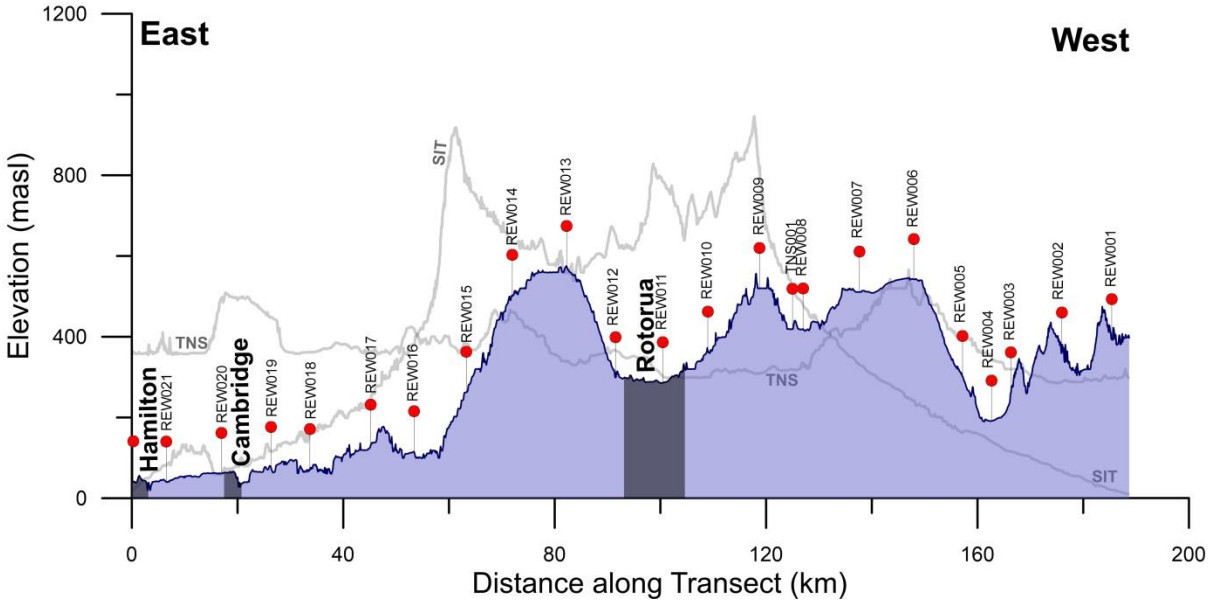

Figure 3.18: Elevation Profile of the REW Transect. Red circles refer to sample sites as labelled, while blue-grey shaded areas show areas of significant landmarks. Pale grey lines in the background show the TNS and SIT transect profiles in comparison, as labelled, with distances normalised to the length of the REW Transect. For GIS data sources see section 0 'GIS Data Sources'.

REW Results

REW: Isotopes

There is a slight west-east decrease in $\delta^{13}C$ ratios, while $\delta^{15}N$ shows a more pronounced negative trend (Figure 3.19A). There are three $\delta^{15}N$ outliers, seen on the western edge of this transect (left in Figure 3.19A); these values are surprising as there is no obvious deviation seen in any of the other parameters at these sites. These sites, REW020 (7.08 ± 1.55‰), REW017 (5.19 ± 5.46‰), and possibly REW016 (0.83 ± 6.90‰), contain some of the most enriched values obtained from any sample in this study, with a maximum sample value of 11.80‰ (REW017-U04).

As site REW002 sampled the genus *Ramalina*, the $\delta^{13}C$ values and nitrogen content for this site are not reported (see Section: 'Variation between Genera', page 53).

REW: C%, N%, and C:N Ratio

Similar to the isotope data, carbon content shows a weak negative trend from west-east, while nitrogen contents show a slightly stronger negative trend (Figure 3.19B). The eastern end of the REW

transect is of interest as the land use changes from intensive farmland, which dominates the western section of the transect, to forested areas (both native and exotic).

There are two sections along the REW transect with low nitrogen content, the first in an area of exotic forest between 120-130km (0.8-1.1%N, REW005-007), and the second in the native forests of the Te Urewera National Park, between 150-160km at the far eastern limit of the transect (0.6-1.1%N, REW001-3). Between these two sections, there is a topographic basin used for farming, in which site REW004 was collected. Like the Canterbury Plains samples sites from the SIT, REW004 shows a spike in nitrogen concentrations.

The low nitrogen contents in the eastern section of the REW Transect result in higher C:N ratios at these sites, as the carbon values do not deviate significantly from their slight negative trend (Figure 3.19C). Other than this, the C:N ratios are very consistent, with the western 110km having an average ratio of 28.8 ± 3.7.

Taupo North-South (TNS)

The TNS transect consists of 11 sites over a Euclidian 92km, five of which were collected for the REW transect (Figure 3.21). The most southern site (TNS006) is halfway between Taupo and Turangi on the shores of Lake Taupo, close to the small town of Tauranga-Taupo. It then follows SH1 north to Taupo, after which it follows SH5 past Wairakei (TNS004), through Rotorua, all the way to the most northern site (REW012) near Ngongotaha and the SH5/36 junction.

Spatial resolution on this transect is much lower than that of the REW transect; sites were selected based on a road distance of 15km, while the average Euclidean distance between sites was 12.9km, and the average true transect distance was 8.4km. As this transect passes the Ngatamariki Geothermal area, the average values of all NGA sample sites are used in this transect as if it were another sample site.

The elevation profile (Figure 3.20) shows that the TNS Transect is much more consistent than the other two transects, averaging 374masl, and ranging between 280 and 560masl.

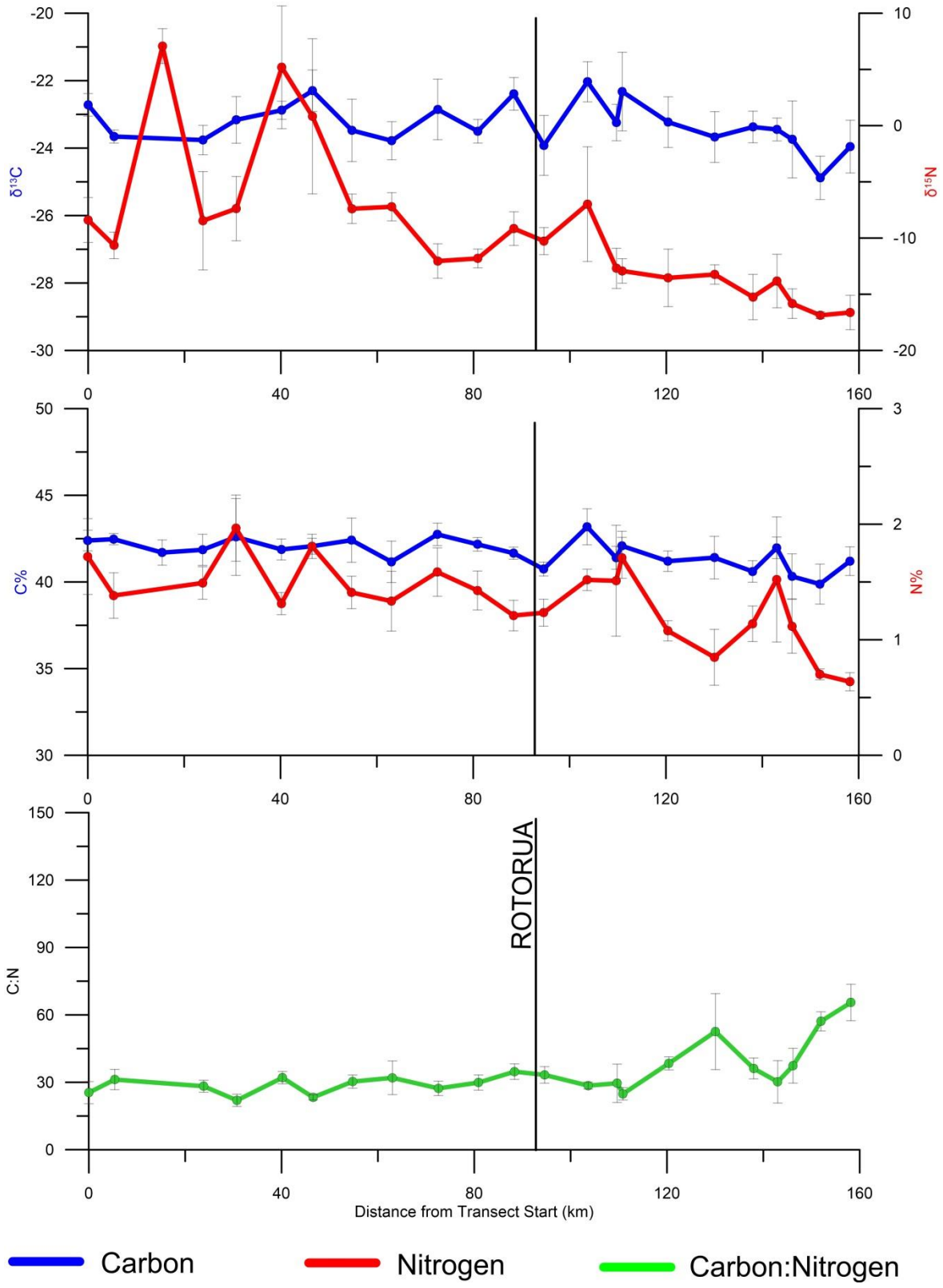

Figure 3.19: Rotorua East-West Transect values for A) $\delta^{13}C$ and $\delta^{15}N$, B) C% and N%, and C) C:N ratios. The x axis ("Distance from Transect Start") starts on the left in the west (Hamilton), and finishes on the right in the east (Te Urewera National Park), almost 160km apart. For more detail on the transect and sample site placement, refer to Figure 3.17. Vertical error bars represent one standard deviation, with each site having a sample size (n) of 5. Solid vertical lines refer to important landmarks as labelled.

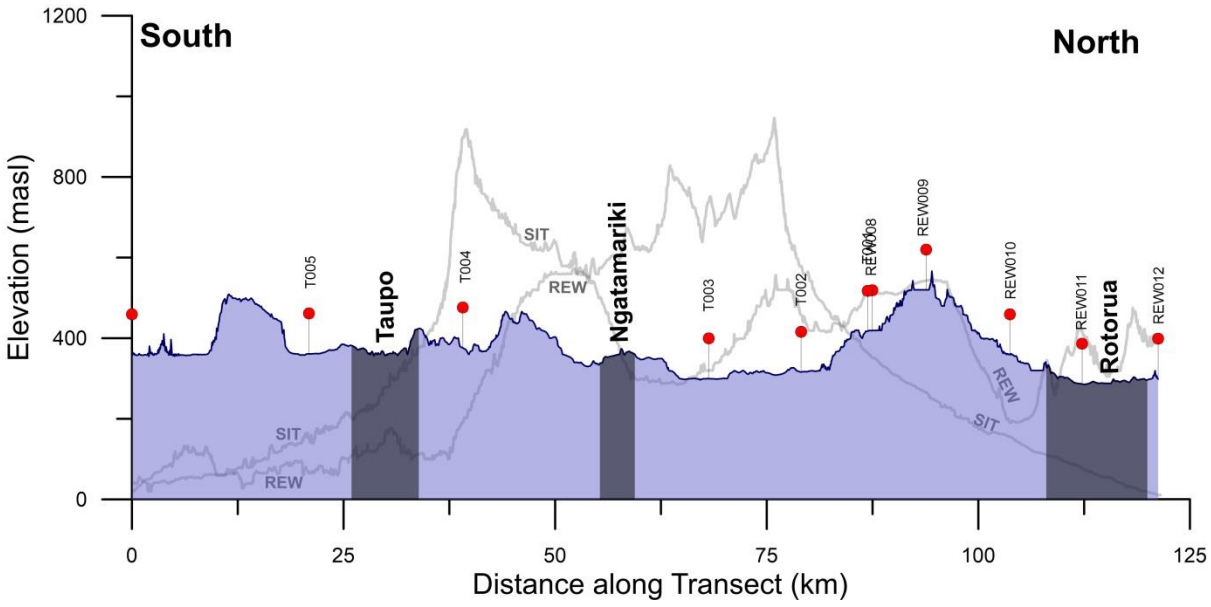

Figure 3.20: Elevation Profile of the TNS Transect. Red circles refer to sample sites as labelled, while blue-grey shaded areas show areas of significant landmarks. Pale grey lines in the background show the SIT and REW transect profiles in comparison, as labelled, with distances normalised to the length of the TNS Transect. For GIS data sources see section 0 'GIS Data Sources'.

TNS Results

TNS: Isotopes

Carbon isotopic compositions show a weak negative trend from north to south, while $\delta^{15}N$ values are higher in the north and south sections of the transect, with lower values in the central area around Ngatamariki (Figure 3.22A). Other than the anomalous sites in the western portion of the REW Transect, the $\delta^{15}N$ values here are fairly similar to those of the REW, both being in the -5 to -15‰ ranges.

TNS: C%, N%, and C:N Ratio

Nitrogen contents along this transect are highest in the central-northern area (50-70km), where values reach 2% nitrogen by dry weight (Figure 3.22B). Nitrogen contents on average remained high, with no site averages falling below 1%.

Other than showing a very slight negative trend from south to north, the carbon contents remain stable. What is interesting is that the high carbon content at Ngatamariki, which is an average of all Ngatamariki sites (n=252), and is >2% greater than all other sites in this transect.

The C:N ratios appear higher in the southern portion of the transect due to both a high nitrogen content and variable-low carbon content (Figure 3.22C). Variation is much lower than both the SIT and REW transect, where the C:N ratio varies between 22-65 and 18-112 respectively, while this transect varies from 23-40.

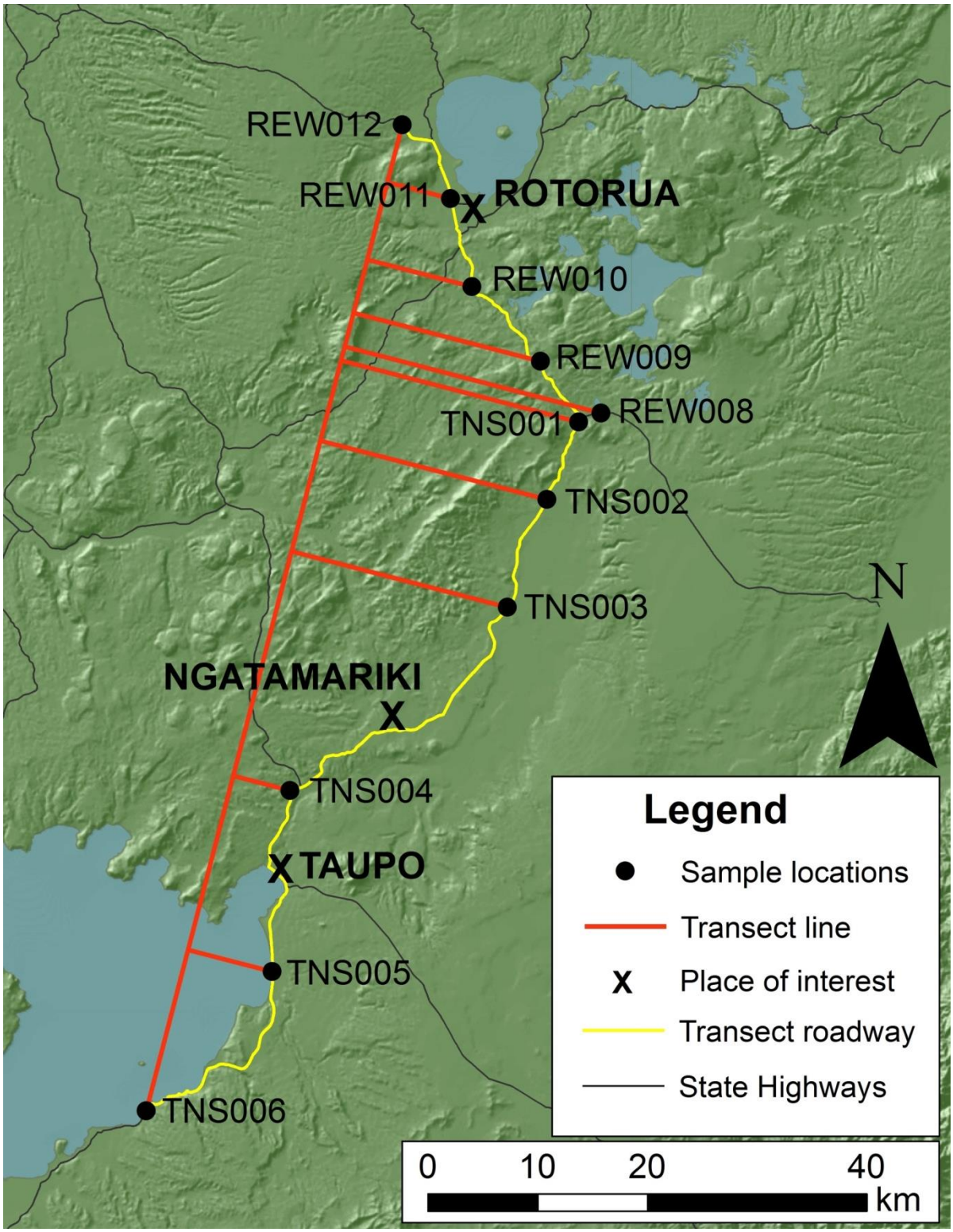

Figure 3.21: A detailed Taupo North-South Transect (TNS) map, indicating sample sites, sample site numbers, major landmarks (bold black text), and the true transect line used (bold red line). For GIS data sources see section 0 'GIS Data Sources'.

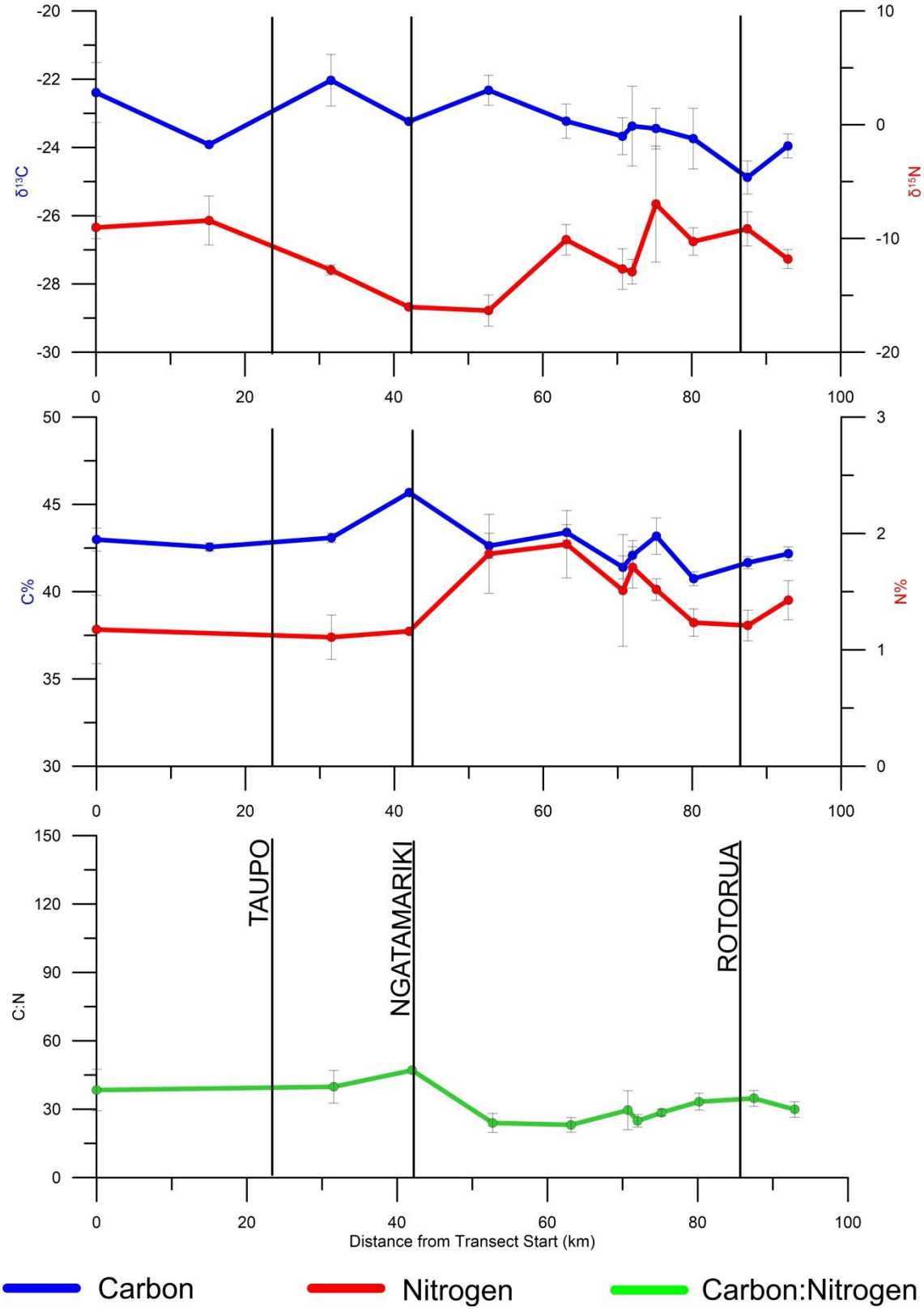

Figure 3.22: Taupo North-South Transect values for A) $\delta^{13}C$ and $\delta^{15}N$, B) C% and N%, and C) C:N ratios. The x axis ("Distance from Transect Start") starts in the south on the left (southern Lake Taupo), and finishes on the right in the north (Rotorua), almost 100km apart. For more detail on transect and sample site placement, refer to Figure 3.21. Vertical error bars represent one standard deviation, with each site having a sample size (n) of 5. Solid vertical lines refer to important landmarks as labelled.

3.2.4 Comparison of SIT, REW, and TNS

There is nothing remarkable about the differences between the SIT, RWE, and TNS transects. Other than the anomalous sites seen in the $\delta^{15}N$ values in the western portion of the REW transect, the three transects follow the same general range of values, between -25 and -22 ‰ for $\delta^{13}C$ and between -15 and -5‰ for $\delta^{15}N$ (Figure 3.23). The reduction in site variability (Section: 'Same-Site Variability', page 54) is clearly seen by the reduction in error bar length between the highly variable SIT sites and the REW and TNS transect.

Carbon contents across the three transects appear to be the most consistent of all measured parameters (Figure 3.23), with minimal variation other than small negative west-east/south-north trends. Values range between 40-45% carbon by dry weight, with the highest value being the average of all of the Ngatamariki sites, along the TNS Transect, with a carbon content of 45.7 ±1.7%.

Nitrogen contents show much greater variation than carbon, for example the SIT data shows two populations of nitrogen contents corresponding to a) the Canterbury Plains (high values) and b) west of Porters Pass (low values; Figure 3.23). The nitrogen contents of the Canterbury Plains are the highest values seen in any of the transects, with six sites over a distance of 100km that are in excess of 2% nitrogen by dry weight. On the other end of the scale, the nitrogen contents of the remainder of the SIT are the lowest values observed in any of the transects, with the majority of values below 1%N. Most of the nitrogen contents of the other transects are generally on the lower end of the 1-2% range.

Due to the lack of variability in carbon contents, the nitrogen contents are well mirrored by the C:N ratios (Figure 3.23), with higher nitrogen contents creating a lower C:N ratio, and vice versa. Due to this, the highest ratios are seen in the SIT, west of Porters Pass, where the lowest nitrogen contents were seen. These ratios are generally in excess of 60:1, with some over 100:1. The REW and TNS transects are remarkably similar, mostly staying between the 30:1 to 40:1 mark.

The relationship between $\delta^{15}N$ and N% shows that while sites generally show the same range of $\delta^{15}N$ ratios, the spread of SIT nitrogen contents is much greater than that of the two North Island Transects (Figure 3.24A). When comparing the relationship between $\delta^{13}C$ and C%, all three transects plot in the same area (Figure 3.24B), although the SIT shows the large variability discussed earlier (see Section: 'Same-Site and Same-Sample Variability', page 54).

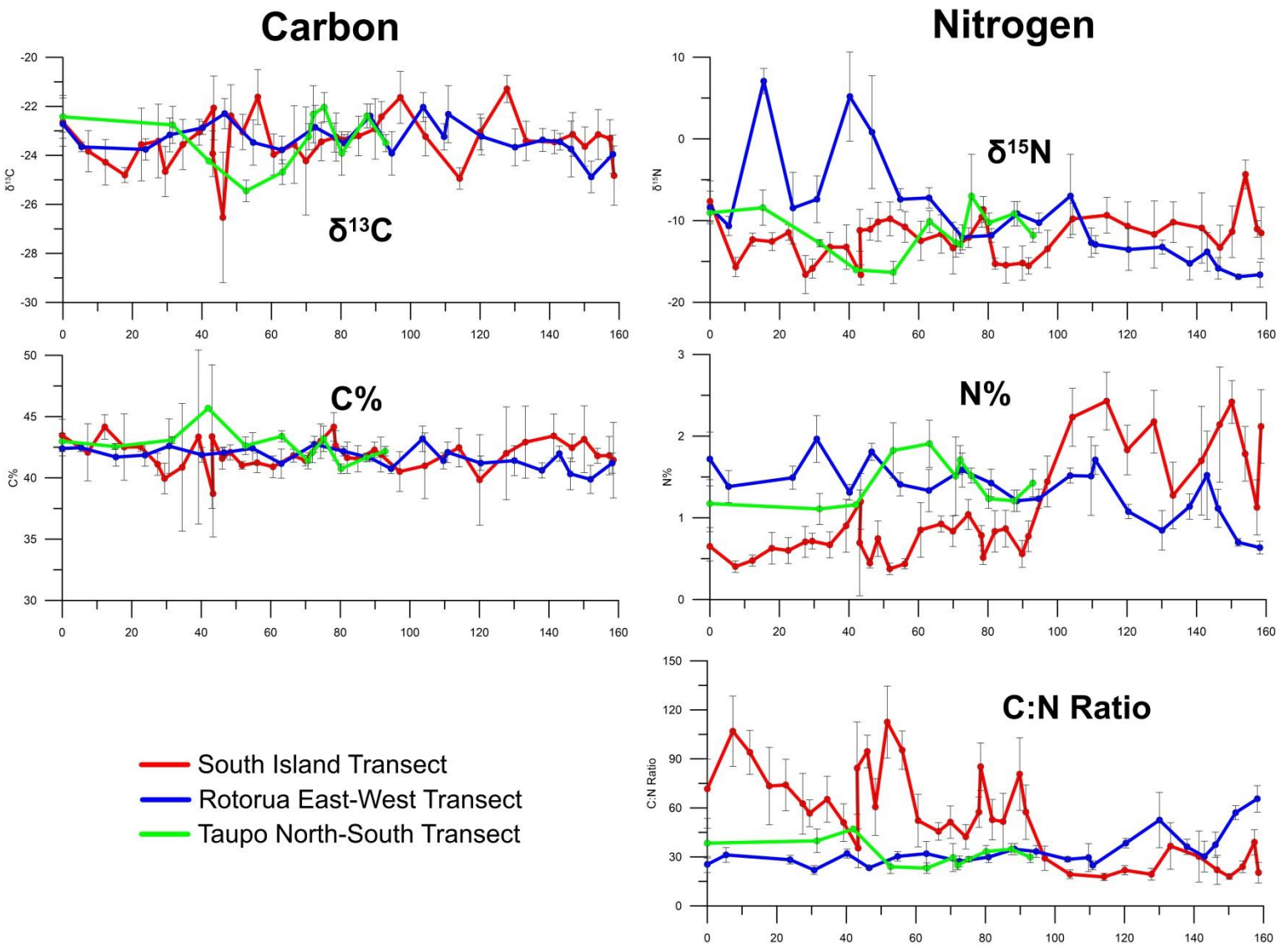

Figure 3.23: Summary graphs of the three transects, comparing each parameter between transects.

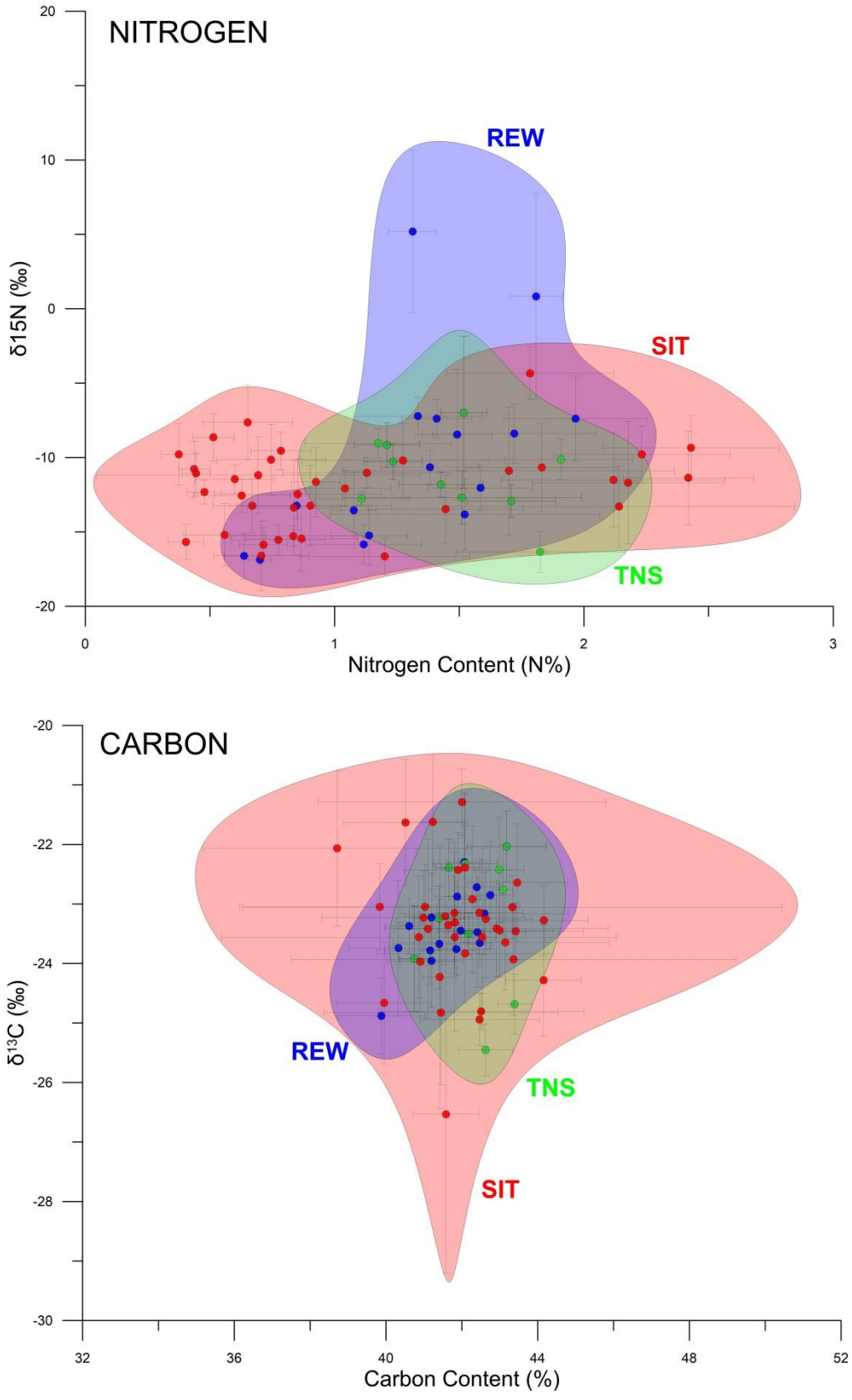

Figure 3.24: Comparison of carbon and nitrogen element concentration to isotopic ratio.

3.3 Ngatamariki

The Ngatamariki Geothermal Area is the site of a recently developed (~2012-13) geothermal field 10-15km north of Taupo. The area hosts a mixture of forestry and farmland, with smaller areas of modified native bush (ie. containing both native and non-native plants). Geothermal surface features are located near to the western boundary of the geothermal field, along the Orakonui river (Orakonui South (OKS) and Orakonui North (OKN)), with smaller springs along the northern boundary of the field along the banks of the Waikato river (Waikato River Springs (WRS)).

3.3.1 Sample Site Distribution

Lichen thalli were collected from sites distributed around the geothermal features of Orakonui North (OKN) and Orakonui South (OKS) with decreasing sample density as distance from OKS and OKN increases (whole field - Figure 3.25 and springs area - Figure 3.26). Sample collection sites were restricted due to a combination of limited land access, especially north of the Waikato River, and heterogeneity in lichen substrate, especially in areas of slash (see Section: 4.4 'Land Use'). Access to the pasture land west of the OKN and OKS springs was not possible.

Five thallus samples were collected at each of the 170 sites (total of 850 samples). At 167 of these sites, lichen of the genus *Usnea* was collected, whilst at three sites (NGA120, 122, 123) *Ramalina* was collected due to lack of available *Usnea* samples in the area. These three sample sites are located on the Somerville's farm area to the north-west of OKN.

3.3.2 Ngatamariki Field Scale

The overarching goal of this thesis is to determine if the stable isotopic composition of lichen is a viable exploration technique in geothermal areas. At the regional scale (10s-100s km), this is determined by comparing samples within geothermal areas (ie. samples from Ngatamariki) to those outside of geothermal areas (ie. samples from the NIT and SIT). At a local scale (ie. the Ngatamariki Geothermal Area) this is determined by comparing samples close to geothermal expressions (ie. near OKN and OKS) to samples at increasing distances. This section reports the Ngatamariki area results in detail.

The lichen samples collected at Ngatamariki had an average isotopic composition of -24.27 ± 0.93 and -16.03 ± 3.67‰ for $\delta^{13}C$ and $\delta^{15}N$, respectively. Due to the large sample size, the population approached a normal distribution; however both were slightly positively skewed towards a less negative isotopic composition (Figure 3.27). This was especially prevalent in the $\delta^{15}N$ values, due to a minority of samples with relatively high isotopic compositions (>0‰) in the north-west of the study area.

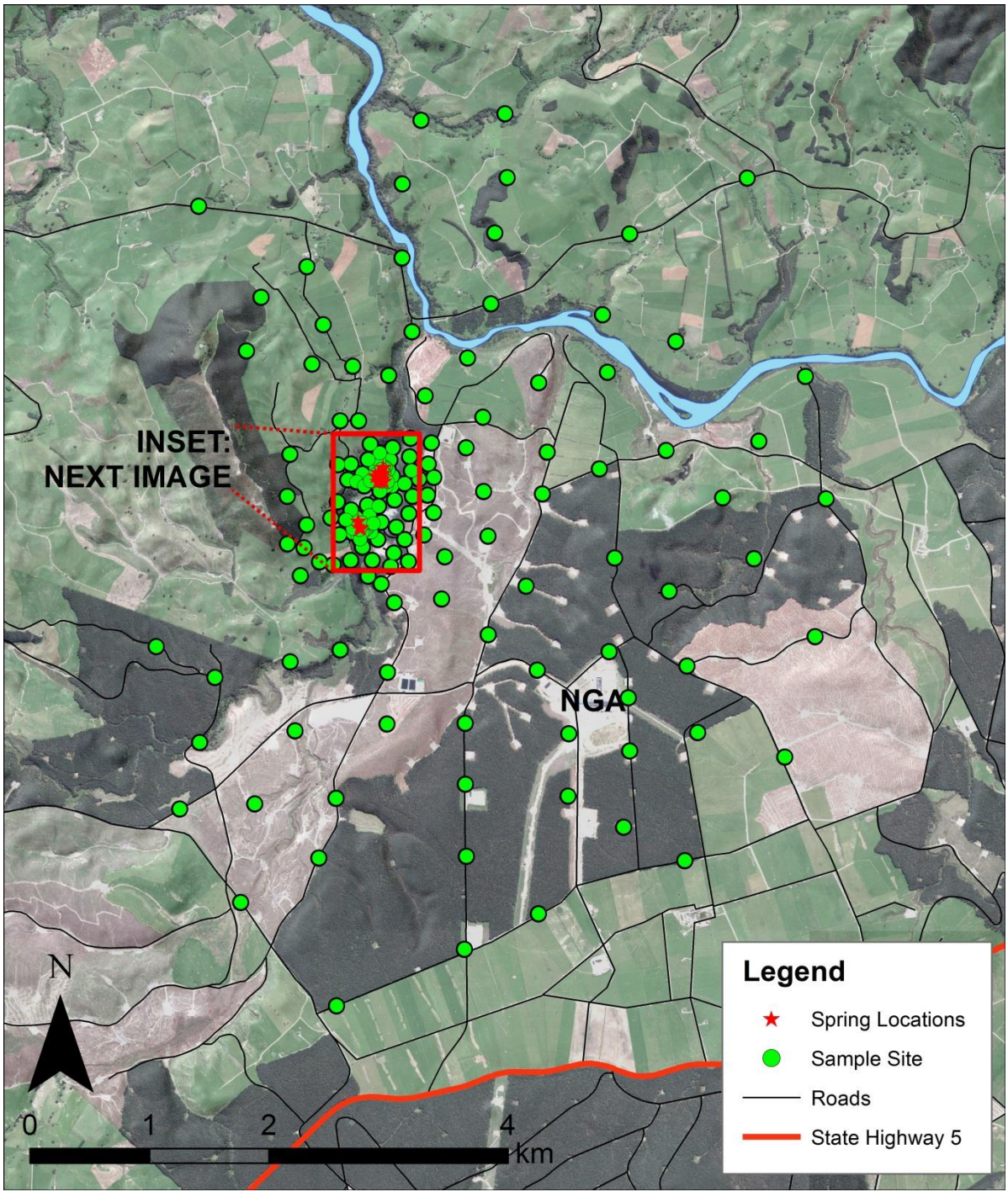

Figure 3.25: Sample sites (green circles) at the Ngatamariki Geothermal Field. The sites are centred around the major geothermal surface expressions, the Orakonui North (OKN) and Orakonui South (OKS) springs. For GIS data sources see section 0 'GIS Data Sources'.

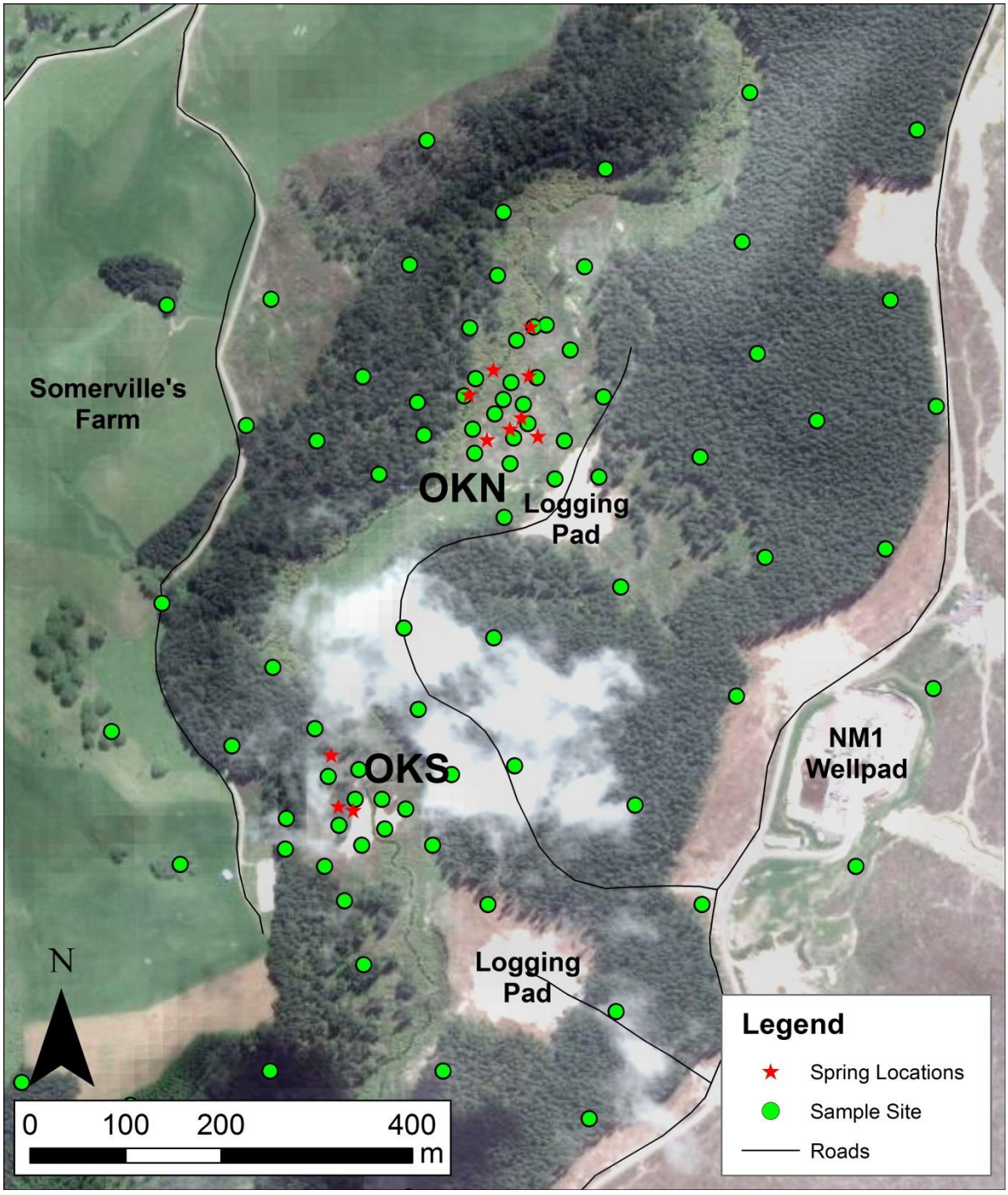

Figure 3.26: Sample sites (green circles) at the Ngatamariki Geothermal Field, focussed on the two geothermal surface expressions, OKN, and OKS. Stars represent individual springs that were identified by this study or through past studies such as O'Brien (2010). For GIS data sources see section 0 'GIS Data Sources'.

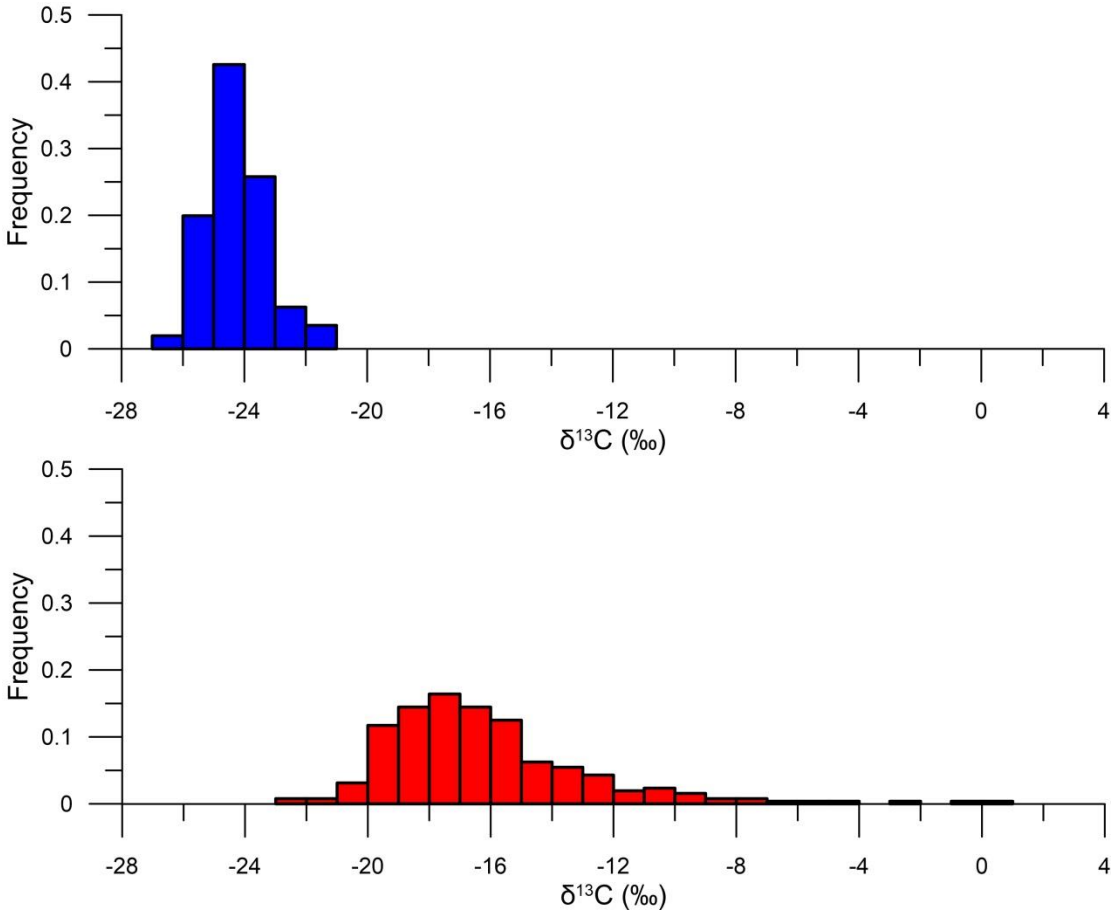

Figure 3.27: Histograms of isotopic composition data from the Ngatamariki Geothermal Area.

Distance to Geothermal Expressions

Using ArcGIS, the distance between each sample site at Ngatamariki to the nearest geothermal expression (either those at OKS or OKN) was derived. Figure 3.28 compares the distance from geothermal expressions to the $\delta^{13}C$ and $\delta^{15}N$ values and shows the grouping of values in the -15 to -20‰ ($\delta^{15}N$) and -23.5 to -25‰ ($\delta^{13}C$) ranges. No obvious patterns are present, other than for a 10% reduction in the standard deviation of $\delta^{13}C$ values as distance increases ($\sigma_{0\text{-}2000m}$: 0.9765‰; $\sigma_{2000\text{-}4000m}$: 0.9053‰).

Figure 3.29 shows the same data, but only the sample sites within 500m of geothermal expressions. There are two $\delta^{13}C$ outliers (-22.621 and -21.444‰), shifted towards more positive values, in the immediate vicinity of geothermal expressions (<25m). Another two outliers (different to the outlier in the $\delta^{13}C$ values) also exist in the $\delta^{15}N$ data (~-10‰) compared to the general clustering of data points (-13 to -20‰). However, when comparing these outliers to the full set of data (0-5000m, Figure 3.28) they appear insignificant.

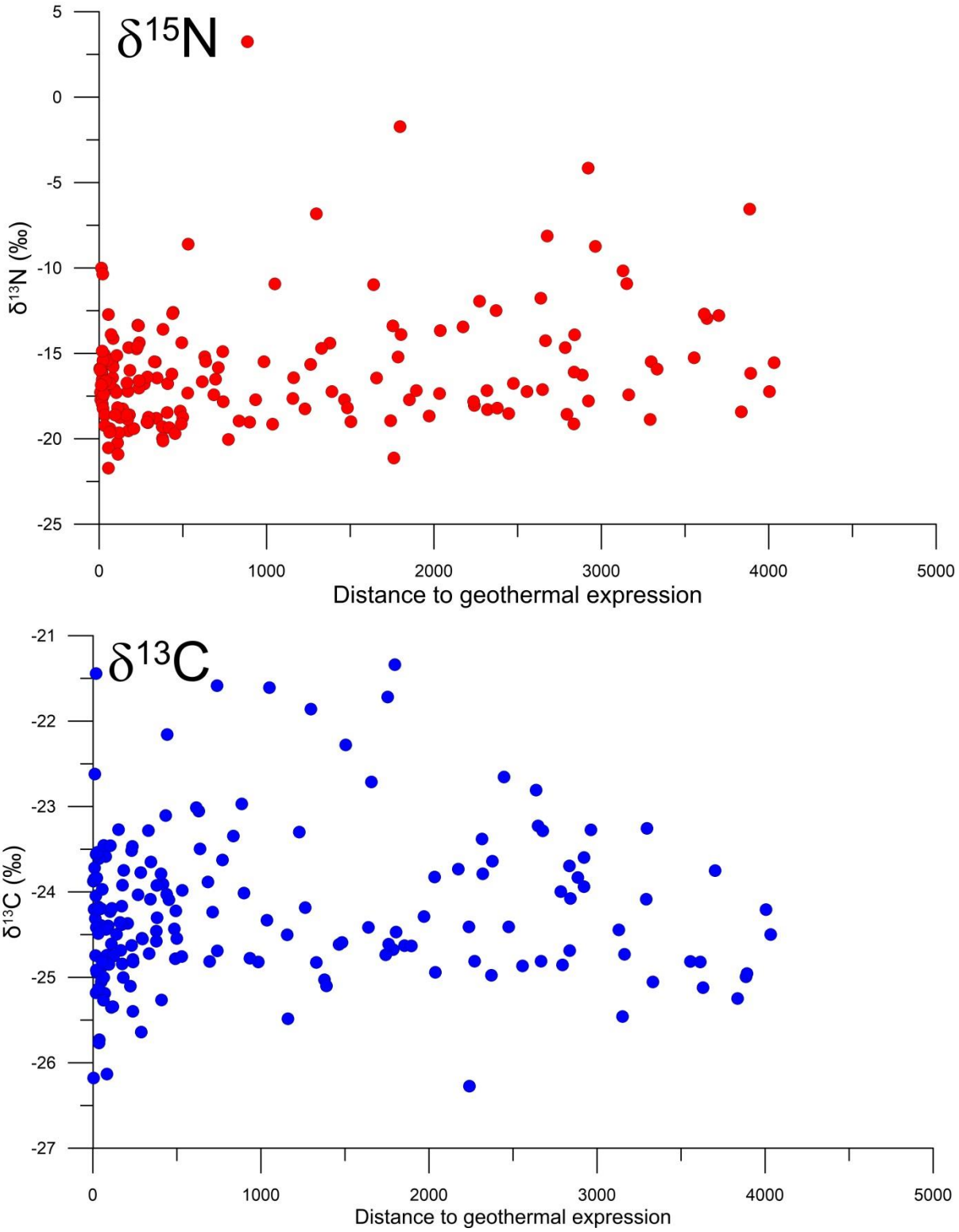

Figure 3.28: Scatterplot to show the relationship between sample sites and the distance to geothermal expressions. Each point represents a single sample site. In the case of a site having two samples; the point is the average of the two.

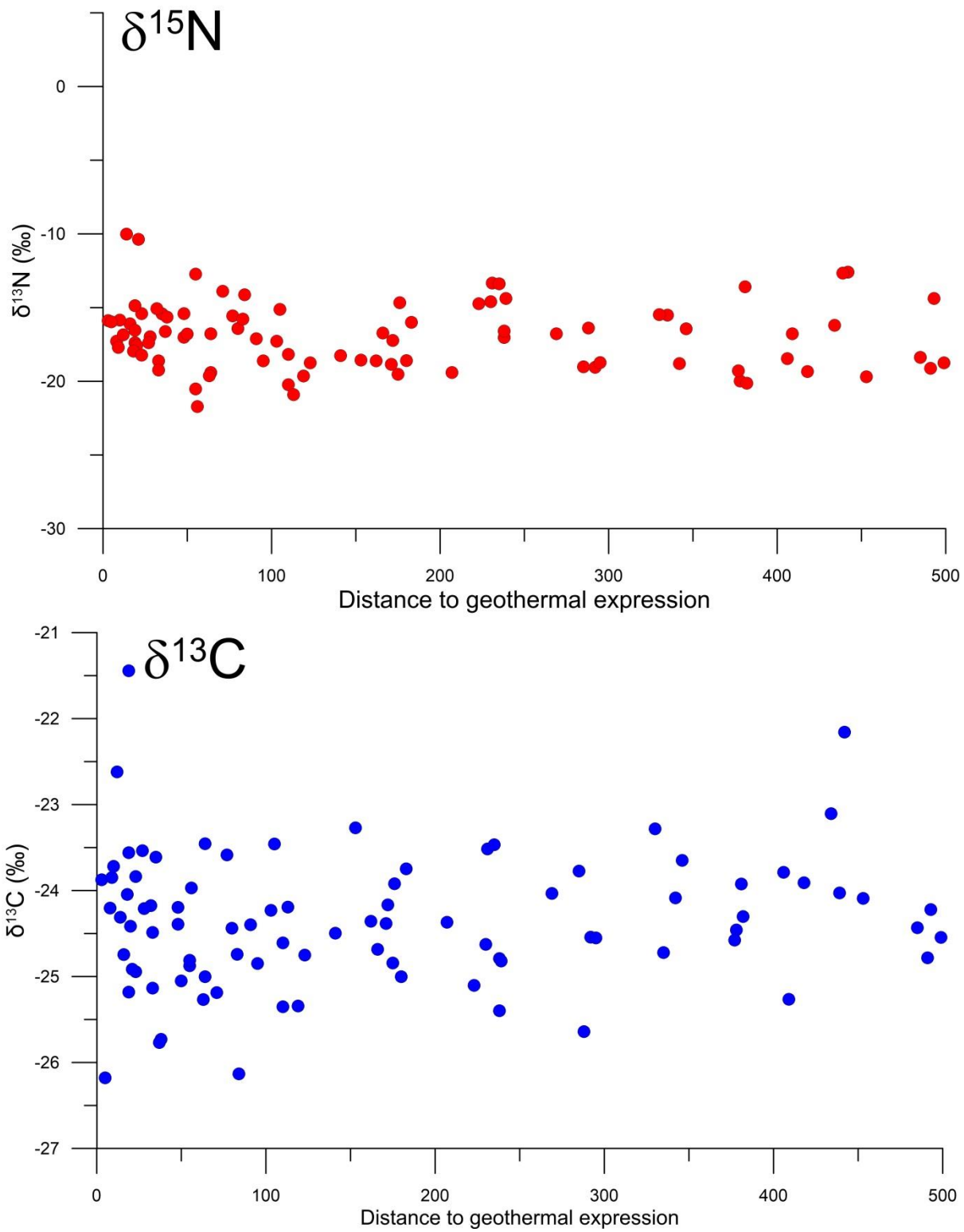

Figure 3.29: Scatterplot to show the relationship between sample sites and the distance to geothermal expressions, restricted to a distance of 500m from geothermal expressions. Each point represents a single sample site. In the case of a site having two samples; the point is the average of the two.

Due to the lack of obvious trends, another approach was used. Each sample site was placed into a distance interval bin. These bin intervals were determined in a way that the sample population within that bin was large enough to assume normality (≥30 samples according to the Central Limit Theorem). T-tests between bin intervals then allowed the testing of significant difference (Student's t-test, α=0.05). The results of these tests, displayed in Table 3.7, show a statistical difference between bins close to (<100m, 100-250m, 250-500m) and far from (2000-3000m, >3000m) geothermal expressions, some at very high degrees of significance (α=0.001).

Table 3.7: Results of the t-tests to determine statistical difference between distance intervals as distance from Ngatamariki geothermal expressions increases.

$\delta^{15}N$

	100-250	250-500	500-1000	1000-1500	1500-2000	2000-3000	>3000
<100m	0.076	0.036*	0.230	0.775	0.324	0.042*	0.007**
100-250m	-	0.744	0.072	0.197	0.129	0.002**	<0.001***
250-500m		-	0.055	0.138	0.105	<0.001***	<0.001***
500-1000m			-	0.357	0.954	0.842	0.602
1000-1500m				-	0.444	0.249	0.050
1500-2000m					-	0.915	0.589
2000-3000m						-	0.271
>3000m							-

$\delta^{13}C$

	100-250	250-500	500-1000	1000-1500	1500-2000	2000-3000	>3000
<100m	0.835	0.049*	0.004**	0.374	0.056	0.017*	0.379
100-250m	-	0.022*	0.002**	0.311	0.043	0.007**	0.457
250-500m		-	0.119	0.810	0.337	0.600	0.009**
500-1000m			-	0.197	0.902	0.261	<0.001***
1000-1500m				-	0.340	0.582	0.170
1500-2000m					-	0.505	0.022*
2000-3000m						-	0.003**
>3000m							-

* significant difference at α=0.05, ** significant difference at α=0.01, *** significant difference at α=0.001.

A statistical difference between isotopic compositions of lichen at increasing distance intervals occurs predominantly in the $\delta^{15}N$ data, while $\delta^{13}C$ is not as distinct. While the $\delta^{15}N$ data shows that there is a statistical difference between samples close to (<100, 100-250mn and 250-500m) and far

away from geothermal expressions (2000-3000m and >3000m), this is not to say these geothermal expressions are the cause (correlation does not imply causation).

The perceived statistical difference may be a result of the increased samples size (n) as distance from OKN and OKS increases. Figure 3.30 shows that the three bins that are greater than 1500m from geothermal features (ie. the “1500-2000m”, “2000-3000m”, and “>3000m” bins), have a greater range which results in these bins becoming statistically different. As the distance from OKN and OKS increases, a greater range of land use classes are present within the distance interval bins. This change in land use class will likely have a concomitant effect on the lichen elemental concentrations and isotope ratios. This issue and the issue of land use impacts are discussed in the following chapter, under Section 4.4 “Land Use”.

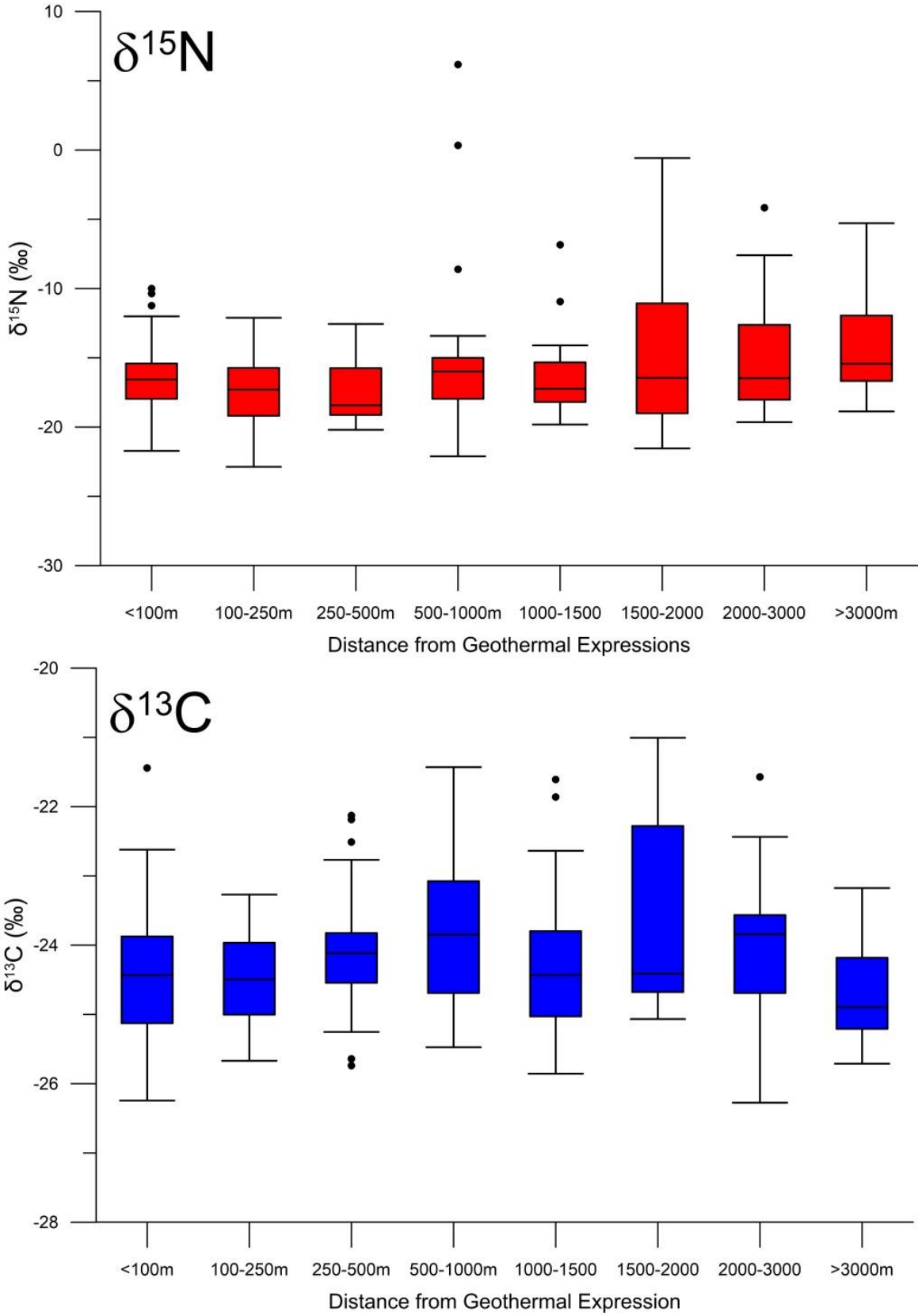

Figure 3.30: Box and whisker representation of the distance interval bins used to determine significant difference between samples close to, and those far away from geothermal expressions. The upper plot (red) shows $\delta^{15}N$, while the lower (blue) represents $\delta^{13}C$. Whiskers represent an IQR factor of 1.5, while black dots represent outliers.

3.3.3 Comparison of Ngatamariki Data with Transect Data

Absolute data ranges from the four study areas (SIT, REW, TNS, and NGA) overlap (Figure 3.32), showing no immediate distinction. The skewed nature of the Ngatamariki samples is similar to those seen in the REW transect, where anomalously high $\delta^{15}N$ values extend well above the mean. These anomalous values are all located in areas of intensive farming (see Section: 4.4 'Land Use').

When 95% confidence intervals are compared (Figure 3.31) it becomes clear that both the $\delta^{13}C$ and the $\delta^{15}N$ values of the lichen populations at Ngatamariki are different from the populations of lichen from all the three transects, at high significance (α=0.001). The differences between carbon contents between Ngatamariki and the three transects is even greater (α=0.001), and while the nitrogen content of Ngatamariki is not significantly different from samples of the SIT (likely due to the wide range of values from the SIT producing a wide confidence interval), there is a significant difference between Ngatamariki and the two North Island transects (α=0.05).

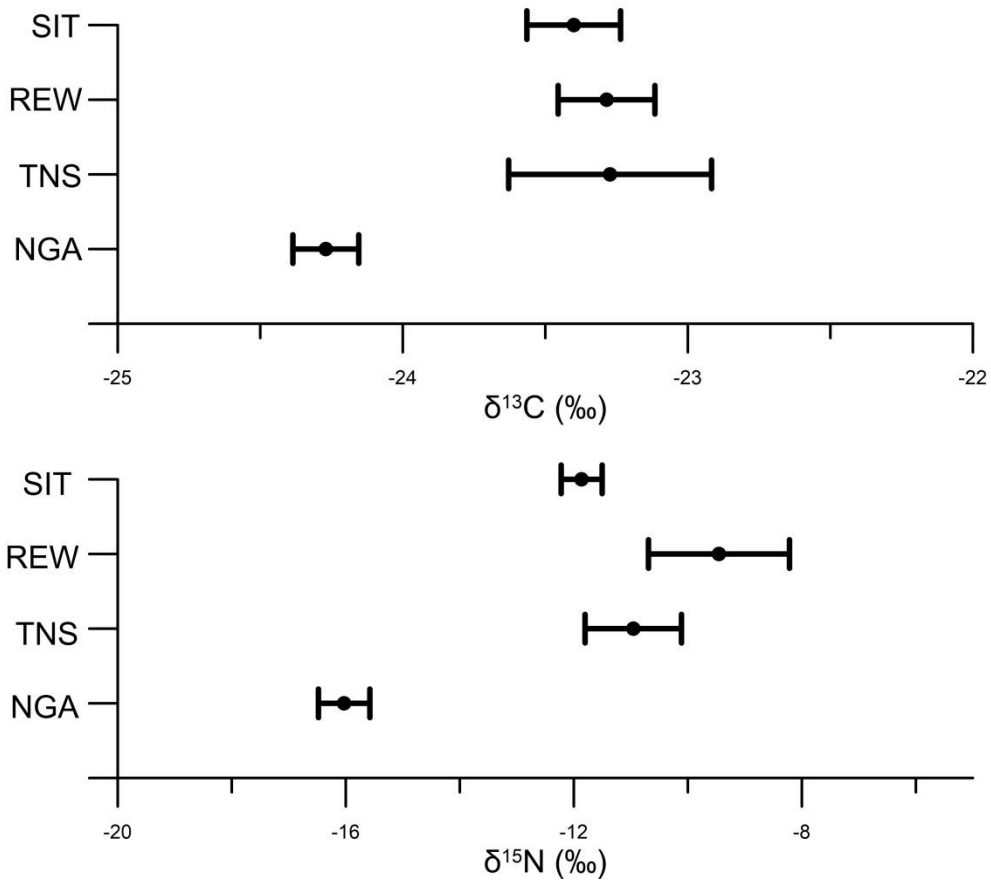

Figure 3.31: Comparison of 95% confidence intervals between the four areas studied in this thesis: South Island Transect (SIT), Rotorua East-West Transect (REW), Taupo North-South Transect (TNS) and the Ngatamariki Geothermal Area (NGA)

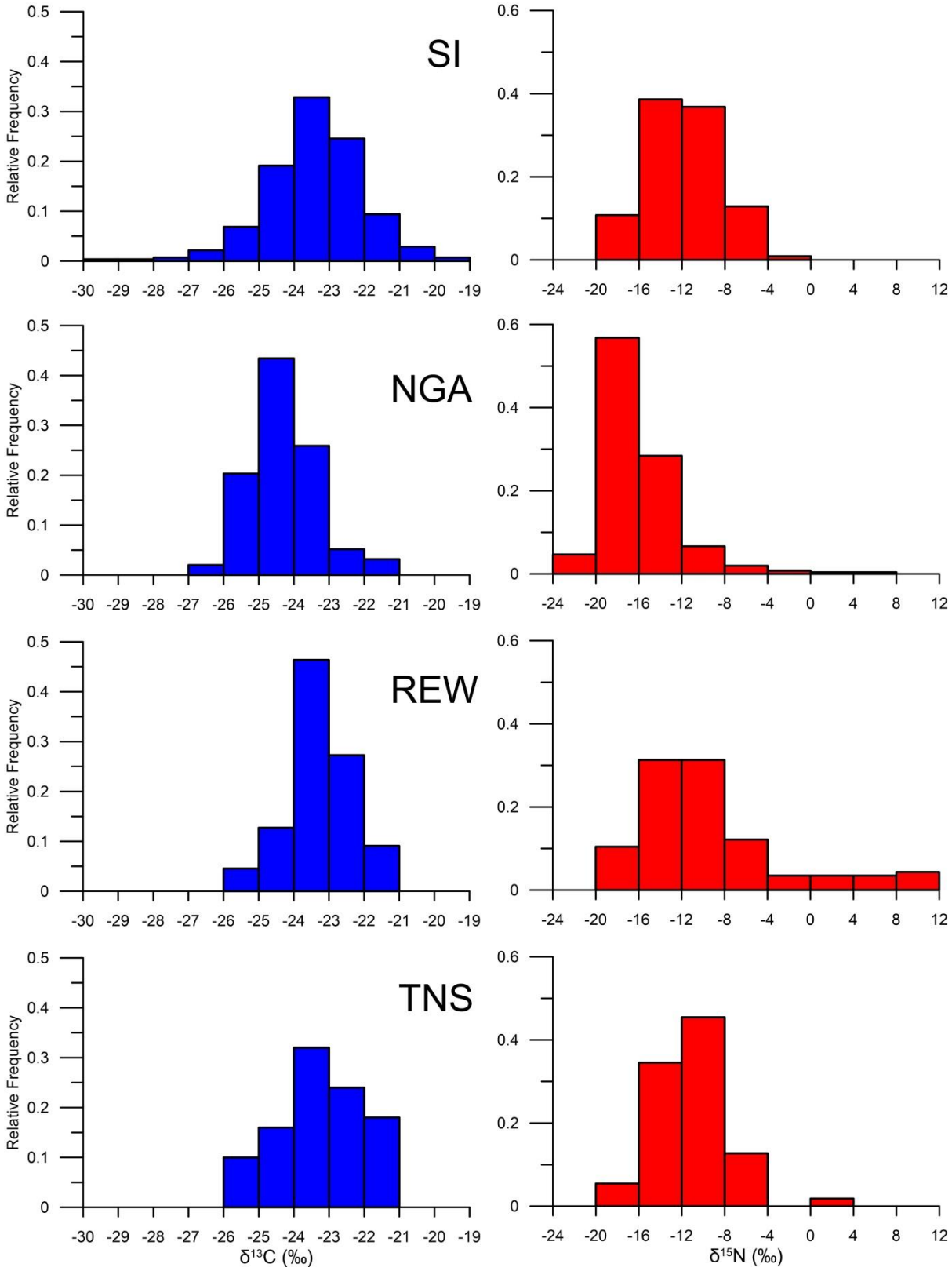

Figure 3.32: Histogram comparison of the four areas investigated in this thesis.

3.4 Chapter Summary

This chapter presented the methodology used to collect and prepare lichen samples and the results from the subsequent analyses. The following section splits these into two parts: first summarising the results of methodology optimisation and secondly summarising the results from the three transects (SIT, TNS, and REW) and the Ngatamariki Geothermal Area.

In terms of methodology and sampling techniques, the follow summary can be made:

- **Washing does not significantly alter (α=0.05) nitrogen or carbon isotopic compositions** (p=0.276 and p=0.901, respectively) or elemental concentrations (p=0.442 and p=0.125, respectively), contrary to data presented by (Gombert *et al.*, 2003). **Page 40**
- **The length of time that samples in this study spent in refrigerated storage (up to 5 months) did not produce a significant difference** (α=0.05) in nitrogen or carbon isotopic compositions (p=0.521 and p=0.979, respectively) or elemental concentrations (p=0.792 and p=0.255, respectively). **Page 41**
- In areas of limited sample availability**, other species may substitute for *Usnea*** (the genus used for the majority of this study) **in terms of δ^{15}N and C%**, while δ^{13}C and N% values appear to be significantly different (α=0.05) between the genera studied. **Page 53**
- There exists **a correlation between isotopic compositions/elemental concentrations and distance to lichen thallus stem** (in *Usnea*). Homogenisation of samples by crushing with liquid nitrogen removes the variability caused by selecting a sample from different parts of the thallus. **Page 57**
- **Homogenisation of lichen samples plays a large part in reducing variability**, shown by the high variability of non-homogenised samples of the SIT (n/site=5, σ=0.976) compared to those of the NIT (n/site=5, σ=0.639). **Page 54**
- **Sample size (number of samples analysed per site) may also play an important part in reducing variability**, shown by the large confidence interval ranges seen in Ngatamariki sites (n/site=2) compared to North Island Transect sites (n/persite=5), which were prepared in the same way. **Page 54**
- Regardless of the prior two points, **sample variability remains high**. **Page 54**

In terms of the SIT, REW, TNS, and Ngatamariki data, the following summary can be made:

- **South Island Transect**: While no patterns are obvious in the δ^{13}C and δ^{15}N values along the SIT, anomalously high nitrogen contents are seen which correlate with samples taken from

the Canterbury Plains. Low nitrogen contents are seen for the remainder of the SIT to the west. **Page 59**

- **Rotorua East-West Transect**: The negative trend of the $\delta^{15}N$ values from west to east correlates with the change in land use type from intensive farming to exotic and native forest. This trend is not reproduced by $\delta^{13}C$ values, but is mirrored by nitrogen content. **Page 67**
- **Taupo North-South Transect**: $\delta^{15}N$ is higher in the northern and southern sections, and lower in the central area (including Ngatamariki). Nitrogen content is again highest in areas of farmland between Rotorua and Ngatamariki. **Page 70**
- **Ngatamariki**: It appears that the $\delta^{15}N$ values of lichen close to geothermal expressions are significantly different to areas further away. However it is unclear whether this difference is a result of geothermal influence or changes in land use. **Page 76**

  Both the $\delta^{13}C$ and $\delta^{15}N$ values of the Ngatamariki lichen population is different to the populations of the three transects at high significance (α=0.001). **Page 85**

A tabulated summary of the three transects and the Ngatamariki data is shown below in Table 3.8.

Table 3.8: Summary table of the four areas investigated in this thesis: South Island Transect (SIT), Rotorua East-West Transect (REW), Taupo North-South Transect (TNS) and the Ngatamariki Geothermal Area (NGA). Table A summarises $\delta^{13}C$ data, while table B summarises $\delta^{15}N$ data. The minimum, maximum, standard deviation, and 95% confidence intervals are in units of per mil (‰).

A)	n	Minimum	Maximum	Std. Deviation	95% Confidence Interval
SIT	277	-29.162	-19.547	1.389	-23.40 ± 0.16
REW	110	-25.696	-21.087	0.898	-23.29 ± 0.17
TNS	50	-25.712	-21.087	1.253	-23.27 ± 0.36
NGA	251	-26.274	-21.004	0.863	-24.27 ± 0.12

B)	n	Minimum	Maximum	Std. Deviation	95% Confidence Interval
SIT	334	-19.551	-1.851	3.340	-11.86 ± 0.36
REW	115	-18.001	11.643	6.696	-9.45 ± 1.24
TNS	55	-18.149	0.049	3.128	-10.96 ± 0.85
NGA	257	-22.870	6.170	3.672	-16.03 ± 0.45

4 Interpreting Controls on Lichen Isotopes

The previous chapter (Chapter 3) examined the results of the analysis of lichen isotopic compositions and elemental concentrations from three transects (South Island, Rotorua East-West, and Taupo North-South Transects) and the Ngatamariki Geothermal area. This chapter aims to examine these results in more detail, ultimately answering the main goal for this thesis: can nitrogen and carbon isotopes in lichen be used for geothermal exploration?

The chapter begins by comparing the isotopic compositions recorded in this study to those presented in the literature, before briefly investigating environmental factors: the effect of elevation (Page 93), sample distance to road (Page 96), and the control of land use on the isotopic compositions of lichen samples (Page 98). The final section presents and discusses isoscapes of the Ngatamariki Geothermal areas and their implications for this study (Page 121).

4.1 Isotopic composition comparison with values in the Literature

A recent paper by Tozer *et al.* (2005) followed a similar hypothesis to that of this study, attempting to examine the relationship between nitrogen isotopic composition and geothermal expressions. Tozer used both lichen (*Usnea*, *Cladia*, *Cladonia*, and *Ramalina* sp.) along with an epiphyte known as *Trentepholia*, a free living alga that is also a common partner in the lichen symbiosis. The study examined *Trentepholia* samples along a transect between Hamilton (non-geothermal source) and Rotorua (geothermal source), on which the REW transect was based, and also analysed samples from Te Kopia, an active geothermal site midway between Taupo and Rotorua.

The Te Kopia geothermal area, roughly 15km north of the Ngatamariki Geothermal Field, is hosted by the Paeroa Fault Zone, and at the surface consists of steaming ground, mud and acid sulphate pools, and multiple fumaroles (Soengkono, 1999). Both *Trentepholia* and lichen samples were collected by Tozer in the immediate vicinity of the major geothermal expression (<40m), finding similar values to the values obtained in this study from Ngatamariki (Figure 4.1). When comparing samples within 40m of geothermal features from Tozer to this study, Tozer's lichen samples were significantly depleted in terms of $\delta^{15}N$ values (~2‰ more depleted, Figure 4.1A, one tailed students t-test, $\alpha=0.01$) while the nitrogen content was very similar (Figure 4.1B, two tailed t-test, $p=0.660$). *Trentepholia* was even more depleted again (~6‰ more depleted than this study, Figure 4.1A), and nitrogen contents were much higher (~2% N by dry weight, Figure 4.1B). These values from *Trentepholia* concur with data presented in Beck & Mayr (2012), showing that the photobiont of the lichen symbiosis (the algal partner), in this case simulated by *Trentepholia,* is more depleted in $\delta^{15}N$ and with a higher nitrogen content.

Over the large scale (Rotorua to Hamilton) *Trentepholia* displays more negative $\delta^{15}N$ values than the $\delta^{15}N$ of this studies lichen (Figure 4.2A), as expected, although nitrogen contents are lower in the western portion, which was not expected (Figure 4.2B). Sampling points are much less consistent in Tozer's study, and large portions of the most western section of Tozer's Rotorua-Hamilton transect lacks observations (0-50km). This hinders comparison, although from the data available it appears that there is no correlation between the two data sets, nor the distance from a geothermal area (Rotorua). This study would benefit if the observations by Tozer continued to the east of Rotorua (100-160km) to confirm the negative trend seen through observations from this study.

Tozer attributes the highly depleted $\delta^{15}N$ values to dual fractionation steps: firstly fractionation from the volatilisation of NH_3 to the atmosphere (diffusion from a source) from intensive farming products (fertilisers, animals wastes etc.), and secondly, fractionation during the diffusive uptake (diffusion into a sink) of already depleted $\delta^{15}N$ by epiphytes (in Tozer's case by the alga genus *Trentepholia*, in this studies case by the lichen genus *Usnea*).

In analysing both large scale (Rotorua to Hamilton) and small scale (<40m from major geothermal expressions) Tozer *et al.* (2005) found "no relationship [between $\delta^{15}N$ values and] proximity to geothermal source, with Trentepholia samples in Hamilton [(far proximity to geothermal expressions)] having similar $\delta^{15}N$ depletion to those in Rotorua [(close proximity to geothermal expressions)]."

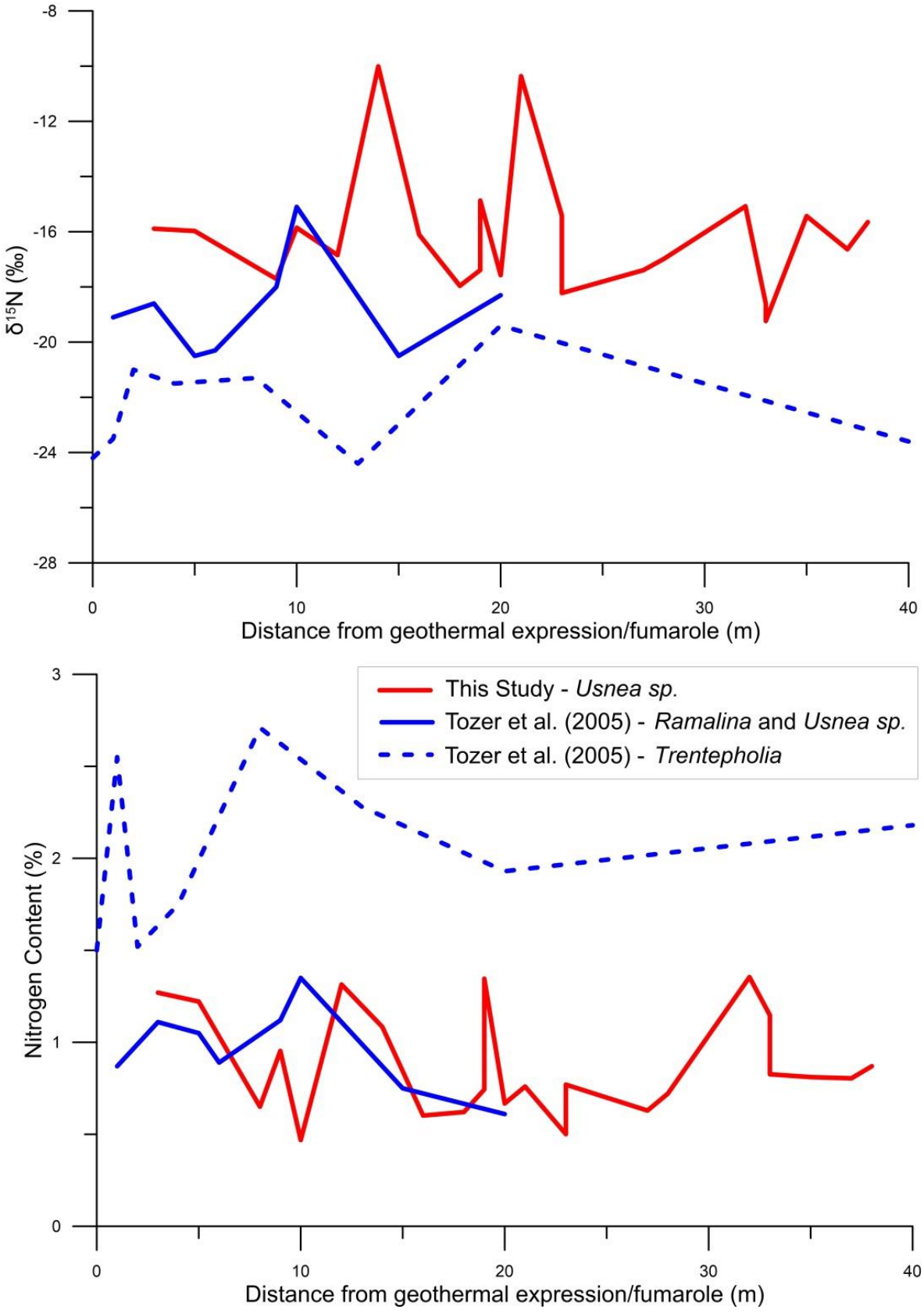

Figure 4.1: Change in $\delta^{15}N$ and nitrogen contents as distance from geothermal expressions increases, comparing data from Tozer *et al.* (2005, dashed and solid blue lines) to values obtained in this study (red line). The dashed blue line refers to values obtained from Trentepholia (an alga that lives freely, but is commonly found as a partner in the lichen symbiosis), while the solid line refers to values obtained from the lichen genera *Ramalina* and *Usnea*.

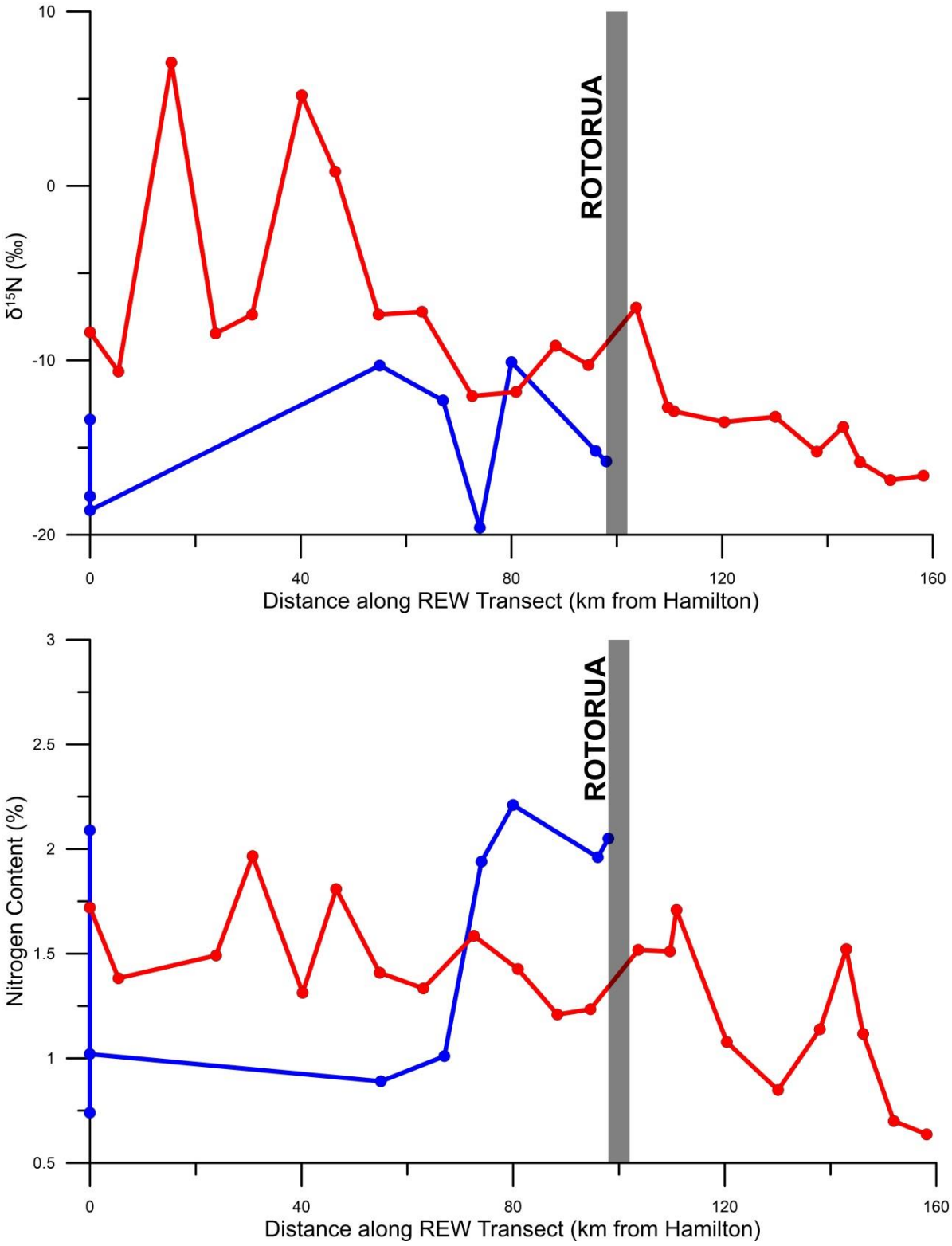

Figure 4.2: Comparison of A) $\delta^{15}N$ values, and B) nitrogen contents between this study and that of Tozer across the western portion of the REW transect.

4.2 Elevation

Elevation is a possible control for nitrogen and carbon isotopes of lichen across the South Island, and was subsequently analysed. Cuna *et al.* (2007) investigated this matter over the elevation range of 1000-1500masl using two lichen species (*Hypogymnia physodes* and *Pseudevernia furfuracea*) and found a positive correlation between altitude and $\delta^{13}C$ values, while Biazrov (2012) completed an altitudinal transect between 1550 and 3250masl and found local scale decrease in $\delta^{15}N$ values as elevation increases, however Biazrov found no correlation between elevation and $\delta^{15}N$ over a regional scale. The South Island Transect collected samples from near sea level (Christchurch, 11m, and Kumara Junction, 30m) to elevations of almost 1000masl. (Porters Pass, 947m, and Arthurs Pass, 918m). Sites were grouped into elevation bins of 200m intervals, as this was the smallest appropriate interval that maintained a sample size of >30 (when any two given bins were combined), and therefore allowed for application of the central limit theorem.

As shown in Table 4.1 and Figure 4.3, change in elevation has no significant impact on carbon or nitrogen isotopes in lichen across the South Island (t-test, $\alpha = 0.05$). An interesting factor shown by the box-and-whisker plots in Figure 4.4, is the decrease in the range of both nitrogen and carbon concentrations as elevation increases. This is likely due to the decreasing sample size of the higher elevation bins, and also due to the lower elevation bins representing large variations in land use class, from highly intensive farming (high N%) to low elevation native bush and urban environments (low N%). The reduction in variability can be seen in the $\delta^{13}C$ and $\delta^{15}N$ graphs in Figure 4.4, however it is much less pronounced, and is likely due to the same factors as mentioned for nitrogen and carbon contents.

Table 4.1: T-test matrix analysing the impact of elevation on $\delta^{13}C$ and $\delta^{15}N$ isotope values. No elevation ranges are significantly different at 95% confidence.

$\delta^{13}C$

	200-400	400-600	600-800	800-1000
0-200m	0.168	0.995	0.002	0.015
200-400m	-	0.493	0.160	0.080
400-600m		-	0.121	0.220
600-800m			-	0.254

$\delta^{15}N$

	200-400	400-600	600-800	800-1000
0-200m	0.773	0.132	0.152	0.523
200-400m	-	0.092	0.580	0.438
400-600m		-	0.205	0.765
600-800m			-	0.613

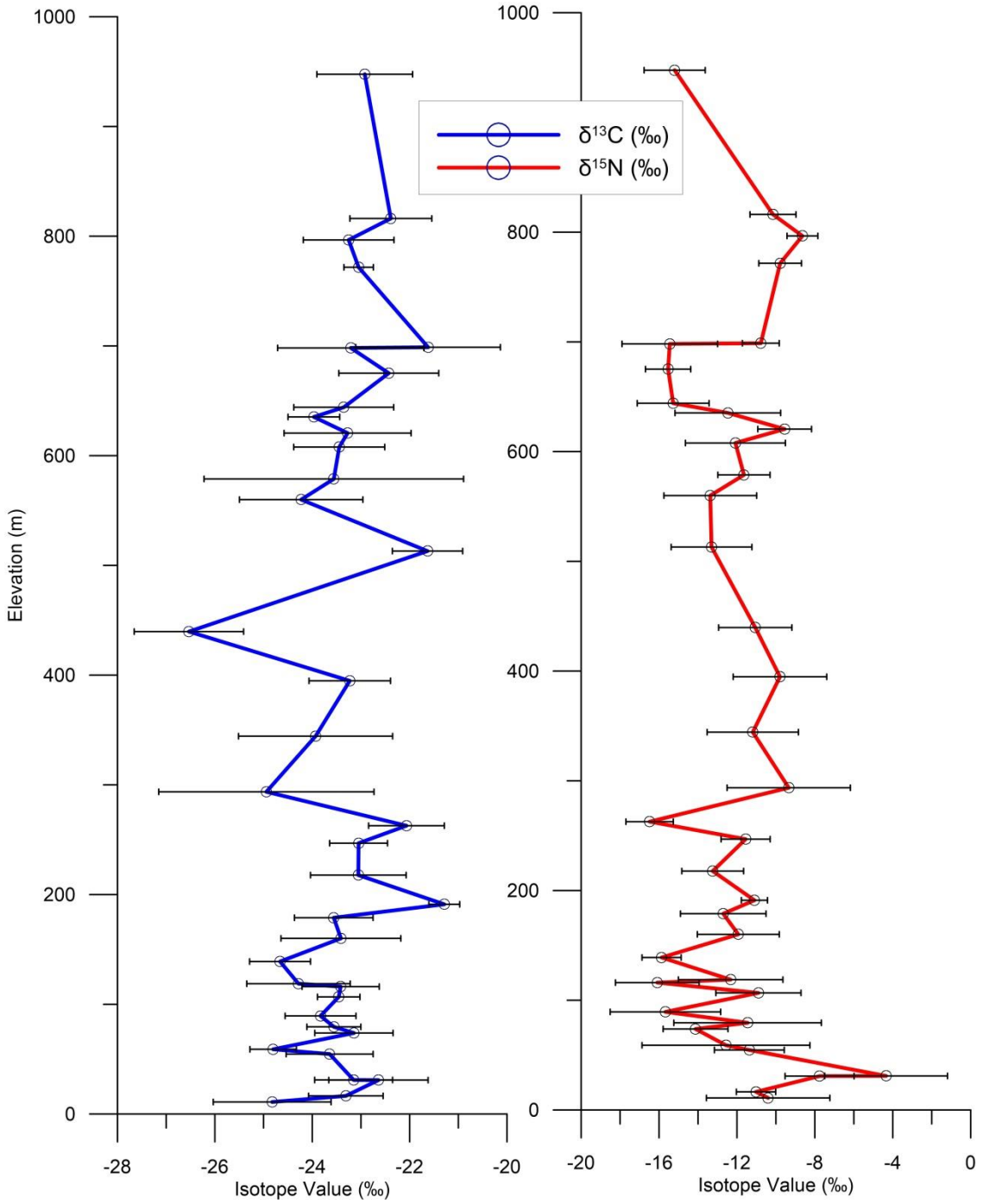

Figure 4.3: The relationship of isotope values and elevation at the sample sites along the South Island Transect. Error bars represent one standard deviation either side of the mean (±1σ).

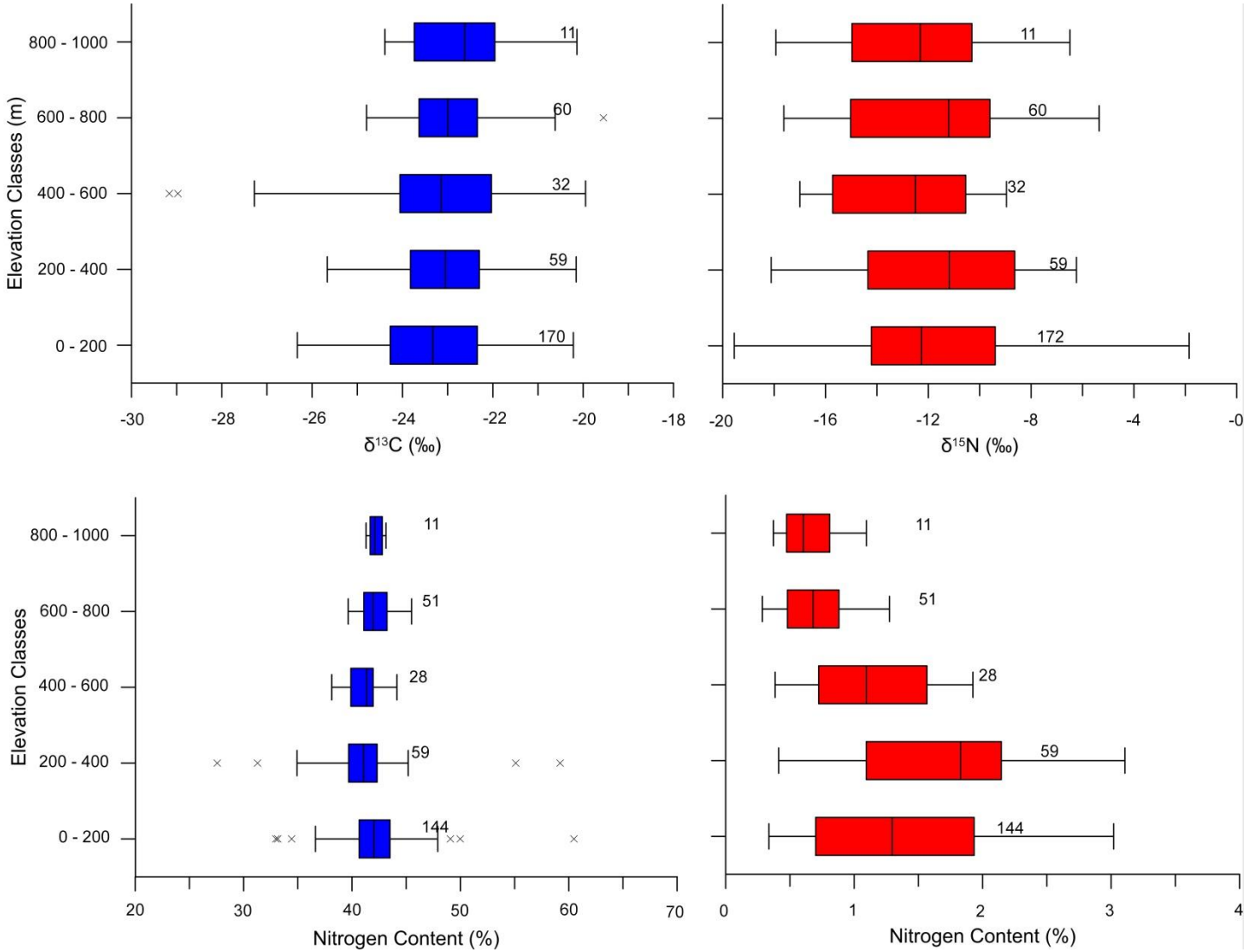

Figure 4.4: The ranges of elevation bins with respect to the parameters analysed in this study. Reading left to right, top to bottom (when reading the correct way up) a) $\delta^{13}C$, b) $\delta^{15}N$, c) C%, d) N%. Whiskers represent a 1.5 IQR factor, while x symbols represent outliers. The numeric value indicates the sample size of the associated elevation range.

4.3 Distance to Road

The proximity of lichen to major roadways has been shown to impact lichen health (Angold, 1997). There are, however, mixed results in terms of the distance of lichen to roadways and the impact on nitrogen concentrations. Gombert *et al.* (2003) showed positive correlations with traffic volume and nitrogen contents, although Frati *et al.* (2006) monitored a highway with traffic volumes of ~10,000 vehicles per day (SIT:<1500 vehicles/day, REW/TNS: 2000-5000 (SH5) and ~8000 (SH1); Department of Conservation, 2007; NZ Transport Agency, 2011) and observed that the proximity to traffic had no significant impact on nitrogen concentrations. Lichen in close proximity (<20m) to roadways are supplied with a nitrogen source (NO_2 and NH_3; Cape *et al.*, 2004; Gadsdon & Power, 2009) that is not usually available in such large quantities to lichen in a completely natural environment, altering the uptake and fractionation pathways of these nutrients, ultimately changing the $\delta^{15}N$ values. Therefore, the contradiction in the literature requires examination in this study.

Distance to road was derived in ArcGIS using the "Near" function on samples sites (corrected where GPS accuracy was low) and the Land Information New Zealand (LINZ) road centrelines (1:25000; corrected using georeferenced satellite imagery from ArcMap's "world Imagery" basemap). Figure 4.5 shows that there is very little/no correlation between isotopic compositions or elemental concentrations of carbon or nitrogen in relation to road proximity.

However, as the SIT covers a range of land use types, which strongly control isotopic composition and elemental concentrations (see Section: 4.4 'Land Use'), a more robust experiment is required to completely dispel this hypothesis, with sampling locations extending perpendicular from roadsides at a single location to determine any possible concentration or isotopic composition gradients.

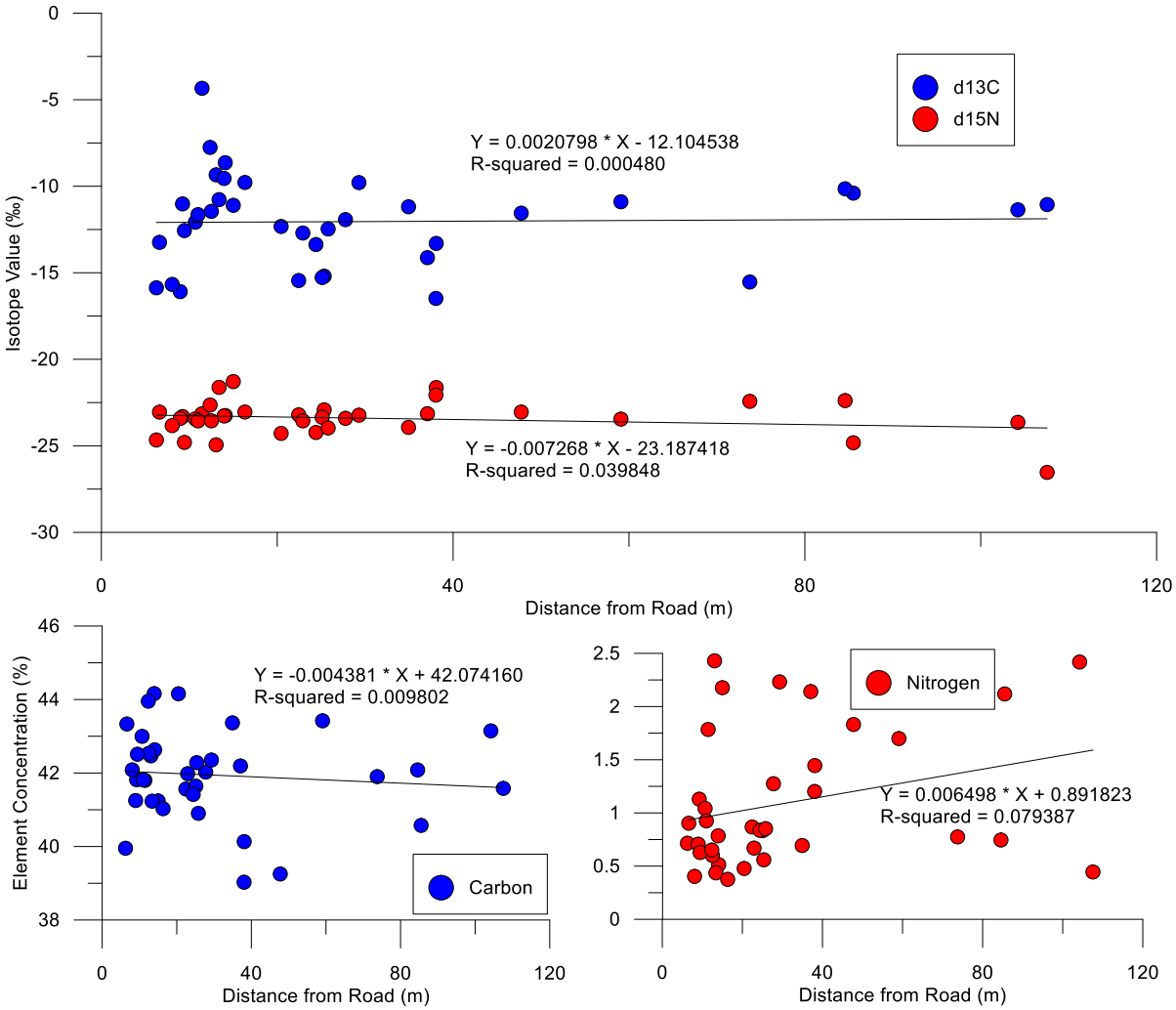

Figure 4.5: Investigation of the distance of SIT sites to the road and the impact of this on the measured parameters. No major correlations can be seen either isotope values or elemental concentrations of nitrogen or carbon.

4.4 Land Use

Land use controls on nitrogen and isotopes are examined on a case-by-case basis at the three major study locations to avoid complications through changing study areas. These three areas are the South Island Transect (SIT), North Island Transects (NIT, including both REW and TNS), and Ngatamariki (NGA).

4.4.1 Land Types

Land use was simplified to **farmland**, **anthropogenic**, **native forest**, **exotic forest**, and in the case of Ngatamariki, **slash**. Farmland is the most common for the two transect groups, while sites in areas of exotic forest far outweigh the other categories at Ngatamariki (Table 4.2).

Table 4.2: Number of sites (SIT, NIT, and NGA) and proportion of land covering the Ngatamariki Geothermal Area (NGA) by different land use types. The bracketed SIT farmland site count shows the number of intensive to extensive farming land types (Intensive: Extensive).

	Farmland	Anthropogenic	Native Forest	Exotic Forest	Slash
SIT	23 (16:7)	2	11	1	-
NIT	15	2	5	5	-
NGA	28 (52.1%)	- (0.6%)	33 (5.5%)	93 (25.6%)	16 (15.3%)

Farmland

Farmland includes areas of intensively cultivated land intended for grazing animals (Figure 4.6 and Figure 4.7). Notable areas in this study include the Canterbury Plains, the western Rotorua East-West transect, and the northern section of the Ngatamariki Geothermal Field.

In the SIT, farming is distinguished as being intensive farming (Canterbury Plains and West Coast) or extensive farming (Porters Pass to Arthurs Pass).

Samples were generally collected from fence-posts or shelter-belt trees (both native and exotic).

Anthropogenic

Anthropogenic refers to sample sites located in established urban areas or areas of extensive construction by humans (Figure 4.8). This is the least common land use type, as most sample sites are well away from these sources, although a number of samples in the eastern SIT were included under this land type.

Samples were generally collected from fence posts, walls, and trees.

Native Forest

Native forest refers to areas of relatively undisturbed flora. It is predominant in this study in the western SIT and the eastern REW transect (Figure 4.9). The scrubland at Ngatamariki is included as native forest and is part of Department of Conservation (DOC) land, although the area is invaded by wild pine (from the adjacent pine plantations) and other non-native species such as gorse, broom, and creepers (Figure 4.10).

Samples were generally collected from tree trunks and branches.

Exotic Forest

Exotic forest refers to areas and stands of non-native/exotic trees, generally from the genus *Pinus*. Sample sites from this land use type occur mostly in the eastern REW and at Ngatamariki (Figure 4.7 and Figure 4.11).

At Ngatamariki, the pine plantations are all approaching harvesting and were planted between 1978 and 1991 (Wairakei Pastoral Ltd., 2013b). Upon harvesting the land use changes to slash, although some farmland in the northern section (immediately south of the Waikato River) was recently (2007) rehabilitated to farmland (Wairakei Pastoral Ltd., 2013a).

Samples were generally collected from tree trunks and branches.

Slash

Slash refers to areas of recently harvested exotic forest stands (Figure 4.12). Slash only occurs at Ngatamariki sites, and is very similar to that of exotic forest. Depending on the time elapsed since deforestation, the area may be still contain tree stumps, roots, branches and other debris, or may have been sieved to remove this debris. In the foreground of Figure 4.7, small patches of weeds can be seen, while the remainder of the ground is bare soil

Problems arise in these areas for sample collection, as there is little for lichen to grow on. All samples from areas of slash were recovered from debris left from deforestation such as branches, although it is unknown how far the samples have been moved from the original growth site. These samples are treated with caution.

Figure 4.6: Satellite view of the 'farmland' type of land use, in this case at sample site CC007 from the South Island Transect. Image is roughly 4km from east to west. From Google Earth & DigitalGlobe (2014).

Figure 4.7: Example of three land use types, exotic forest (background), farmland (midground), and slash (foreground). Land use type 'slash' is only applicable to Ngatamariki samples. Image taken immediately south of the Waikato River near the confluence of the Orakonui Stream and Waikato River (Site: NGA143). Image looks to the south-east.

Figure 4.8: Satellite view of the 'anthropogenic' type of land use. In this case it is near the start of the SIT, in western Christchurch. Field of view is roughly 1km from east to west. From Google Earth (2014).

Figure 4.9: Satellite view of the 'native forest' type of land use. In this case it is at the sample site REW002 (green circle, centre) along the Rotorua East-West transect, in the Te Urewera National Park. Field of view is roughly 2km east to west. From Google Earth & DigitalGlobe (2014e).

Figure 4.10: An example of the 'scrubland' at Ngatamariki that has been labelled as Native Bush, although the area is invaded by non-native plants such as pine trees (background), gorse, and broom (lower right). Image taken to the north-east of the OKN springs, facing roughly north down the Orakonui Stream.

Figure 4.11: Satellite view of the 'exotic forest' type of land use. In this case it shows sample sites (green circles) in the eastern section of the Ngatamariki Geothermal Field, and shows the area of pine in the background of Figure 4.7. Field of view is roughly 2km east to west. From Google Earth & DigitalGlobe(2014c).

Figure 4.12: Satellite view of the 'slash' type of land use. In this case it shows sample sites (green circles) in the central section of the Ngatamariki Geothermal Field. The built-up area in the top-right is a well pad (NM1), and the Orakonui springs are to the west (left) and north-west (upper left corner) of the image. Field of view is roughly 1km east to west. From Google Earth & DigitalGlobe (2014d).

4.4.2 SIT Land Use

Along the SIT, the $\delta^{13}C$ of extensive farmland is not significantly different to native forest (p=0.081) or intensive farmland (p=0.238; Table 4.3A), while intensive farmland is significantly different to native forest (p=<0.001) and anthropogenic (p=<0.001) land uses. In terms of $\delta^{15}N$, there is no significant difference between anthropogenic land use and native forest (p=0.123) and intensive farmland (p=0.977), while all other pairs there is significant difference (Table 4.3B). This matches well with the data seen comparing the Canterbury Plains (mostly intensive farmland) to the values seen in the western portion of the SIT (see Section: 'SIT Results', page 59).

There is no significant difference between any two land use types in terms of carbon content (Table 4.3C), while all land use types are significantly different in terms or nitrogen content, apart from the comparison of anthropogenic to intensive farmland (p=0.105; Table 4.3D)

Table 4.3: Students t-test results for the difference in land use types across the SIT for A) $\delta^{13}C$, B) $\delta^{15}N$, C) C%, and D) N%. All use the same null hypothesis (H_o: $\mu_{(Land\ Use\ Type\ A)} = \mu_{(Land\ Use\ Type\ B)}$) and level of significance (α=0.05).

A)

	Native	Farmland (Intensive)	Farmland (Extensive)	Anthropogenic
Native	-	<0.001	0.081	0.056
Farmland (Intensive)		-	0.238	<0.001
Farmland (Extensive)			-	0.002
Anthropogenic				-

B)

	Native	Farmland (Intensive)	Farmland (Extensive)	Anthropogenic
Native	-	0.036	0.003	0.123
Farmland (Intensive)		-	<0.001	0.977
Farmland (Extensive)			-	<0.001
Anthropogenic				-

C)

	Native	Farmland (Intensive)	Farmland (Extensive)	Anthropogenic
Native	-	0.622	0.661	0.624
Farmland (Intensive)		-	0.164	0.894
Farmland (Extensive)			-	0.323
Anthropogenic				-

D)

	Native	Farmland (Intensive)	Farmland (Extensive)	Anthropogenic
Native	-	<0.001	<0.001	<0.001
Farmland (Intensive)		-	<0.001	0.105
Farmland (Extensive)			-	<0.001
Anthropogenic				-

4.4.3 NIT Land Use

The results of statistical testing from the NIT (both REW and TNS combined) show that there is no significant difference between land use types in terms of $\delta^{13}C$ (Table 4.4A). This is surprising as it is contrary to the data presented from the Ngatamariki land use types, which used a very similar classification system.

There is no significant difference between exotic and native forest in terms of $\delta^{15}N$ ($p=0.201$; Table 4.4B), while farmland is different to both ($p<0.001$ and $p=0.009$, respectively). Anthropogenic land use, while having a low sample count (Table 4.2), appears significantly different to exotic forest ($p<0.001$), but not to farmland ($p=0.213$) or native forest ($p=0.068$).

In terms of carbon content, only farmland and exotic forest have statistically different data populations (Table 4.4C), although both intensive land use types – farmland and anthropogenic – show significant difference to exotic ($p<0.001$ and $p=0.013$, respectively) and native forest ($p=0.002$ and $p=0.049$, respectively; Table 4.4D). There is no significant difference between the nitrogen content of lichen in farmland and anthropogenic ($p=0.565$) or exotic and native forest ($p=0.812$).

Table 4.4: Students t-test results for the difference in land use types across the NIT for A) $\delta^{13}C$, B) $\delta^{15}N$, C) C%, and D) N%. All use the same null hypothesis (H_o: $\mu_{(Land\ Use\ Type\ A)} = \mu_{(Land\ Use\ Type\ B)}$) and level of significance ($\alpha=0.05$).

A)

	Exotic	Native	Farmland	Anthropogenic
Exotic	-	0.068	0.250	0.584
Native		-	0.304	0.374
Farmland			-	0.843
Anthropogenic				-

B)

	Exotic	Native	Farmland	Anthropogenic
Exotic	-	0.201	<0.001	<0.001
Native		-	0.009	0.068
Farmland			-	0.213
Anthropogenic				-

C)

	Exotic	Native	Farmland	Anthropogenic
Exotic	-	0.868	0.046	0.871
Native		-	0.076	0.993
Farmland			-	0.081
Anthropogenic				-

D)

	Exotic	Native	Farmland	Anthropogenic
Exotic	-	0.812	<0.01	0.013
Native		-	0.002	0.049
Farmland			-	0.565
Anthropogenic				-

4.4.4 Ngatamariki Land Use

The distribution of land use at Ngatamariki (Figure 4.13) consists of an east-west belt of exotic forest, slash, and native bush, bound to the north and south by farmland. Under the map extent of Figure 4.13, farmland covers the greatest area (52.5%), with exotic forest (25.6%), slash (15.3%) and native forest (5.5%) covering the majority of the remaining area. Small areas of land are attributed to anthropogenic (0.6%; well pads, power plant infrastructure) and river (0.8%).

In terms of $\delta^{13}C$, farmland is significantly different to all other land use types (students t-test, H_o: $\mu_{(Land\ Use\ Type\ A)} = \mu_{(Land\ Use\ Type\ B)}$, α=0.05; vsExotic: p=0.003; vsNative: p=0.008; vsSlash: p= 0.044; Table 4.5A). Exotic forest, native forest and slash all appear to be similar, with p values greater than 0.5.

The results from $\delta^{13}C$ are similar to those of $\delta^{15}N$, with farmland being significantly different to areas of exotic forest, native forest, and slash (students t-test, H_o: $\mu_{(Land\ Use\ Type\ A)} = \mu_{(Land\ Use\ Type\ B)}$, α=0.05; vsExotic: p<0.001; vsNative: p=0.001; vsSlash: p<0.001, Table 4.5B). Native forest and slash are not significantly different to exotic forest.

Carbon content data shows that carbon content may not be useful in identifying land use type, as all comparisons reject the null hypothesis (H_o: $\mu_{(Land\ Use\ Type\ A)} = \mu_{(Land\ Use\ Type\ B)}$; Table 4.5C) at α=0.05, except for the farmland and native forest, which do not appear to be statistically different (p=0.615).

Farmland again shows a very significant difference from the other three land use types examined when comparing nitrogen contents (students t-test, H_o: $\mu_{(Land\ Use\ Type\ A)} = \mu_{(Land\ Use\ Type\ B)}$, α=0.05; vsExotic: p<0.001; vsNative: p<0.001; vsSlash: p<0.001; Table 4.5D). Interestingly, slash has a significant difference in nitrogen content to exotic forest (p=0.02).

Different land use types appear to occupy the same range across both carbon and nitrogen isotopes and concentrations (Figure 4.14), although farmland can be seen to be generally higher in both carbon and nitrogen isotope ratios as well as nitrogen content, reflecting the results of statistical testing.

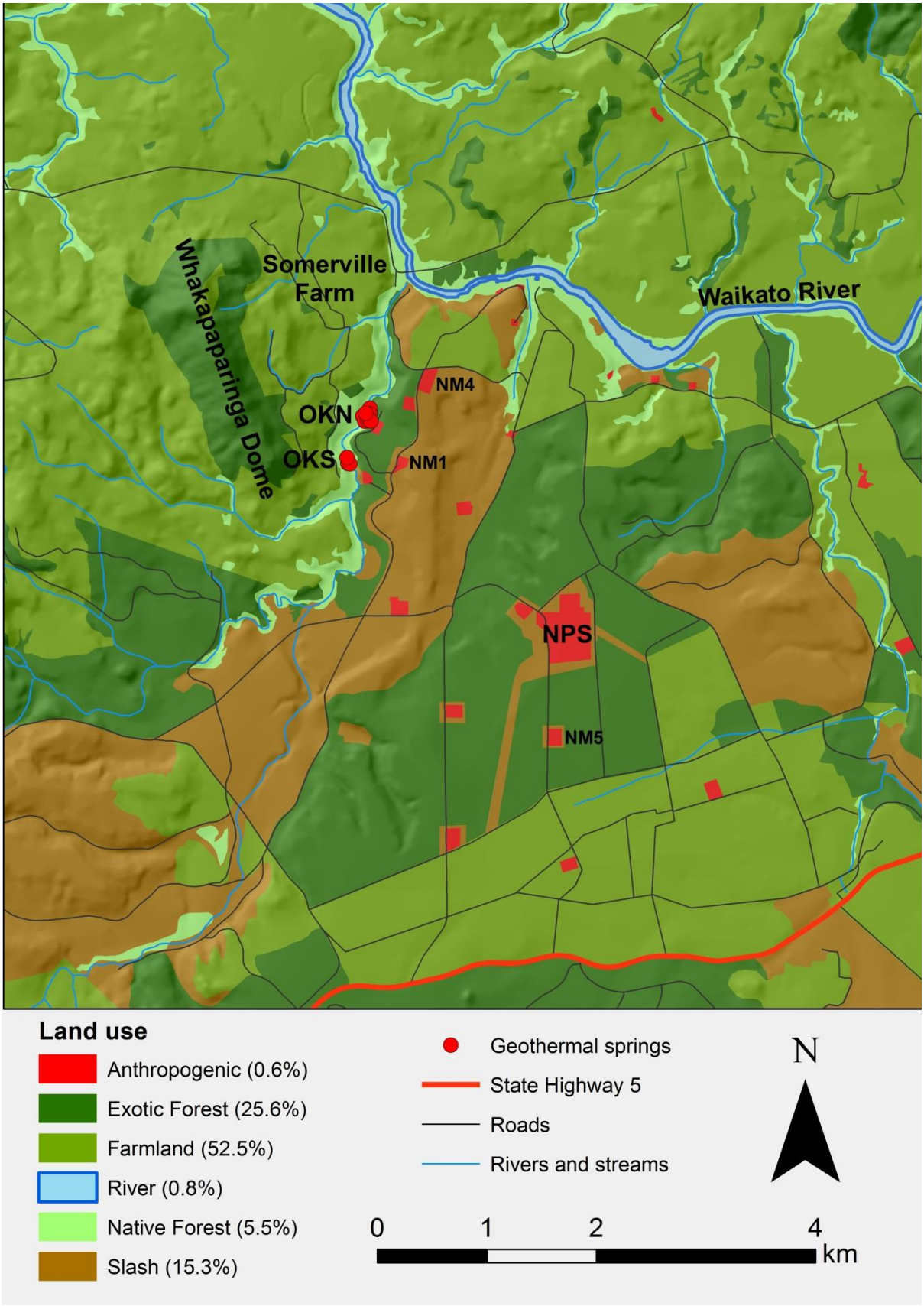

Figure 4.13: Distribution of land use classes at the Ngatamariki Geothermal Area. Bracketed percentages next to land use types refer to total proportion of land cover when seen using this map extent. For GIS data sources see section 0 'GIS Data Sources'.

Table 4.5: Students t-test results for the difference in land use types across the Ngatamariki Geothermal Area for A) $\delta^{13}C$, B) $\delta^{15}N$, C) C%, and D) N%. All use the same null hypothesis (H_o: $\mu_{(Land\ Use\ Type\ A)} = \mu_{(Land\ Use\ Type\ B)}$) and level of significance (α=0.05).

A)

	Exotic	Native	Farmland	Slash
Exotic	-	0.866	0.003	0.499
Native		-	0.008	0.509
Farmland			-	0.044
Scrub				-

B)

	Exotic	Native	Farmland	Slash
Exotic	-	0.069	<0.001	0.223
Native		-	0.001	0.009
Farmland			-	<0.001
Scrub				-

C)

	Exotic	Native	Farmland	Slash
Exotic	-	0.002	0.039	0.020
Native		-	0.615	<0.001
Farmland			-	0.001
Scrub				-

D)

	Exotic	Native	Farmland	Slash
Exotic	-	0.053	<0.01	0.002
Native		-	<0.01	0.113
Farmland			-	<0.001
Scrub				-

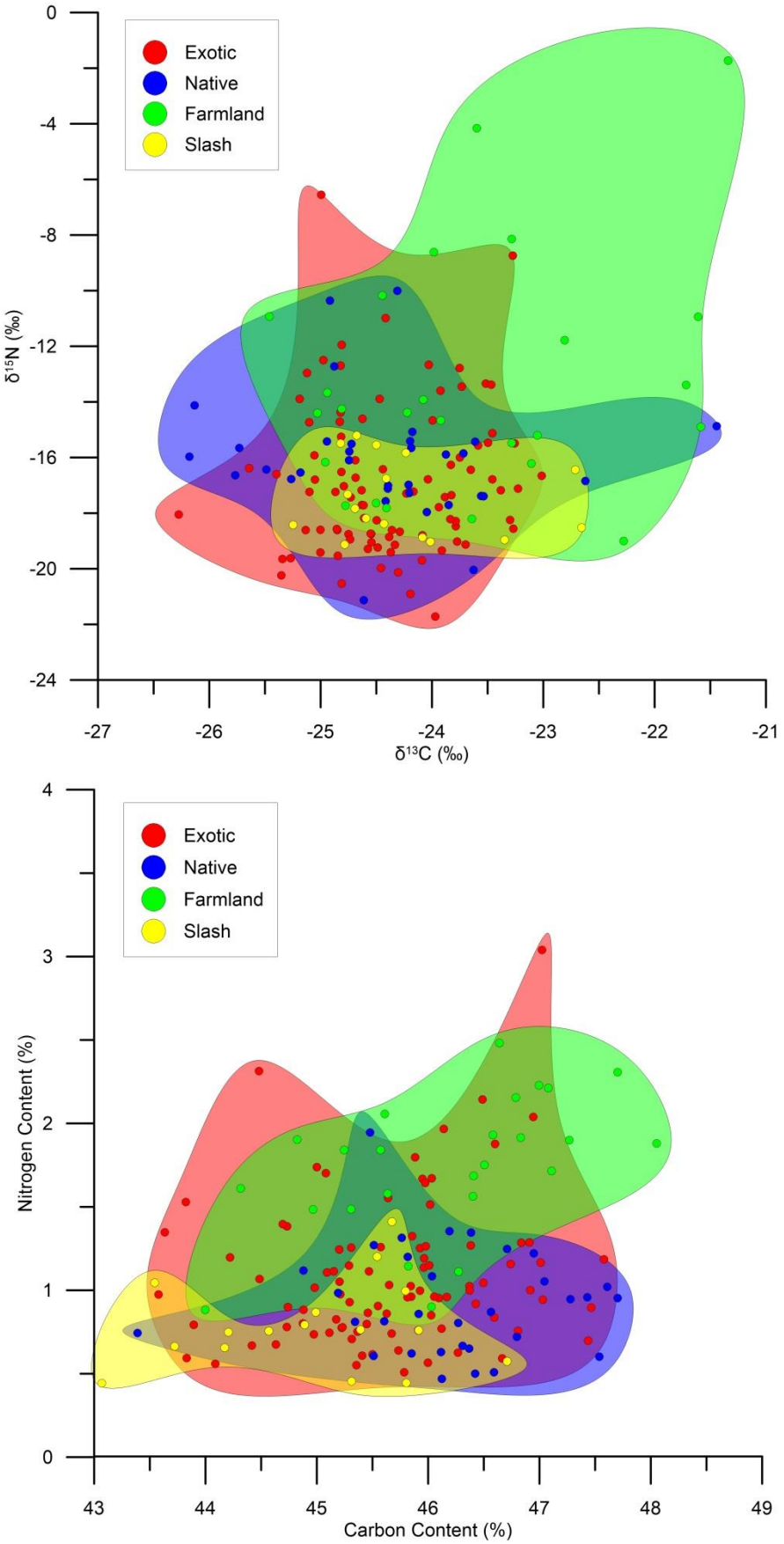

Figure 4.14: Comparison of different land use types: a) $\delta^{15}N$ against $\delta^{13}C$, and b) nitrogen content against carbon content

4.4.5 Land Use Discussion

The results from the analysis of land use show that some isotope and element concentrations lack the ability to differentiate between land use types, while others show strong distinctions.

Both nitrogen isotopic compositions and elemental concentrations strongly distinguish between farmland compared to other land uses across all four study areas, although it does not show significant difference between farmland and anthropogenic land use (ie. Urban environments). This may, in part, be due to the sample size (n) of anthropogenic sites being low (n=2 for both NIT and SIT).

Areas of intensive farmland are by far the largest producers of NH_3 to the atmosphere, mostly due to volatilization from animal wastes, soil organic matter, and intensive feedlots and fertilisation (Krupa, 2003; Petersen, Sommer, Aaes, & Søegaard, 1998; Ping, Bremer, & Janzen, 2000). Typical atmospheric levels of NH_3 in New Zealand, the nitrogen species most readily available to lichen, are generally low (31-74 ng/m^3; Allen, Dick, & Davison, 1997). A study by Tozer *et al.* (2005) found much higher than average atmospheric $NH_{3(g)}$ concentrations above farmland near the western portion of the REW; highest above grazed (80µgN/m^3) than ungrazed pasture (25µgN/m^3; Tozer *et al.*, 2005). Data from Tozer *et al.* (2005) also shows $\delta^{15}N$ values of acidified mats (to simulate diffusive uptake of nutrients by epiphytes) above the same pasture to be more depleted than atmospheric $NH_{3(g)}$ $\delta^{15}N$ in the same area by -4 and -5.5‰ for ungrazed and grazed pasture respectively. These values show the fractionation step of diffusive atmospheric uptake, with grazed farmland (Tozer's 'grazed pasture') exhibiting greater fractionation.

The $\delta^{15}N$ values obtained in this study over intensive farmland[2] (-9.44 ± 0.39‰ (±1σ)) are similar to those of acidified mats over ungrazed farmland in the western REW presented by Tozer (ungrazed: ~-10‰, grazed: ~-14-18‰). However, the farmland $\delta^{15}N$ values show less depletion than native[2] (-12.09 ± 0.45‰) and exotic[2] forests (-12.94 ± 0.26‰) which, if these values had arisen from diffusion of atmospheric NH_3 volatilisation used by Tozer to explain the values of farmland, would be expected to be more enriched comparatively.

Two hypotheses exist to explain the statistical difference between lichen isotopes from farmland and forested land use classes.

Hypothesis 1: Variation in biological components

The first hypothesis is that the difference in lichen isotopic compositions between farmland and forest land use classes can be explained by variations in the proportion of biological components

[2] From North Island samples only, including: REW, TNS, and NGA samples

making up the lichen thallus, either on a large scale – the proportion of photobiont (alga) to mycobiont (fungus), or on a microscale – changes in biological compounds.

Previously (see Section: 'Same-Site Variability', page 54), variations across the extent of a single lichen thallus were attributed to the proportion of each lichen partner to the other, as mycobionts were shown by Beck & Mayr (2012) to have more enriched $\delta^{13}C$ and $\delta^{15}N$ values when compared to the photobiont. A tolerance for the higher nitrogen concentrations seen in farmland areas depends on the capability of the photobiont to produce sufficient amounts of carbon skeletons for ammonia assimilation (Hauck, 2010), and as such we would expect an increase in the proportion of the photobiont. However, as outlined by Beck and Mayr, an increase in the proportion of photobiont partner will deplete the $\delta^{15}N$ and $\delta^{13}C$ values, which are actually more enriched than the values seen in areas of lower nitrogen concentration.

If an increase in the mycobiont proportion relative the photobiont was used to explain the more enriched isotopic composition of farmland lichen, then the measured C:N ratios would present a problem. C:N ratios are lowest for areas of farmland (28.3 ± 6.6 (±1σ)) compared to areas of native (50.4 ± 19.3) and exotic forest (46.0 ± 15.1). Further data from the study by Beck and Mayr show that mycobionts have much higher C:N ratios, as much of the nitrogen taken in by the mycobiont is transferred to the photobiont.

The other section of this hypothesis (hypothesis 1) is that the altered proportions of various biological compounds related to the increase in nitrogen uptake are responsible for the enrichment in $\delta^{15}N$ of farmland samples compared to exotic and native forest samples. A study by Dahlman *et al.* (2003) showed that when highly fertilised lichen (equivalent to our farmland samples) were compared to a control population (equivalent to our exotic and native forest samples), the fertilised lichen thalli had significantly higher protein and chitin contents (the nitrogenous component of fungal cell walls), among other compounds outside of the scope of this study.

Hypothesis 2: Change in nitrogen source

The second hypothesis is that the difference in lichen isotopic compositions between farmland and forest land use classes can be explained by variations in the isotopic composition of the nitrogen source. As mentioned, nitrogen over farmland is mostly the result of volatilization of NH_3 from fertilisers and animal waste, with atmospheric NH_3 shown to have a $\delta^{15}N$ value between -6 and -10‰ which would result in fractionation during uptake of <3‰ (Tozer *et al.*, 2005), while nitrogen in forested areas is the result of biogenic decomposition.

At a basic level, a more negative nitrogen source for lichen in native and exotic forests relative to farmland could explain the observed differences in lichen isotopic composition. However, due to the complicated nature of the nitrogen cycle (ie. large variability in soil $\delta^{15}N$) and the limited available data on expected values, it is not certain that the nitrogen pool assimilated by lichen in exotic and native forests is more depleted than that of farmland (Evans, 2008; Hogberg, 1997). This requires further testing similar to that of Tozer *et al.* (2005) which is outside the scope of this study.

Summary

Clearly there is a significant divide between the nitrogen and carbon isotopic compositions and elemental concentrations of lichen of the same genera on differing land use types. Two hypotheses are presented. The first hypothesis, that changes in isotopic composition are controlled by variation in proportions of biological compounds, has been shown to be correct in the literature, but does not match well with values obtained in this study. The second hypothesis, that changes in isotopic composition are controlled by variation in the isotopic composition of the nitrogen source, presents a much stronger case, with data from this study matching the expected nitrogen source isotopic compositions of farmland areas.

Limitations of this approach

Complications arise when a sample location is along the boundary of two major land use types, as occurred frequently at Ngatamariki (Figure 4.15). Usually the lichen sample will have been taken slightly within one or the other of the land types, and is such attributed to that land use type. However, the impact of the adjacent land use type is not taken into account, and a sample from a boundary site is treated in the same way as a sample site that is nested well within a certain land use type.

Figure 4.15: A satellite view of a sample site along the boundary of two major land use types: exotic forest to the north and south, and farmland to the east and west. Sample site is NGA093 at Ngatamariki geothermal field, in the south-western limit of the field, and in this case was treated as an 'exotic forest' site as it was collected 5m into the stand of trees. Field of view is 1.5km wide. From Google Earth & DigitalGlobe (2014b).

4.5 Isoscapes at Ngatamariki

Isoscapes were created in ArcMap 10.1 using the Nearest Neighbour interpolation tool, due to the uneven distribution of sample points, producing much smoother contours than the available Kriging and associated semivariograms. Colour schemes were then applied and contours added for display purposes, with red representing a more depleted isotope ratio (most negative/lowest number) and green a less depleted ratio (least negative/highest number).

The results are examined at a field scale, covering the full extent of Ngatamariki sample sites, before being examined on an 'outcrop' scale, covering OKS and OKN, the two main areas of geothermal activity at Ngatamariki.

4.5.1 Carbon Isotopes

Carbon isotopes in the study area range between -26 up to -21‰. The field isoscape is shown in Figure 4.16, while an isoscape focused and zoomed in on the Orakonui Springs is shown in Figure 4.17.

Field Scale

The $\delta^{13}C$ isoscape displays a major positive (relative) anomaly to the north and north-west of the study area, with four sites being enriched above -22‰. This location is on the eastern side of the north-west striking Whakapaparinga dome (see Section: 2.5.1 'Geology of the Ngatamariki Area'), a rhyolitic dome believed to mark part of the western boundary of the Whakamaru Caldera (Urzúa-Monsalve, 2008; Wilson *et al.*, 1986).

This anomaly would possibly be larger, but for the omission of three sample sites, NGA120, 122, and 123. At these sites, *Usnea* was not found, so *Ramalina* was collected. Linking back to the Section: 'Variation between genera' (Page 53), there is a significant difference between $\delta^{13}C$ values in *Usnea* and *Ramalina* (students t-test, α=0.05), while there is no statistical difference between $\delta^{15}N$ values of the two genera (students t-test, α=0.05). Therefore, *Usnea* may substitute for *Ramalina* in terms of $\delta^{15}N$, but not in terms of $\delta^{13}C$. As a result, these three points are omitted in the $\delta^{13}C$-Isoscape. However, were they included, they would add to the spatial extent of the north-west anomaly.

A smaller anomaly exists over the developed area of the geothermal field around the power-plant area and the major well stations, with two sites being enriched above -23‰, and thirteen sites enriched above -24‰. Over the past 6 months, this area has hosted the greatest anthropogenic activity of the Ngatamariki area, with extensive forest harvesting and geothermal power plant construction. A significant portion of heavy logging traffic follows Arawa road, while the majority of MRP and plant construction traffic follows Tokomaru road (For place names refer to Figure 2.7).

In the south-west of the field area a single point anomaly exists (NGA131), with an isotopic composition of -26.27‰. This anomalous value is the result of a single sample (as half of the NGA samples are), and is the most depleted value seen in the Ngatamariki area, and is the second most depleted site seen in this study, the other being site CC026 in the SIT in which three values were obtained between -27 and -29.16‰. This site would benefit from another sample being run to verify this value (as five samples were collected for each site, but only 1-2 we analysed), and will be treated as an outlier.

Outcrop Scale

As shown in the Section 'Distances to Geothermal Expressions' (Page 79), a correlation between carbon isotopic compositions and distances to geothermal expressions is not obvious. Again, obvious trends around the geothermal expressions in the isoscapes of Figure 4.17 are lacking, although some of the most enriched samples and some of the more depleted samples are located around the Orakonui Stream Springs.

The major feature of the springs isoscapes is the more enriched $\delta^{13}C$ sites at OKS, immediately adjacent to the Main Pool (see Section: 2.5.2 'Geothermal Features of Ngatamariki'), the largest and most active geothermal feature in the Ngatamariki Geothermal Area. The anomaly is made up by two sample sites, although three other sites around these appear to verify that this is an area of enriched $\delta^{13}C$ values. One site is one of the most enriched sample analysed in the whole Ngatamariki area (-21.44‰ at NGA111 (n=1)), which was collected from a log overhanging the steaming surface of the Main Crater, albeit at the opposite side of the pool from the major geothermal upwelling. This site is similar to the enriched values seen on the Somerville Farm in the north-west of the study area, and approaches the most enriched site near the Somerville farm house (-21.34‰ at NGA124 (n=2)). The second site of the anomaly was more enriched than average (-22.62‰ at NGA105 (n=1)), which was collected from bush overhanging the outflow for the Main Crater to the Orakonui Stream.

Around the OKN springs, sites generally have $\delta^{13}C$ values of between -24.5 to -24‰, although a single site above the high temperature (96˚ at time of sampling) Clear Black Spring (see Section: 2.5.2 'Geothermal Features of Ngatamariki') returned a highly depleted $\delta^{13}C$ value of -26.18‰ (NGA057, n=1).

4.5.2 Nitrogen Isotopes

Nitrogen isotopic composition in the study area ranges between -21.71 up to +3.25‰. The field isoscape is shown in Figure 4.18, while an isoscape focused and zoomed in on the Orakonui Springs is shown in Figure 4.19.

Field Scale

The major feature of the nitrogen isoscape is the anomaly to the north-west of the study area. Two points, NGA122 and NGA124, exhibit the highest $\delta^{15}N$ values in the Ngatamariki area, with ratios of +6.17 and -0.58‰ respectively. This area of relatively enriched nitrogen is in the same general area as the $\delta^{13}C$ anomaly, on the Somerville's Farm between Whakapaparinga Dome and Orakonui Stream/Waikato River.

The above anomaly may be connected to the area to the north and north-east of the study area, an area that shows less depleted isotope ratios than the central field area. This area, which exhibits $\delta^{15}N$ ratios of >-15‰, matches areas of long term farmland reasonably well, bar a few sites which are more depleted, such as the native bush/river bank site NGA170 (NE corner of the Somerville's Farm), which has a $\delta^{15}N$ ratio of -21.1‰, the most depleted seen at Ngatamariki.

Two anomalous points are seen along south-eastern boundary, although they are not nearly as enriched as the larger north-west anomaly. Each anomaly stems from one site that is much more enriched (less depleted) than the immediately surrounding samples (NGA078: -8.75 (n=2); NGA082: -6.56‰ (n=2)).

In the spring area and to the immediate east and west of these, the isotope ratios appear consistently depleted (-16 to -19‰) relative to the rest of the field area.

Outcrop Scale

No obvious trends are visible in the isoscapes centred on the Orakonui Stream Springs (Figure 4.19)

Around the OKN springs, two sample sites appear to more enriched than the surround isoscape, with values of -10.36‰ (NGA071, n=1) and -10.01‰ (NGA043, n=1). The remaining sites around the OKN are similar to those seen in the central area of Ngatamariki (Figure 4.18) at between -16 and -19‰.

At the OKS springs, the isoscape is even less remarkable, with a minor enriched anomaly 50m to the east of the Main Crater (-12.72‰, NGA006 (n=2)), and a minor depleted anomaly 50m to the west (-21.71‰, NGA113 (n=1)).

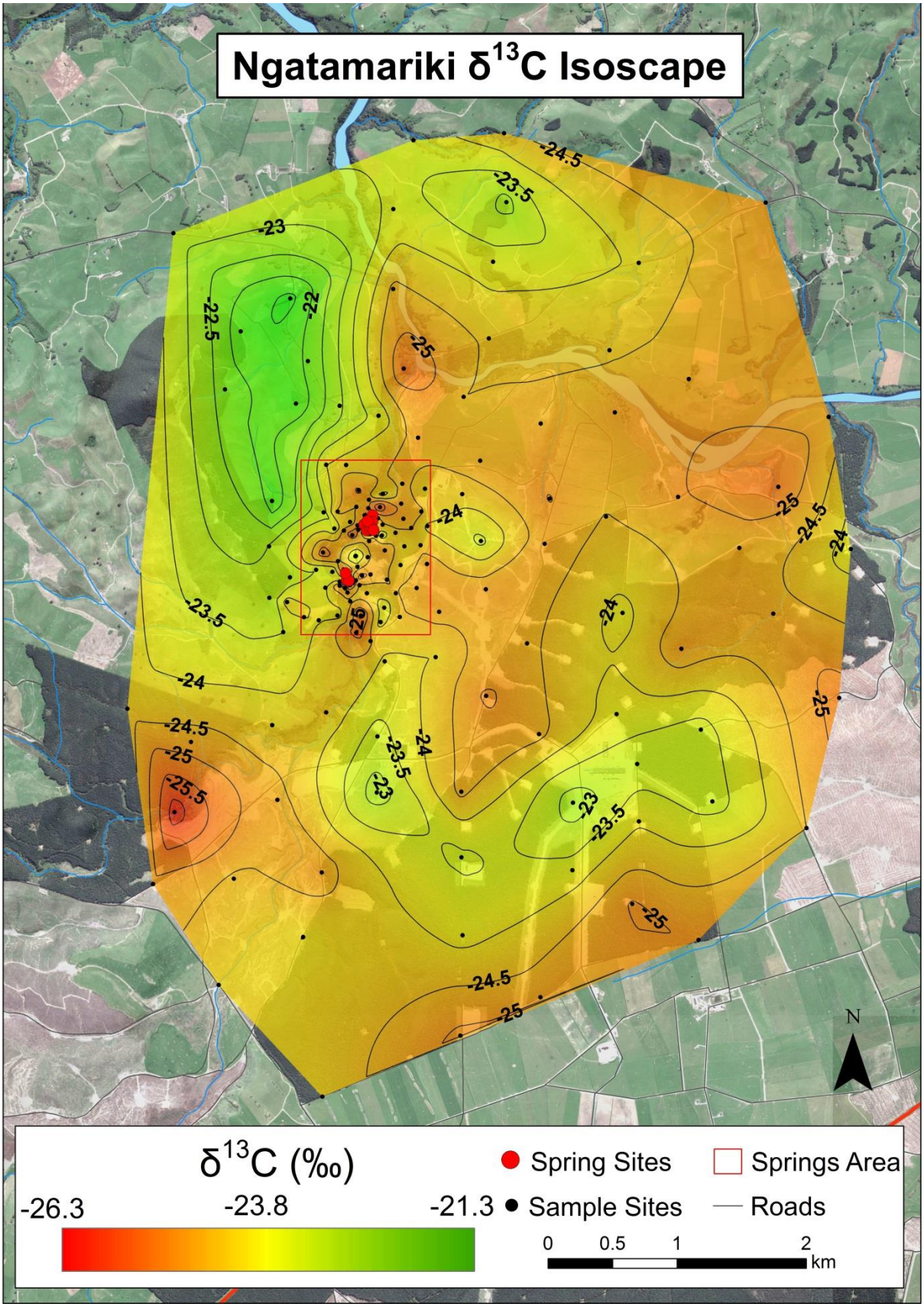

Figure 4.16: Field-scale isoscape of the $\delta^{13}C$ ratios in lichen thalli (*Usnea* sp.) at the Ngatamariki Geothermal Field. For GIS data sources see section 0 'GIS Data Sources'.

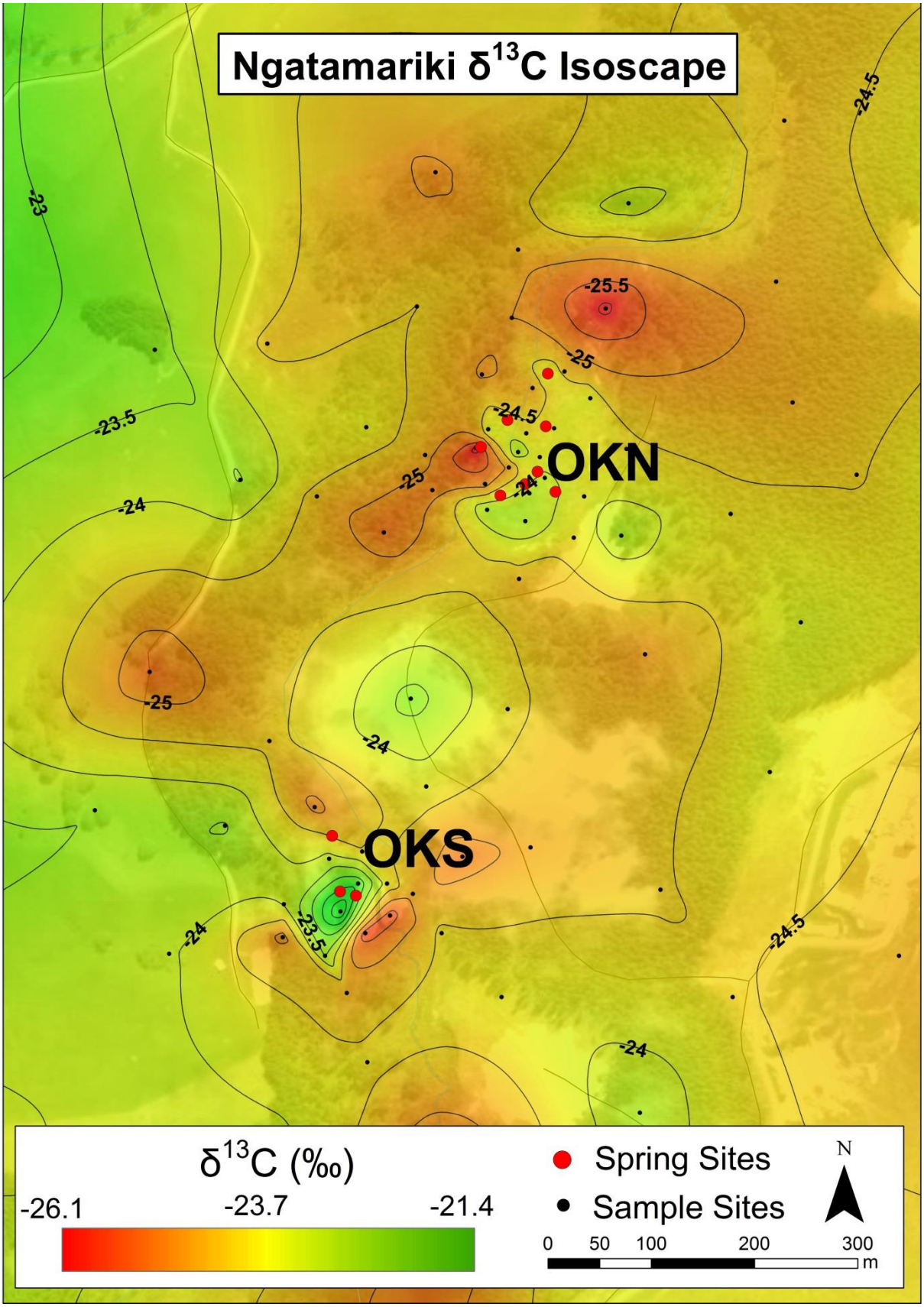

Figure 4.17: Outcrop scale isoscape of the $\delta^{13}C$ ratios in lichen thalli (*Usnea* sp.) at the Ngatamariki Geothermal Field, focused on the Orakonui Springs. For GIS data sources see section 0 'GIS Data Sources'.

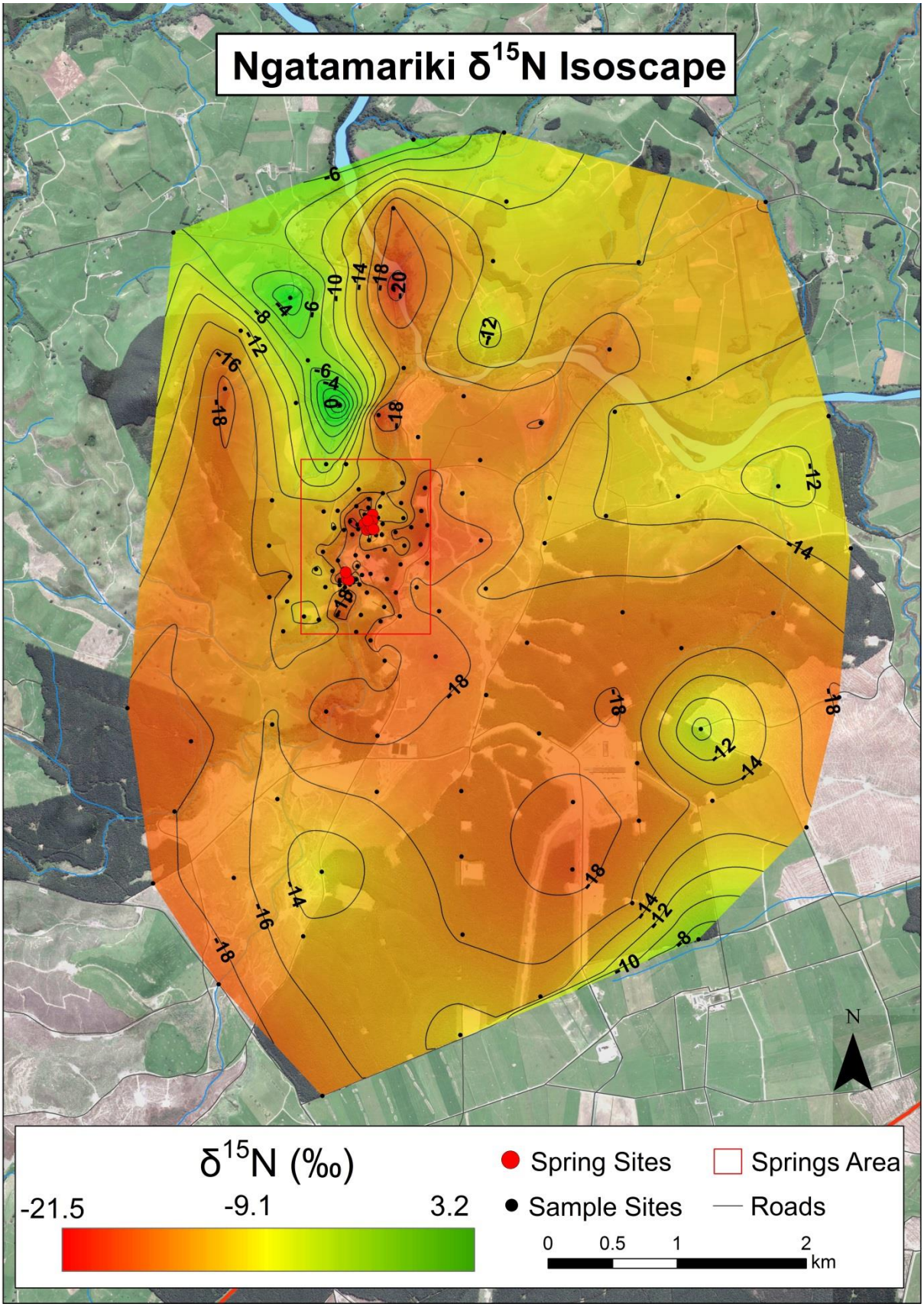

Figure 4.18: Field-scale isoscape of the $\delta^{15}N$ ratios in lichen thalli (*Usnea* sp. and *Ramalina* sp.) at the Ngatamariki Geothermal Field. For GIS data sources see section 0 'GIS Data Sources'.

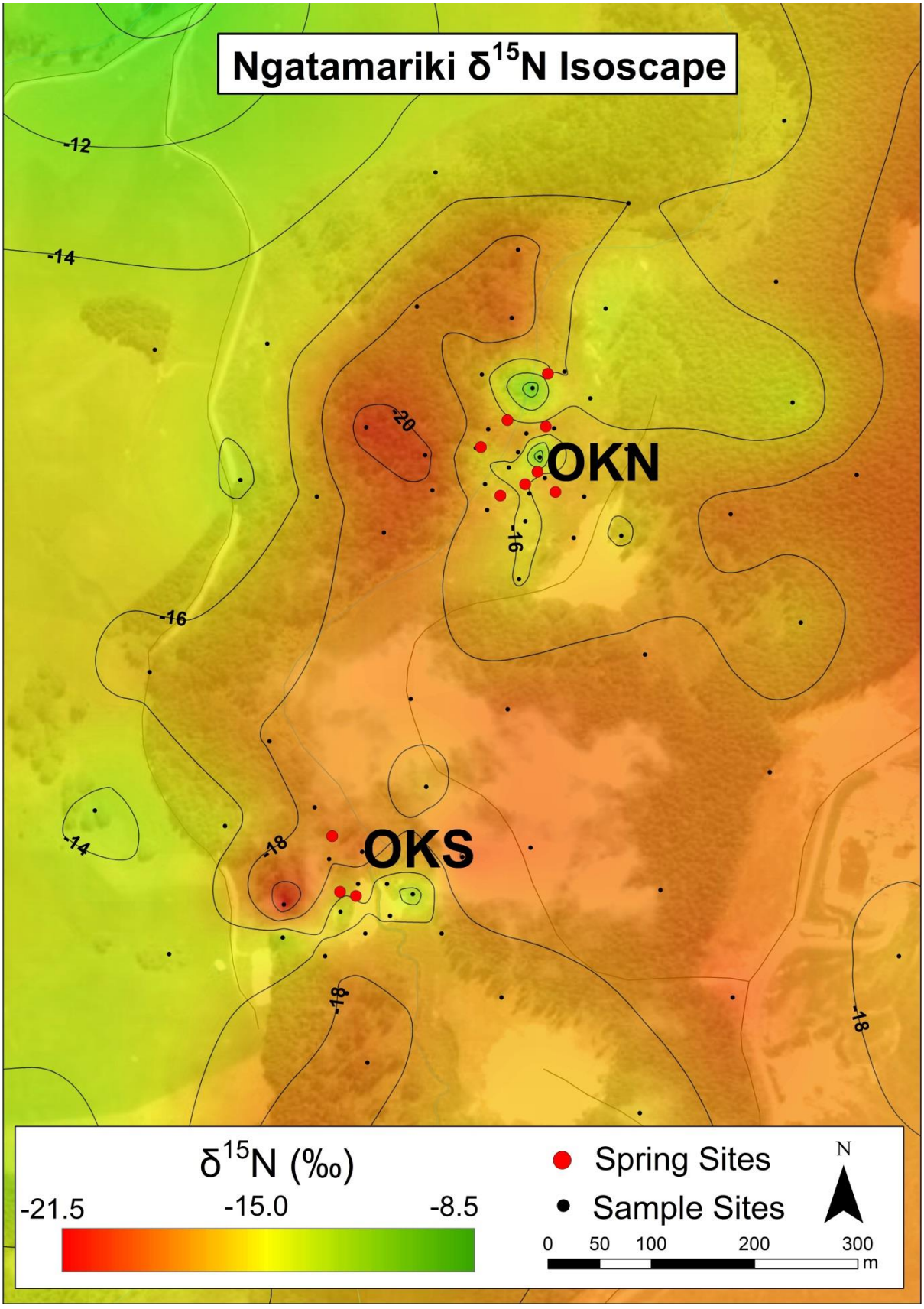

Figure 4.19: Outcrop scale isoscape of the $\delta^{15}N$ ratios in lichen thalli (*Usnea* sp. and *Ramalina* sp.) at the Ngatamariki Geothermal Field, focused on the Orakonui Springs. The area focussed on is referenced by the red square in Figure 4.18. For GIS data sources see section 0 'GIS Data Sources'.

4.5.3 Isoscape Discussion

Due to a greater collection of literature on the subject, the relationship between carbon isotopes and lichen and the relationship between carbon isotopes and geothermal activity both in the Ngatamariki area and worldwide is relatively clearer than nitrogen isotope relationships.

The intake of carbon in the lichen symbiosis is the responsibility of the photobiont (alga), and intake varies depending on factors such as light intensity, moisture content, species-specific differences in CO_2 intake resistance, and the photobiont's CO_2-fixation mechanism (Cristina Máguas *et al.*, 2013). The resulting $\delta^{13}C$ of the assimilated carbon is controlled by the original $\delta^{13}C$ of the source carbon and the degree of fractionation that occurs during assimilation.

A recent study by Hanson (2014) investigating the use of carbon isotopes and CO_2 flux at Ngatamariki as an exploration tool identified three end member CO_2 sources in the area around the Orakonui springs (OKS and OKN):

- **Geothermal Reservoir CO_2** – A sample of deep well fluids from NM4 (2749m deep, 500m north-east of OKN) found the $\delta^{13}CO_2$ composition to be **-6.8‰** (Giggenbach, 1995).
- **Atmospheric CO_2** – Based on $\delta^{13}CO_2$ data from the (US) National Oceanic and Atmosphere Administration (NOAA) for the five years prior to lichen sample collection (2008-13), the average δ^{13}CO2 isotopic composition was **-8.2 ±0.10‰** (www.esrl.noaa.gov).
- **Biogenic derived CO_2** – Decomposition of C3 plants produces CO_2 with an average $\delta^{13}CO_2$ value of **-27‰** (Cheng, 1996), while respiration from C3 plants ranges between -19.0 to -32.6‰ with a mean of **-26.2‰** (Pataki *et al.*, 2003).

The majority of gas flux analysed by Hanson (2014) was found to plot along the continuum between atmospheric CO_2 and biogenic CO_2, however, a number of sites closer to OKN and OKS were found be similar to the $\delta^{13}CO_2$ of the atmospheric end member, but the flux differed in terms of the CO_2 concentration and was attributed to flux from the geothermal reservoir. All measurements that were attributed to geothermal $\delta^{13}CO_2$ end members were located in the immediate vicinity of the OKS Main Crater, while gas samples with potential geothermal influence (between geothermal and atmospheric $\delta^{13}CO_2$ end members) were located in the vicinity of both OKS and OKN.

When compared to the data presented by Hanson (2014), all of the lichen carbon isotopes sampled in this study in the Ngatamariki area plot in the vicinity of the biogenic $\delta^{13}CO_2$ end member (c. -27‰). However, the degree of fractionation that occurs during photosynthesis by the photobiont of the lichen symbiosis is generally between 13.6-30.4‰ (Farquhar, Ehleringer, & Hubick, 1989 and references therein). This would indicate the source of CO_2 for lichen at Ngatamariki to be mostly

atmospheric in origin (likely between -9 and -13‰), assuming fractionation to be on the lower end of the scale, with a minor component of biogenically derived CO_2.

OKS Main Crater Enriched Carbon Isotope Anomaly

The OKS Carbon Isotope Anomaly is possible evidence that carbon isotopes in lichen are suitable for geothermal exploration. As the only flux measurements attributed to geothermal reservoir source by Hanson (2014) were within close proximity to the Main Crater at OKS, it would make this area the likely starting place to identify a geothermal signature of carbon isotopes in lichen. Unfortunately, this anomaly is not observed in the $\delta^{15}N$ isoscape, therefore if this anomaly is attributed to geothermal influences, then using nitrogen isotopes to identify the volatilisation of ammonia from geothermal features may not be a suitable geothermal exploration technique.

When analysed, the two sites on the edge of the Main Crater returned highly enriched values (1.6 (2σ) and 2.7‰ (>3σ) greater than the mean) relative to the majority of the field (enriched at a similar level to the Somerville Farm anomaly). **The hypothesis is that the lichen samples at these two sites were dominated by CO_2 from a geothermal end member ($\delta^{13}CO_2$ = -6.8‰), rather than an atmospheric end member ($\delta^{13}CO_2$ = -8.2‰), resulting in enriched $\delta^{13}C$ values**. While this hypothesis would demonstrate that carbon isotopes in lichen may act as a geothermal exploration tool, other hypothesis remain that are worthy of deliberation.

One such hypothesis considers that the anomaly is not a repercussion of the $\delta^{13}CO_2$ of the geothermal gas, but of the impact that heated air and raised humidity would have on the lichen thallus. Green-algal photobionts (as opposed to cyanobiont; All lichen in this study contain green-algae photobionts) are known to photosynthesise at low moisture contents (Lange, 1980), and net photosynthesis increases as moisture content increases, but as lichen reach saturation photosynthetic capabilities drop to near zero due to increased CO_2 diffusion resistances (Smith & Griffiths, 1998). Máguas *et al.* (1995) found this limitation in CO_2 diffusion to decrease fractionation by 3-4‰, resulting in more enriched $\delta^{13}C$ product. Increasing temperature reduces the moisture content required to engage photosynthesis and while it is unclear whether this reduces the saturation limit at which photosynthesis decreases, increased temperature is known to increase respiration (O. L. Lange, 1980; Palmqvist, 2000). Batts *et al.* (2004) found that increases in the humidity of the environment altered the $\delta^{13}C$ value of lichen, but by less than 1‰, and in a negative direction resulting in more depleted $\delta^{13}C$. The lichen samples at the two sites were collected close to the Main Crater, as shown in Figure 4.20, but the effect of the steam from the pool on the lichen microclimate is unknown. It is unlikely that the steam increases the water content to a level of thallus saturation that impedes photosynthesis, although it is likely that these lichen samples

experience some increase in humidity as shown in lichen close to geothermal pools at Te Kopia (geothermal area 15km to the north; Tozer *et al.*, 2005); the exact impact requires further investigation.

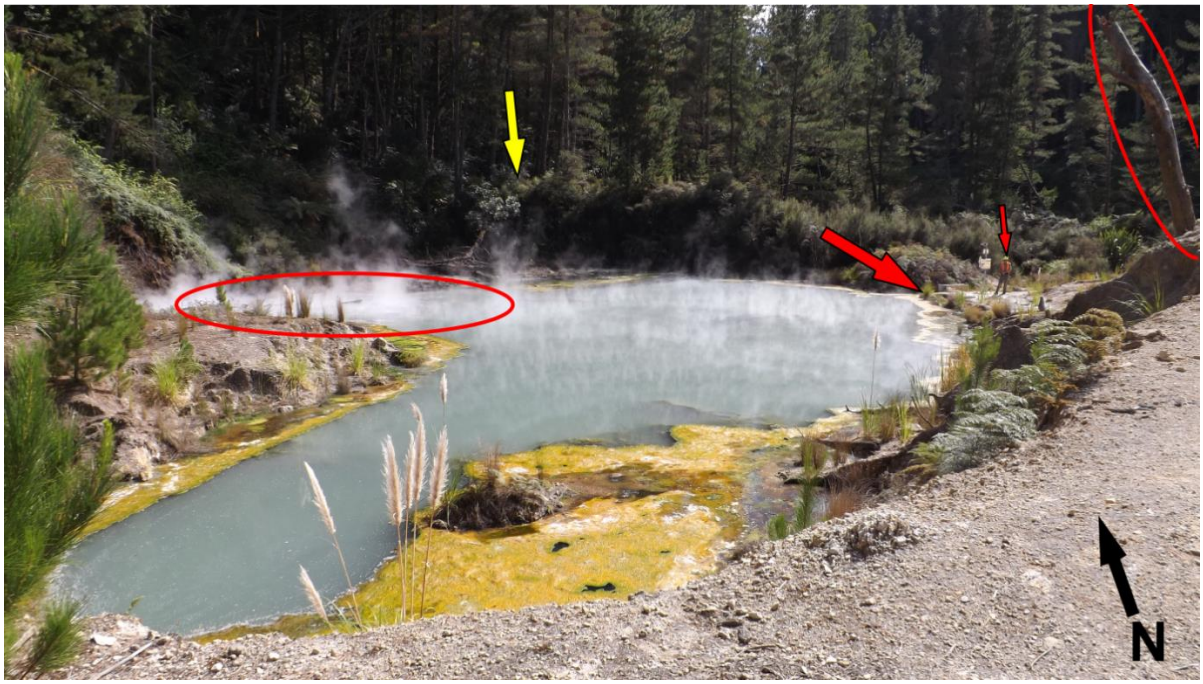

Figure 4.20: Locations of the two highly enriched samples relative to the Main Crater at OKS. The most enriched sample (-21.44‰) is located on the overhanging log in the top-right right of the image, while the second sample (-22.62‰) is located on a bush overhanging the outflow stream (large red arrow in centre-right, behind the person (for scale; small red arrow in centre-right). The third sample site referred to in the text is shown by the yellow arrow (upper-centre) roughly 10m from the cater edge. The major upflow of the Main Crater is shown by the red circle to the centre-left, although the whole pool exhibits a bubbling a steaming surface.

The samples for these two enriched sites are collected from dead logs embedded in eruption breccia, from the 2005 hydrothermal eruption which spewed hydrothermal breccia up to 100m east across the Orakonui stream (O'Brien, 2010). The following hypothesis exists as a hypothesis not just for these OKS samples, but for all samples on fence-posts (ie. farmland areas) or non-living (but non-decomposing) substrates. For samples growing on biogenic substrates such as branches and tree bark, respiration provides CO_2 that is not available to lichen growing on minerogenic or anthropogenic surfaces, increasing the ratio of biogenic(relatively depleted) to atmospheric (relatively enriched) sourced $\delta^{13}CO2$ and depleting the $\delta^{13}C$ of the lichen. A geological understanding of the area may aid this hypothesis, as the hydrothermal eruption breccia on which these samples are located likely has very limited soil formation due to both the impermeability of the clay rich breccia and the age (~8 years at time of sampling). This would result in limited or no soil respiration (highly depleted $\delta^{13}CO2$). **It is hypothesised that as the samples making up the OKS Main Crater anomaly are essentially on non-biogenic substrates, the depleted $\delta^{13}CO_2$ source from respiration (both soil, bark and plant respiration) is not available and a larger proportion of atmospheric CO_2**

is assimilated, resulting in more enriched $\delta^{13}C$ values relative to lichen from biogenic sources. This hypothesis is supported by a site that is located in the scrub to the north of the crater rim (yellow arrow in Figure 4.20). This site does not exhibit the same enriched $\delta^{13}C$ values as the two samples that make up this anomaly, yet is of equal distance to the geothermal pool, the only difference being that this sample was found to be living on a biogenic substrate.

All three of these hypotheses show merit towards explaining the enriched carbon isotope anomaly at the OKS Main Crater. With the available data, the hypothesis that the anomaly is controlled by substrate appears the strongest, due to the lack of anomalous $\delta^{13}C$ values at a site to the north of the pool edge but at roughly equal distance. Further sampling and analysis at a higher spatial around OKS Main Crater resolution would aid in explaining this anomaly.

Somerville Farm Enriched Anomaly

From the field scale isoscape of Ngatamariki ($\delta^{13}C$: Figure 4.16, $\delta^{15}N$: Figure 4.18), it is clear that there is a large anomaly in the north-west of the study area, seen through both nitrogen and carbon isotopic compositions. Following on from the previous section on the impact of land use on isotopic composition (see Section: 4.4 'Land Use') this enriched anomaly is situated in an area of farmland (Figure 4.13); areas of farmland show enriched nitrogen isotopic composition along the three transects (SIT, TNS, and REW) as we see here. Anomalous $\delta^{13}C$ values, enriched to a lesser extent, continue around the northern boundary of the study area covering the majority of the land area attributed to farmland, although the extent of long-term farmland is most accurately represented by the nitrogen isotopic composition.

The relatively large $\delta^{13}C$ and $\delta^{15}N$ enrichment of lichen around the Somerville farm may be a result of recent fertilisation efforts. During the initial days of sample collection at Ngatamariki (late-March), **aerial spraying operations** were seen, the result of which would be higher nitrogen availability over the Somerville farm area. High nitrogen contents are seen around the Somerville farm area parallel to the direction of aerial spraying (aerial spraying was restricted to a north-south direction due to the orientation of Whakapaparinga Dome topographical high), with most sites in excess of 1.75%, and some reaching almost 3% (nitrogen by dry weight). However, it is unknown if the time interval of 2-3 days between aerial spraying and collection would have a profound influence over the long-term carbon and nitrogen isotopic compositions of the lichen present, and it could be assumed that sample collection would coincide with fertilisation efforts on at least one other farm (the north-eastern section of the study area is split into many independently operated farms), resulting in this highly enriched anomaly continuing in strength to the north-east, which is not seen.

In terms of wind direction, this large enriched anomaly is located on the lee side of the Whakapaparinga dome, relative to the predominant wind direction from the west (Figure 4.21). A possible explanation revolves around the **diffusion of the heavier isotope** (^{13}C and ^{15}N), becoming 'trapped' to a greater extent behind the sheltered side of the topographical high and enriching the resident lichen in the area. As this is the only major topographical feature in the area, this cannot be reproduced at other locations, and sites along the three transects are not sampled at a high enough density to reproduce this effect.

Whakapaparinga Dome is a rhyolitic dome that extends along north-west trending fractures, parallel to the Whakamaru caldera boundary (Wilson *et al.*, 1986). The caldera margin has been projected to continue to the south, cutting across the Orakonui Stream approximately 1km upstream of the OKS springs. The possibility of a **geological control on the isotopic composition** cannot be ruled out without further investigation into the area around the north and west side of the dome, which was not sampled due to land access restrictions. The lack of the continuation of a positive anomaly to the south following the projected boundary through areas in which lichen samples were analysed is suspect, although there is also a lack of surficial geological features related to the caldera margin in this area.

Similar to the OKS Main Crater enriched carbon isotope anomaly discussed in the previous section (see Section: 4.5.3 'OKS Main Crater Enriched Carbon Isotope Anomaly') **the substrate from which the lichen samples were collected may play a role in producing such a significant anomaly**. As many of the samples from the Somerville Farm (and other farmland areas) were sampled from fence posts, the depleted $\delta^{13}CO_2$ from soil and plant respiration is unavailable, resulting in a greater proportion of CO_2 for photosynthesis being derived from the atmospheric CO_2 pool. However, the carbon anomaly, which covers a greater area than the nitrogen anomaly, includes sites at which lichen was collected from biogenic material (tree bark) and sites at which lichen was collected from non-biogenic material (fence posts), both of which indicate highly enriched $\delta^{13}C$ values with no distinction between the two. Due to this, the strength of this hypothesis is severely reduced.

Without further investigation, the Somerville Farm isotopic anomaly is attributed to the farmland class of land use, as similar trends to this are observed in other areas of both the North Island and South Island Transects, although the cause of the relatively large enrichment compared to other areas of farmland to the north-east of the study area is unclear.

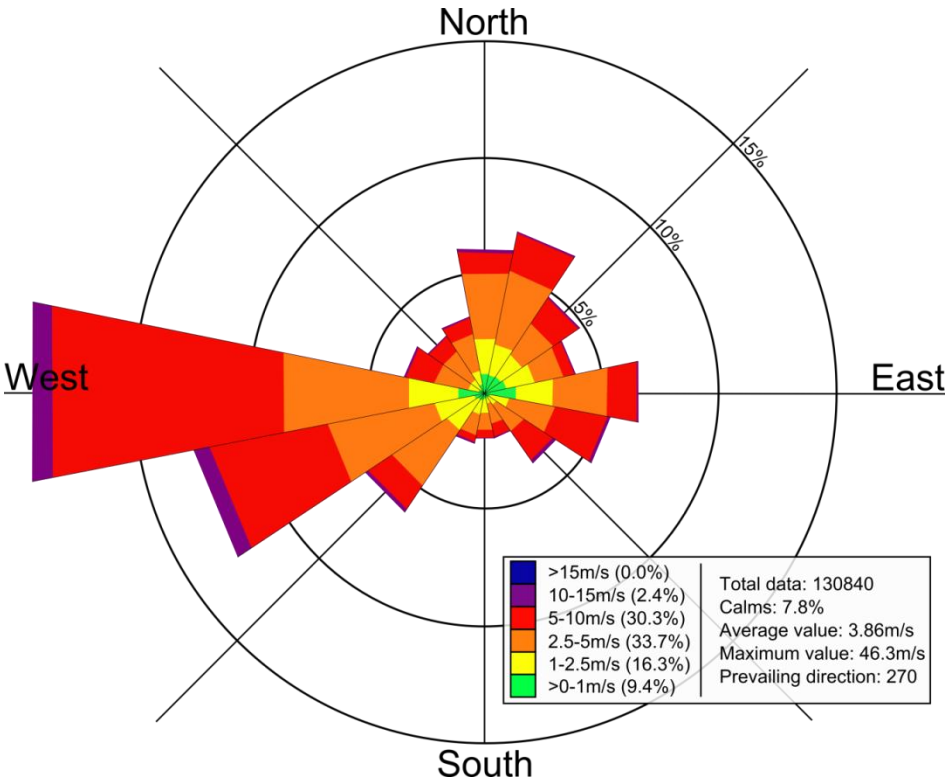

Figure 4.21: Long-term average (1983-2013) wind direction and speed in the central North Island, New Zealand. Derived from data from the Taupo Aerodrome AWS, retrieved from NIWA's CliFlo database (www.cliflo.niwa.co.nz). Modified from plot originally created using Enviroware's Windrose Pro.

5 Conclusion

Ultimately, do we see anomalous isotope ratios around the geothermal expressions that may allow isotopes of nitrogen and carbon in lichen to be used as a geothermal exploration technique?

The $\delta^{13}C$ enriched (less depleted) anomaly from two sample collection sites directly overhanging the major geothermal expressions (Main Pool – OKS) at the Ngatamariki Geothermal Area correlates well with gas flux measurements that show this geothermal feature to display the only distinct surficial geothermal signature (Hanson, 2014). Based on this, this technique may have applications in geothermal settings. However, conflicting hypotheses exist, attributing the isotopic anomaly around OKS Main crater to the substrate from which the lichen were collected, which has been shown to influence lichen isotopes (Beck & Mayr, 2012) and to a similarity between geothermal and atmospheric $\delta^{13}CO_2$ values. Additionally, as this anomaly is less than 100m across this technique may not be suitable for low flux geothermal areas, and further investigations into higher flux systems (eg. Rotokawa – see Bloomberg *et al.*, 2012) may be appropriate.

Land use plays a major part in controlling not only isotopic value, but also elemental concentrations of both nitrogen and carbon, observed in samples across both the South (SIT) and North Island (NGA, REW, TNS). The combination of two major land use types (Forestry – low nitrogen, depleted $\delta^{15}N$; Farmland – high nitrogen, enriched $\delta^{13}C$ and $\delta^{15}N$) in the Ngatamariki area may mask subtle trends. The geothermal exploration technique used in this study may be better suited to geothermal areas of homogenous land use.

5.1 Further work:

The distribution of sampling sites at Ngatamariki is suitable to produce isoscapes of the area, however, the main aim of this study was to determine if the isotopes of lichen are a suitable exploration tool for geothermal areas. While a high spatial sampling resolution was used around the geothermal features of Ngatamariki, this study would benefit from a) high spatial scale straight-line transects extending away from the geothermal features in both upwind, downwind, and crosswind directions, and b) a greater emphasis on identifying boundary effects between major land use classes.

6 References

6.1 In-text citations

Allen, A. G., Dick, A. L., & Davison, B. M. (1997). Sources of atmospheric methanesulphate, non-sea-salt sulphate, nitrate and related species over the temperate South Pacific. *Atmospheric Environment*, *31*(2), 191–205. doi:10.1016/1352-2310(96)00194-X

Angold, P. G. (1997). The Impact of a Road Upon Adjacent Heathland Vegetation: Effects on Plant Species Composition. *Journal of Applied Ecology*, *34*(2), 409–417.

Barbier, E. (2002). Geothermal energy technology and current status: an overview. *Renewable and Sustainable Energy Reviews*, *6*(1-2), 3–65. doi:10.1016/S1364-0321(02)00002-3

Batts, J. E., Calder, L. J., & Batts, B. D. (2004). Utilizing stable isotope abundances of lichens to monitor environmental change. *Chemical Geology*, *204*(3-4), 345–368. doi:10.1016/j.chemgeo.2003.11.007

Beck, A., & Mayr, C. (2012). Nitrogen and carbon isotope variability in the green-algal lichen Xanthoria parietina and their implications on mycobiont-photobiont interactions. *Ecology and Evolution*, *2*(12), 3132–44. doi:10.1002/ece3.417

Bennett, J. P., & Wetmore, C. M. (1999). Geothermal elements in lichens of Yellowstone National Park, USA. *Environmental and Experimental Botany*, *42*(3), 191–200. doi:10.1016/S0098-8472(99)00036-2

Bennie, S. L. (1983). *Geophysical Investigations of the Ngatamariki Geothermal Area* (p. 35). Wellington, New Zealand.

Bertani, R. (2010). Geothermal Power Generation in the World 2005 – 2010 Update Report. In *World Geothermal Congress 2010* (Vol. 2015, pp. 25–29).

Bettinelli, M., Spezia, S., & Bizzarri, G. (1996). Trace element determination in lichens by ICP-MS. *Atomic Spectroscopy*, *17*(3), 133–141.

Biazrov, L. G. (2012). Stable nitrogen isotopes (δ15N) in thalli of arid vagrant lichen Xanthoparmelia camtschadalis across an altitudianl gradient of the Khangai Plateau of Mongolia. *Contemporary Problems of Ecology*, *5*(2), 200–207.

Bibby, H. M., Caldwell, T. G., Davey, F. J., & Webb, T. H. (1995). Geophysical evidence on the structure of the Taupo Volcanic Zone and its hydrothermal circulation. *Journal of Volcanology and Geothermal Research*, *68*(1-3), 29–58. doi:10.1016/0377-0273(95)00007-H

Blanco, M., Suárez, C., & Vicente, C. (1984). The use of urea by Evernia prunastri thalli. *Planta*, *162*, 305–310. doi:10.1007/BF00396741

Blasco, M., Domeño, C., & Nerín, C. (2006). Use of lichens as pollution biomonitors in remote areas: comparison of PAhs extracted from lichens and atmospheric particles sampled in and around the Somport tunnel (Pyrenees). *Environmental Science and Technology*, *40*(20), 6384–91.

Bloomberg, S. (2012). *Looking for Permeability: Mass and Heat Flow assessment Using High Resolution Soil CO2 Flux Surveys within the Taupo Volcanic Zone, New Zealand*. University of Canterbury.

Bloomberg, S., Rissmann, C., Mazot, A., Oze, C., Horton, T., Kennedy, B., … Pawson, J. (2012). Soil gas flux exploration at the Rotokawa Geothermal Field on White Island, New Zealand. In *Thirty-Sixth Workshop on Geothermal Reservoir Engineering* (p. 11). Stanford, California.

Boonpragob, K., & Nash, T. H. I. (1990). Seasonal variation of elemental status in the lichen Ramalina Menziesii Tayl. from two sites in Southern California: Evidence for dry deposition accumulation. *Environmental and Experimental Botany*, *30*(4), 415–428.

Boseley, C., Cumming, W., Urzúa-Monsalve, L. A., Powell, T., & Grant, M. A. (2010). A Resource Conceptual Model for the Ngatamariki Geothermal Field Based on Recent Exploration Well Drilling and 3D MT Resistivity Imaging. In *Proceedings for the World Geothermal Congress* (Vol. 4, pp. 25–29).

Brotheridge, J. M. A. (1995). *Surface manifestations - Past and present - of the Ngatamariki Geothermal Field, Taupo Volcanic Zone, New Zealand*. University of Auckland.

Brotheridge, J. M. A., Browne, P. R. L., & Hochstein, M. P. (1995). The Ngatamariki Geothermal Field, NZ: surface manifestations - past and present. In *Proceedings of the 17th NZ Geothermal Workshop* (pp. 61–66).

Büdel, B., & Scheidegger, C. (2008). Thallus morphology and anatomy. In T. H. I. Nash (Ed.), *Lichen Biology* (2nd ed., pp. 37–64). Cambridge University Press.

Cape, J. N., Tang, Y. S., van Dijk, N., Love, L., Sutton, M. a, & Palmer, S. C. F. (2004). Concentrations of ammonia and nitrogen dioxide at roadside verges, and their contribution to nitrogen deposition. *Environmental Pollution (Barking, Essex : 1987)*, *132*(3), 469–78. doi:10.1016/j.envpol.2004.05.009

Carlisle, A., Brown, A. H. F., & White, E. J. (1966). The organic matter and nutrient elements in the precipitation beneath a sessile oak (Quercus Petraea) canopy. *Journal of Ecology*, *54*(1), 87–89.

Chandrasekharam, D., & Bundschuh, J. (2008). *Low-Enthalpy Geothermal Resources for Power Generation* (p. 149). Leiden, The Netherlands: CRC Press/Balkema.

Cheng, W. (1996). Measurement of rhizosphere respiration and organic matter decomposition using natural 13C. *Plant and Soil*, *183*(2), 263–268. doi:10.1007/BF00011441

Cole, J. (1990). Structural control and origin of volcanism in the Taupo volcanic zone, New Zealand. *Bulletin of Volcanology*, 445–459.

Cole, J. W., & Lewis, K. B. (1981). Evolution of the Taupo-Hikurangi Subduction System. *Tectonophysics*, *72*, 1–21.

Conti, M. E., & Cecchetti, G. (2001). Biological monitoring: lichens as bioindicators of air pollution assessment--a review. *Environmental Pollution*, *114*(3), 471–92.

Crittenden, P. D. (1988). Nitrogen Relations of Mat-forming Lichens. In L. Boddy, R. Marchant, & D. J. Read (Eds.), *Nitrogen, Phosphorus and Sulphur Utilization by Fungi* (pp. 243–268). Cambridge, England: Cambridge University Press.

Cuna, S., Balas, G., & Hauer, E. (2007). Effects of natural environmental factors on delta13C of lichens. *Isotopes in Environmental and Health Studies*, *43*(2), 95–104. doi:10.1080/10256010701362401

Dahlman, L., Nasholm, T., & Palmqvist, K. (2002). Growth, nitrogen uptake, and resource allocation in the two tripartite lichens Nephroma arcticum and Peltigera aphthosa during nitrogen stress. *New Phytologist*, *153*(2), 307–315. doi:10.1046/j.0028-646X.2001.00321.x

Dahlman, L., Persson, J., Näsholm, T., & Palmqvist, K. (2003). Carbon and nitrogen distribution in the green algal lichens Hypogymnia physodes and Platismatia glauca in relation to nutrient supply. *Planta*, *217*(1), 41–8. doi:10.1007/s00425-003-0977-8

Dahlman, L., Persson, J., Palmqvist, K., & Näsholm, T. (2004). Organic and inorganic nitrogen uptake in lichens. *Planta*, *219*(3), 459–67. doi:10.1007/s00425-004-1247-0

Dawson, T. E., Mambelli, S., Plamboeck, A. H., Templer, P. H., & Tu, K. P. (2002). Stable Isotopes in Plant Ecology. *Annual Review of Ecology and Systematics*, *33*(1), 507–559. doi:10.1146/annurev.ecolsys.33.020602.095451

De Lange, P. J., Galloway, D. J., Blanchon, D. J., Knight, A., Rolfe, J. R., Crowcroft, G. M., & Hitchmough, R. (2012). Conservation status of New Zealand lichens. *New Zealand Journal of Botany*, *50*(3), 303–363. doi:http://dx.doi.org/10.1080/0028825X.2012.691426

Department of Conservation. (2007). *Arthur's Pass National Park Management Plan* (p. 223). Christchurch.

Di Lella, L. A., Frati, L., Loppi, S., Protano, G., & Riccobono, F. (2003). Lichens as biomonitors of uranium and other trace elements in an area of Kosovo heavily shelled with depleted uranium rounds. *Atmospheric Environment*, *37*, 5445–5449. doi:10.1016/j.atmosenv.2003.09.009

Ellis, A. J., & Mahon, W. A. J. (1977). *Chemistry and Geothermal Systems*. (J. Denton, Ed.) (p. 392). New York: Academic Press.

Ellis, C. J., Crittenden, P. D., Scrimgeour, C. M., & Ashcroft, C. J. (2005). Translocation of 15N indicates nitrogen recycling in the mat-forming lichen Cladonia portentosa. *The New Phytologist*, *168*(2), 423–34. doi:10.1111/j.1469-8137.2005.01524.x

Evans, R. D. (2008). Soil Nitrogen Isotope Composition. In R. Michener & K. Lajtha (Eds.), *Stable Isotope in Ecology and Environmental Science*. John Wiley and Sons Ltd.

Fahselt, D. (2008). Individuals and Populations of Lichens. In T. H. I. Nash (Ed.), *Lichen Biology* (2nd ed.). Cambridge, England: Cambridge University Press.

Farquhar, G. D., Ehleringer, J. R., & Hubick, K. T. (1989). Carbon Isotope Discrimination and Photosynthesis. *Annual Review of Plant Physiology and Plant Molecular Biology*, *40*, 503–37.

Frati, L., Caprasecca, E., Santoni, S., Gaggi, C., Guttova, A., Gaudino, S., … Loppi, S. (2006). Effects of NO2 and NH3 from road traffic on epiphytic lichens. *Environmental Pollution*, *142*(1), 58–64. doi:10.1016/j.envpol.2005.09.020

Fry, B. (2006). *Stable Isotope Ecology* (p. 308). New York: Springer Science+Business Media.

Gadsdon, S. R., & Power, S. a. (2009). Quantifying local traffic contributions to NO2 and NH3 concentrations in natural habitats. *Environmental Pollution (Barking, Essex : 1987)*, *157*(10), 2845–52. doi:10.1016/j.envpol.2009.04.010

Galun, M. (1988a). Carbon Metabolism. In M. Galun (Ed.), *Handbook of Lichenology Vol.1* (pp. 197–200). Boca Raton, Florida: CRC Press, Inc.

Galun, M. (1988b). *Handbook of Lichenology: Volume 1*. (M. Galun, Ed.) (p. 297). Boca Raton, Florida: CRC Press, Inc.

Gauslaa, Y., & Solhaug, K. A. (1996). Difference in the susceptibility to light stress between epiphytic lichens of ancient and young boreal forest stands. *Functional Ecology*, *10*(3), 344–354.

Giggenbach, W. F. (1995). Variations in the chemical and isotopic composition of fluids discharged from the Taupo Volcanic Zone, New Zealand. *Journal of Volcanology and Geothermal Research*, *68*(1-3), 89–116. doi:10.1016/0377-0273(95)00009-J

Gombert, S., Asta, J., & Seaward, M. R. D. (2003). Correlation between the nitrogen concentration of two epiphytic lichens and the traffic density in an urban area. *Environmental Pollution (Barking, Essex : 1987)*, *123*(2), 281–90.

González, C. M., Casanovas, S. S., & Pignata, M. L. (1996). Biomonitoring of air pollutants from traffic and industries employing Ramalina ecklonii (Spreng.) Mey. and Flot. in Córdoba, Argentina. *Environmental Pollution (Barking, Essex : 1987)*, *91*(3), 269–77.

González, C. M., & Pignata, M. L. (1999). Effect of pollutants emitted by different urban-industrial sources on the chemical response of the transplanted Ramalina ecklonii (Spreng.) Mey & Flot. *Toxicological and Environmental Chemistry*, *69*(1-2), 61–73.

Google Earth. (2014). Western Christchurch. Latitude: 43°31’35.34“S, Longitude: 172°34’28.12”E.

Google Earth, & DigitalGlobe. (2014a). Canterbury Plains (Farmland). Latitude: 43°31’52.20“S, Longitude: 172°15’55.72”E.

Google Earth, & DigitalGlobe. (2014b). Ngatamariki Geothermal Field (Exotic Forest and Farmland Sample Site Conflict). Latitude: 38°34’11.17“S, Longitude: 176°10’17.86”E.

Google Earth, & DigitalGlobe. (2014c). Ngatamariki Geothermal Field (Exotic Forest). Latitude: 38°32’19.94“S, Longitude: 176°12’8.41”E.

Google Earth, & DigitalGlobe. (2014d). Ngatamariki Geothermal Field (Slash). Latitude: 38°32’4.63“S, Longitude: 176°11’2.84”E.

Google Earth, & DigitalGlobe. (2014e). Te Urewera National Park. Latitude: 38°33’43.09“S, Longitude: 176°45’2.71”E.

Google Earth, & Landsat. (2013). NIT Area. Latitude: 38°27’24.34“S, Longitude: 176° 9’23.57”E.

Green, T. G. A., Nash, T. H. I., & Lange, O. L. (2008). Physiological Ecology of Carbon Dioxide Exchange. In T. H. I. Nash (Ed.), *Lichen Biology* (2nd ed., pp. 152–181). Cambridge, England: Cambridge University Press.

Grenon, J. A. (2012). *Epiphytic Lichens, Nitrogen Deposition and CLimate In The US Northern Rocky Mountain States*. Montana State University.

Grindley, G. W. (1960). Geological Map of New Zealand - Sheet 8 Taupo. New Zealand Geological Survey, D.S.I.R.

Grindon, L. H. (1859). *The Manchester Flora* (p. 593). London: William White.

Hanson, M. C. (2014). *Carbon Isotope and CO2 Flux Analysis for Geothermal Resource Exploration of Surface Blind Systems*. University of Canterbury.

Hauck, M. (2010). Ammonium and nitrate tolerance in lichens. *Environmental Pollution*, *158*(5), 1127–33. doi:10.1016/j.envpol.2009.12.036

Heaton, T. H. E., Spiro, B., & Robertson, S. M. C. (1997). Potential canopy influences on the isotopic compostion of nitrogen and sulphur in atmospheric desposition. *Oecologia*, *109*(4), 600–607.

Henley, R. W., & Ellis, a. J. (1983). Geothermal systems ancient and modern: a geochemical review. *Earth-Science Reviews*, *19*(1), 1–50. doi:10.1016/0012-8252(83)90075-2

Hibbett, D. S., Binder, M., Bischoff, J. F., Blackwell, M., Cannon, P. F., Eriksson, O. E., … Zhang, N. (2007). A higher-level phylogenetic classification of the Fungi. *Mycological Research*, *111*(5), 509–47. doi:10.1016/j.mycres.2007.03.004

Hietz, P., Wanek, W., Wania, R., & Nadkarni, N. M. (2002). Nitrogen-15 natural abundance in a montane cloud forest canopy as an indicator of nitrogen cycling and epiphyte nutrition. *Oecologia*, *131*(3), 350–355. doi:10.1007/S00442-002-0896-6

Hochstein, M. P. (1995). Crustal heat transfer in the Taupo Volcanic Zone (New Zealand) comparison with other volcanic arcs and explanatory heat source models. *Journal of Volcanology and Geothermal Research*, *68*(1-3), 117–151. doi:10.1016/0377-0273(95)00010-R

Hoefs, J. (2004). *Stable Isotope Geochemistry* (5th ed., p. 244). Berlin, Germany: Springer.

Hogberg, P. (1997). Tansley Review No . 95: 15N natural abundance in soil-plant systems. *New Phytologist*, *137*, 179–203.

Honegger, R. (2008). Morphogenisis. In T. H. I. Nash (Ed.), *Lichen Biology* (2nd ed., pp. 69–93). Cambridge, England: Cambridge University Press.

Hyvärinen, M., & Crittenden, P. D. (1998). Relationships between atmospheric nitrogen inputs and the vertical nitrogen and phosphorus concentration gradients in the lichen Cladonia portentosa. *New Phytologist*, *140*, 519–530.

Jahns, H. M. (1988). The Lichen Thallus. In M. Galun (Ed.), *Handbook of Lichenology Vol.1* (pp. 95–143). Boca Raton, Florida: CRC Press, Inc.

Johansson, O. (2011). *Epiphytic lichen responses to nitrogen deposition*.

Kappen, L., Meyer, M., & Bolter, M. (1988). Photosynthetic Production of the Lichen Ramalina terebrata Jook. f. et Tayl., in the Mritime Antarctic. *Polarforschung*, *58*, 181–188.

Kendall, C., & Caldwell, E. A. (2006). Fundamentals of Isotope Geochemistry. In C. Kendall & J. J. McDonnell (Eds.), *Isotope Tracers in Catchment Hydrology* (3rd ed., pp. 50–86). Amsterdam, The Netherlands: Elsevier B.V.

Kirk, P. M., Cannon, P. F., David, J. C., & Stalpers, J. A. (Eds.). (2008). *Ainsworth & Bisby's Dictionary of the Fungi* (10th ed., p. 770). CABI Publishing.

Kissling, W. M., & Weir, G. J. (2005). The spatial distribution of the geothermal fields in the Taupo Volcanic Zone, New Zealand. *Journal of Volcanology and Geothermal Research*, *145*(1-2), 136–150. doi:10.1016/j.jvolgeores.2005.01.006

Klusman, R. W., Moore, J. N., & Leroy, M. P. (2000). Potential for surface gas flux measurements in exploration and surface evaluation of geothermal resources. *Geothermics*, *29*, 637–670.

Krupa, S. (2003). Effects of atmospheric ammonia (NH3) on terrestrial vegetation: a review. *Environmental Pollution*, *124*(2), 179–221. doi:10.1016/S0269-7491(02)00434-7

Lange, O. L. (1980). Moisture content and CO2 exchange of lichens. *Oecologia*, *45*(1), 82–87.

Lange, O. L., Büdel, B., Heber, U., Meyer, A., Zellner, H., & Green, T. G. A. (1993). Temperate rainforest lichens in New Zealand: High thallus water content can severely limit photosynthetic CO2 exchange. *Oecologia*, *95*(3), 303–313.

Lange, O. L., & Tenhunen, J. D. (1981). Moisture content and CO2 exchange of lichens II : Depression of net photosynthesis in Ramalina maciformis at high water content is caused by increased thallus carbon dioxide diffusion resistance. *Oecologia*, *51*(3), 426–429.

Lewis, B., Chambefort, I., & Rae, A. J. (2012). *Geology of Injection Well NM8-NM8A, Ngatamariki Geothermal Field* (p. 81). GNS Science Consultancy Report 2012/188.

Lewis, B., Chambefort, I., Rae, A. J., & Sanders, F. (2012). *Geology of Injection Well NM10, Ngatamariki Geothermal Field* (p. 28). GNS Science Consultancy Report 2012/231.

Lewis, B., Chambefort, I., Rae, A. J., & Sanders, F. (2013). *Geology of Well NM9, Ngatamariki Geothermal Field* (p. 58). GNS Science Consultancy Report 2012/330.

Lewis, B., Chambefort, I., Rae, A. J., Sanders, F., & Massiot, C. (2013). *Geology of Well NM11, Ngatamariki Geothermal Field* (p. 58). GNS Science Consultancy Report 2013/33.

Lim, H. S., Han, M. J., Seo, D. C., Kim, J. H., Lee, J. Il, Park, H., … Cho, J.-S. (2009). Heavy Metal Concentrations in the Fruticose Lichen Usnea aurantiacoatra from King George Island, South Shetland Islands, West Antarctica. *Journal of the Korean Society for Applied Biological Chemistry*, *52*(5), 503–508. doi:10.3839/jksabc.2009.086

Liu, X.-Y., Xiao, H.-Y., Liu, C.-Q., Li, Y.-Y., & Xiao, H.-W. (2008). Stable carbon and nitrogen isotopes of the moss Haplocladium microphyllum in an urban and a background area (SW China): The role of environmental conditions and atmospheric nitrogen deposition. *Atmospheric Environment*, *42*(21), 5413–5423. doi:10.1016/j.atmosenv.2008.02.038

Lloyd, E. F. (1972). *Geology and Hot Springs of Orakeikorako* (p. 164). Wellington, New Zealand Geological Survey.

Loppi, S. (1996). Lichens as Bioindicators of Geothermal Air Pollution in Central Italy. *American Bryological and Lichenological Society*, *99*(1), 41–48.

Loppi, S., Malfatti, A., Sani, M., & Whitehead, N. E. (1997). Lichens as biomonitors of geothermal radionuclide pollution. *Geothermics*, *26*(4), 535–540. doi:10.1016/S0375-6505(97)00005-9

Loppi, S., & Nascimbene, J. (1998). Lichen bioindication of airquality in the Mt. Amiata geothermal area (Tuscany, Italy). *Geothermics*, *27*(3), 295–304.

Loppi, S., & Nascimbene, J. (2010). Monitoring H2S air pollution caused by the industrial exploitation of geothermal energy: the pitfall of using lichens as bioindicators. *Environmental Pollution (Barking, Essex : 1987)*, *158*(8), 2635–9. doi:10.1016/j.envpol.2010.05.002

MacFarlane, J. D., & Kershaw, K. A. (1985). Some Aspects of Carbohydrate Metabolism. In D. H. Brown (Ed.), *Lichen Physiology and Cell Biology* (p. 8). Springer, US.

Máguas, C., & Brugnoli, E. (1996). Spatial variation in carbon isotope discrimination across the thalli of several lichen species. *Plant, Cell and Environment*, *19*, 437–446.

Máguas, C., Griffiths, H., & Broadmeadow, M. S. J. (1995). Gas exchange and carbon isotope discrimination in lichens : Evidence for interactions between CO2-concentrating mechanisms and diffusion limitation. *Planta*, *196*, 95–102.

Máguas, C., Pinho, P., Branquinho, C., Hartard, B., & Lakatos, M. (2013). Carbon-Water-Nitrogen relationships between lichens and the atmosphere: Tools to understand metabolism and ecosystem change. *MycoKeys*, *6*, 95–106. doi:10.3897/mycokeys.6.4814

Martin, W., & Child, J. (1972). *Lichens of New Zealand* (p. 193). Wellington: A. H. & A. W. Reed Ltd.

Matthews, K. M. (1981). The use of lichens in a study of geothermal radon emissions in New Zealand. *Environmental Pollution Series A, Ecological and Biological*, *24*(2), 105–116. doi:10.1016/0143-1471(81)90072-6

Mighty River Power. (2013, September 2). New Ngatamariki Station boosts Mighty River Power's geothermal production, driving earnings growth. *Mighty River Power News Release*, pp. 1–2. Retrieved from http://www.mightyriver.co.nz/PDFs/PDFs/New-Ngatamariki-Station-boosts-MRPs-geothermal-pro.aspx

Mulligan, L. (2009). *An Assessment of Epiphytic Lichens , Lichen Diversity and Environmental Quality in the Semi-natural Woodlands of Knocksink Wood Nature Reserve, Enniskerry, County Wicklow*. Dublin Institute of Technology.

Nash, T. H. I. (2008a). *Lichen Biology* (2nd ed., p. 498). Cambridge, England: Cambridge University Press.

Nash, T. H. I. (2008b). Nitrogen, its metabolism and potential contributin to ecosystem. In T. H. I. Nash (Ed.), *Lichen Biology* (2nd ed., pp. 216–233). Cambridge, England: Cambridge University Press.

Nash, T. H. I. (2008c). Nitrogen, its metabolism and potential contribution to ecosystems. In *Lichen Biology* (2nd ed., pp. 216–233). Cambridge University Press.

Neuhäuser, B., Dynowski, M., Mayer, M., & Ludewig, U. (2007). Regulation of NH4+ transport by essential cross talk between AMT monomers through the carboxyl tails. *Plant Physiology*, *143*(4), 1651–9. doi:10.1104/pp.106.094243

Nicholson, K. (1993). *Geothermal Fluids: Chemistry and Exploration Techniques* (p. 263). Berlin, Germany: Springer-Verlag.

NZ Transport Agency. (2011). *State Highway Traffic Data Booklet 2006-2010* (p. 50). Retrieved from http://www.nzta.govt.nz/resources/state-highway-traffic-volumes/docs/SHTV-2006-2010.pdf

O'Brien, J. M. (2010). *Hydrogeochemical Characteristics of the Ngatamariki Geothermal Field and a Comparison with the Orakei Korako Thermal Area, Taupo Volcanic Zone, New Zealand*. Unpublished M.Sc Thesis, University of Canterbury.

Osyczka, P., Dutkiewicz, E. M., & Olech, M. (2007). Trace elements concentrations in selected moss and lichen species collected within Antarctic research stations. *Polish Journal of Ecology*, *55*(1), 39–48.

Palmqvist, K. (2000). Tansley Review No. 117: Carbon economy in lichens. *New Phytologist*, *148*(1), 11–36.

Palmqvist, K., Dahlman, L., Valladares, F., Tehler, A., Leopoldo, G., & Mattsson, J. (2002). CO2 exchange and thallus nitrogen across 75 contrasting lichen associations from different climate zones. *Oecologia*, *133*, 295–306.

Paoli, L., & Loppi, S. (2008). A biological method to monitor early effects of the air pollution caused by the industrial exploitation of geothermal energy. *Environmental Pollution*, *155*(2), 383–8. doi:10.1016/j.envpol.2007.11.004

Pataki, D. E., Ehleringer, J. R., Flanagan, L. B., Yakir, D., Bowling, D. R., Still, C. J., … Berry, J. a. (2003). The application and interpretation of Keeling plots in terrestrial carbon cycle research. *Global Biogeochemical Cycles*, *17*(1), n/a–n/a. doi:10.1029/2001GB001850

Petersen, S. O., Sommer, S. G., Aaes, O., & Søegaard, K. (1998). Ammonia losses from urine and dung of grazing cattle: Effect of N intake. *Atmospheric Environment*, *32*(3), 295–300.

Ping, J., Bremer, E., & Janzen, H. H. (2000). Foliar uptake of volatilized ammonia from surface-applied urea by spring wheat. *Communications in Soil Science and Plant Analysis*, *31*(1-2), 165–172. doi:10.1080/00103620009370427

Poblet, A., Andrade, S., Scagliola, M., Vodopivez, C., Curtosi, A., Pucci, A., & Marcovecchio, J. (1997). The use of epilithic Antarctic lichens (Usnea aurantiacoatra and U. antartica) to determine deposition patterns of heavy metals in the Shetland Islands, Antarctica. *The Science of the Total Environment*, *207*(2-3), 187–94.

Proemse, B. C., & Mayer, B. (2012). Tracing Industrial Nitrogen and Sulfur Emissions in the Athabasca Oil Sands Region Using Stable Isotopes. In K. E. Percy (Ed.), *Alberta Oil Sands: Energy, Industry and the Environment* (p. 528). Newnes. Retrieved from http://books.google.co.nz/books?id=Eqgr3HF7WR8C&printsec=frontcover#v=onepage&q&f=false

Rae, A. J., Ramirez, L. E., & Bardsley, C. (2009). *Geology of Exploration Well NM6, Ngatamariki Geothermal Field* (p. 68). GNS Science Consultancy Report 2009/130.

Rae, A. J., Ramirez, L. E., & Boseley, C. (2009). *Geology of Geothermal Well NM7, Ngatamariki Geothermal Field* (p. 57). GNS Science Consultancy Report 2009/289.

Rai, A. N. (1988). Nitrogen Metabolism. In M. Galun (Ed.), *Handbook of Lichenology Vol.1* (pp. 201–237). Boca Raton, Florida: CRC Press, Inc.

Ramirez, L. E., & Rae, A. J. (2009). *Geology of Injection Well NM5, NM5A, Ngatamariki Geothermal Field* (p. 29). GNS Science Consultancy Report 2009/41.

Riera, P. (2005). δ13C and δ15N comparisons among different co-occurring lichen species from littoral rocky substrata. *The Lichenologist*, *37*(1), 93–95. doi:10.1017/S0024282904014446

Robinson, D. (2001). δ15N as an integrator of the nitrogen cycle. *Ecology and Evolution*, *16*(3), 153–162.

Scerbo, R., Possenti, L., Lampugnani, L., Ristori, T., & Barale, R. (1999). Lichen (Xanthoria parietina) biomonitoring of trace element contamination and air quality assessment in Livorno Province (Tuscany , Italy). *The Science of the Total Environment*, *241*, 91–106.

Schofield, J. C. (1965). The Hinuera formation and associated quaternary events. *New Zealand Journal of Geology and Geophysics*, *8*(5), 772–791. doi:10.1080/00288306.1965.10422116

Sharp, Z. (2007). *Principles of Stable Isotope Geochemistry* (p. 344). New Jersey: Pearson Education, Inc.

Skinner, R. a., Ineson, P., Jones, H., Sleep, D., Leith, I. D., & Sheppard, L. J. (2006). Heathland vegetation as a bio-monitor for nitrogen deposition and source attribution using δ15N values. *Atmospheric Environment*, *40*(3), 498–507. doi:10.1016/j.atmosenv.2005.09.054

Smith, E. G. C., & Griffiths, H. (1998). Intraspecific variation in photosynthetic responses of trebouxioid lichens with reference to the activity of a carbon-concentrating mechanism. *Oecologia*, *113*(3), 360–369.

Soengkono, S. (1999). Te Kopia geothermal system (New Zealand) - the relationship between its structure and extent. *Geothermics*, *28*, 767–784.

Taiz, L., & Zeiger, E. (2002). *Plant Physiology* (3rd ed., p. 690). Sunderland, Massachusetts: Sinauer Associaties, Inc.

Thell, A., Crespo, A., Divakar, P. K., Kärnefelt, I., Leavitt, S. D., Lumbsch, H. T., & Seaward, M. R. D. (2012). A review of the lichen family Parmeliaceae - history, phylogeny and current taxonomy. *Nordic Journal of Botany*, *30*(6), 641–664. doi:10.1111/j.1756-1051.2012.00008.x

Tozer, W. C., Hackell, D., Miers, D. B., & Silvester, W. B. (2005). Extreme isotopic depletion of nitrogen in New Zealand lithophytes and epiphytes; the result of diffusive uptake of atmospheric ammonia? *Oecologia*, *144*(4), 628–35. doi:10.1007/s00442-005-0098-0

Truong, C., Divakar, P. K., Yahr, R., Crespo, A., & Clerc, P. (2013). Testing the use of ITS rDNA and protein-coding genes in the generic and species delimitation of the lichen genus Usnea (Parmeliaceae, Ascomycota). *Molecular Phylogenetics and Evolution*. doi:10.1016/j.ympev.2013.04.005

Turkenburg, W., Arent, D. J., Bertani, R., Faaij, A., Hand, M., Krewitt, W., … Usher, E. (2012). Renewable Energy. In J. Schmid (Ed.), *Global Energy Assessment - Toward a Sustainable Future* (pp. 761–900). Elsevier.

Ulloa, M., & Hanlin, R. T. (2000). *Illustrated Dictionary of Mycology* (p. 448). St. Paul, Minnesota: APS Press.

United States Department of Agriculture. (2013). Plant Profile: Usnea. Retrieved February 25, 2013, from http://plants.usda.gov/java/profile?symbol=USNEA2

Urzúa-Monsalve, L. A. (2008). *Integration of a preliminary one-dimensional MT analysis with geology and geochemistry in a conceptual model of the Ngatamariki geothermal field*. Unpublished M.Sc Thesis, University of Auckland.

Van Dobben, H. F., Wolterbeek, H. T., Wamelink, G. W., & Ter Braak, C. J. (2001). Relationship between epiphytic lichens, trace elements and gaseous atmospheric pollutants. *Environmental Pollution*, *112*(2), 163–9.

Vingiani, S., Adamo, P., & Giordano, S. (2004). Sulphur, nitrogen and carbon content of Sphagnum capillifolium and Pseudevernia furfuracea exposed in bags in the Naples urban area. *Environmental Pollution*, *129*(1), 145–158. doi:10.1016/j.envpol.2003.09.016

Wadleigh, M. a, & Blake, D. M. (1999). Tracing sources of atmospheric sulphur using epiphytic lichens. *Environmental Pollution (Barking, Essex : 1987)*, *106*(3), 265–71.

Wairakei Pastoral Ltd. (2013a). *Wairakei Estate/MRP Site: Harvest Dates*.

Wairakei Pastoral Ltd. (2013b). *Wairakei Estate/MRP Site: Stand Establishment Dates*.

Wania, R., Hietz, P., & Wanek, W. (2002). Natural 15N abundance of epiphytes depends on the position within the forest canopy: source signals and isotope fractionation. *Plant, Cell and Environment*, *25*, 581–589.

West, J. B., Bowen, G. J., Dawson, T. E., & Tu, K. P. (Eds.). (2010). *Isoscapes: Understandaing Movement, Pattern, and Process on Earth Through Isotope Mapping* (p. 487). Springer.

Wilson, C. J. N., Houghton, B. F., & Lloyd, E. F. (1986). Volcanic history and evolution of the Maroa-Taupo area, central North Island. In I. E. M. Smith (Ed.), *Late Cenozoic Volcanism in New Zealand. Royal Society of New Zealand Bulletin, 23* (pp. 194–223).

Wilson, C. J. N., Houghton, B. F., McWilliams, M. O., Lanphere, M. A., Weaver, S. D., & Briggs, R. M. (1995). Volcanic and structural evolution of Taupo Volcanic Zone, New Zealand: A review. *Journal of Volcanology and Geothermal Research*, *68*, 1–28.

Wirtz, N., Printzen, C., Sancho, L. G., & Lumbsch, H. T. (2006). The phylogeny and classification of Neuropogon and Usnea (Parmeliaceae, Ascomycota) revisited. *Taxon*, *55*(2), 367–376.

Wood, C. P. (1985a). *Straigraphy and Petrology of NM2, Ngatamriki Geothermal Field* (p. 5).

Wood, C. P. (1985b). *Stratigraphy and Petrology of NM1, Ngatamariki Geothermal Field* (p. 6).

Wood, C. P. (1986a). *Straigraphy and Petrology of NM4, Ngatamariki Geothermal Field* (p. 7).

Wood, C. P. (1986b). *Stratigraphy and Petrology of NM3, Ngatamariki Geothermal Field* (p. 5).

GIS Data Sources

6.1.1 Chapter 2: Lit Review/Background

Figure 2.5: Extent of TVZ

Hillshade sourced from the Koordinates data sevice (https://koordinates.com/layer/515-nz-greyscale-hillshade-100m/) and licensed by Geographx for re-use under the Creative Commons Attribution 3.0 New Zealand licence

Figure 2.6: Calderas and Geothermal Systems of the TVZ

Hillshade sourced from the Koordinates data sevice (https://koordinates.com/layer/515-nz-greyscale-hillshade-100m/) and licensed by Geographx for re-use under the Creative Commons Attribution 3.0 New Zealand licence

Figure 2.7: Geography of the Ngatamariki Area

River data sourced from the LINZ Data Service (River Polygons: https://data.linz.govt.nz/layer/328-nz-mainland-river-polygons-topo-150k/ and River Polylines: https://data.linz.govt.nz/layer/327-nz-mainland-river-centrelines-topo-150k/) and licensed by the LINZ/National Topographic Office re-use under the Creative Commons Attribution 3.0 New Zealand licence.

Road data sourced from the Koordinates Data Service (All Roads: https://koordinates.com/layer/40-nz-roads-centrelines/ and State Highways: https://koordinates.com/layer/1331-nz-state-highway-centrelines/) and licensed by Land Transport New Zealand for re-use under the Creative Commons Attribution 3.0 New Zealand licence.

Satellite Imagery sourced from the ArcMap 10.1 Basemap "World Imagery" (http://www.arcgis.com/home/item.html?id=10df2279f9684e4a9f6a7f08febac2a9) and licenced by ESRI under the Esri Master License Agreement.

Hillshade sourced from the Koordinates Data Service (https://koordinates.com/layer/515-nz-greyscale-hillshade-100m/) and licensed by Geographx for re-use under the Creative Commons Attribution 3.0 New Zealand licence.

Figure 2.8: Geology of the Orakonui Springs Area

Hillshade sourced from the Koordinates Data Service (https://koordinates.com/layer/515-nz-greyscale-hillshade-100m/) and licensed by Geographx for re-use under the Creative Commons Attribution 3.0 New Zealand licence.

River data sourced from the LINZ Data Service (River Polygons: https://data.linz.govt.nz/layer/328-nz-mainland-river-polygons-topo-150k/ and River Polylines: https://data.linz.govt.nz/layer/327-nz-mainland-river-centrelines-topo-150k/) and licensed by the LINZ/National Topographic Office re-use under the Creative Commons Attribution 3.0 New Zealand licence.

Figure 2.9: OKS and OKN Map

Aerial imagery sourced from the LINZ Data Service (https://data.linz.govt.nz/layer/1760-bay-of-plenty-025m-rural-aerial-photos-2011-2012/) and licensed by BOPLASS Limited for re-use under the Creative Commons Attribution 3.0 New Zealand licence.

6.1.2 Chapter 3: Lichen Isotopes Spatially

Figure 3.7: Elevation Profile of the SIT

Elevation data derived from DEM, sourced from the LRIS Data Service (https://lris.scinfo.org.nz/layer/127-nzdem-south-island-25-metre/) and reproduced with the permission of Landcare Research New Zealand Limited.

Road data sourced from the Koordinates Data Service (https://koordinates.com/layer/40-nz-roads-centrelines/) and licensed by Land Transport New Zealand (LTNZ) for re-use under the Creative Commons Attribution 3.0 New Zealand licence.

Error! Reference source not found.: Sample locations along the SIT (with lichen ssociations)

Hillshade sourced from the Koordinates Data Service (https://koordinates.com/layer/515-nz-greyscale-hillshade-100m/) and licensed by Geographx for re-use under the Creative Commons Attribution 3.0 New Zealand licence.

NZ Coastline sourced from the Koordinates Data Service (https://koordinates.com/layer/41-new-zealand-coastline-polygon-2007/) and licensed by Land Information New Zealand (LINZ) for re-use under the Creative Commons Attribution 3.0 New Zealand licence.

Figure 3.8: Sample locations along the SIT (with sample sites)

Hillshade sourced from the Koordinates Data Service (https://koordinates.com/layer/515-nz-greyscale-hillshade-100m/) and licensed by Geographx for re-use under the Creative Commons Attribution 3.0 New Zealand licence.

NZ Coastline sourced from the Koordinates Data Service (https://koordinates.com/layer/41-new-zealand-coastline-polygon-2007/) and licensed by Land Information New Zealand (LINZ) for re-use under the Creative Commons Attribution 3.0 New Zealand licence.

Figure 3.17: Sample locations along the REW Transect

Hillshade sourced from the Koordinates Data Service (https://koordinates.com/layer/515-nz-greyscale-hillshade-100m/) and licensed by Geographx for re-use under the Creative Commons Attribution 3.0 New Zealand licence.

NZ Coastline sourced from the Koordinates Data Service (https://koordinates.com/layer/41-new-zealand-coastline-polygon-2007/) and licensed by Land Information New Zealand (LINZ) for re-use under the Creative Commons Attribution 3.0 New Zealand licence.

Lake data (modified) sourced from the Koordinates Data Service (https://koordinates.com/layer/150-nz-lakes/) and licensed by Land Information New Zealand (LINZ) for re-use under the Creative Commons Attribution 3.0 New Zealand licence.

State Highway Data sourced from the Koordinates Data Service (https://koordinates.com/layer/1331-nz-state-highway-centrelines/) and licensed by the New Zealand Transport Agency (NZTA) for re-use under the Creative Commons Attribution 3.0 New Zealand licence.

Figure 3.18: Elevation Profile of the REW Transect

Elevation data derived from DEM, sourced from the LRIS Data Service (https://lris.scinfo.org.nz/layer/131-nzdem-north-island-25-metre/) and reproduced with the permission of Landcare Research New Zealand Limited.

State Highway Data sourced from the Koordinates Data Service (https://koordinates.com/layer/1331-nz-state-highway-centrelines/) and licensed by the New Zealand Transport Agency (NZTA) for re-use under the Creative Commons Attribution 3.0 New Zealand licence.

Figure 3.20: Elevation Profile of the TNS Transect

Elevation data derived from DEM, sourced from the LRIS Data Service (https://lris.scinfo.org.nz/layer/131-nzdem-north-island-25-metre/) and reproduced with the permission of Landcare Research New Zealand Limited.

State Highway Data sourced from the Koordinates Data Service (https://koordinates.com/layer/1331-nz-state-highway-centrelines/) and licensed by the New Zealand Transport Agency (NZTA) for re-use under the Creative Commons Attribution 3.0 New Zealand licence.

Figure 3.21: Sample locations along the TNS Transect

Hillshade sourced from the Koordinates Data Service (https://koordinates.com/layer/515-nz-greyscale-hillshade-100m/) and licensed by Geographx for re-use under the Creative Commons Attribution 3.0 New Zealand licence.

NZ Coastline sourced from the Koordinates Data Service (https://koordinates.com/layer/41-new-zealand-coastline-polygon-2007/) and licensed by Land Information New Zealand (LINZ) for re-use under the Creative Commons Attribution 3.0 New Zealand licence.

Lake data (modified) sourced from the Koordinates Data Service (https://koordinates.com/layer/150-nz-lakes/) and licensed by Land Information New Zealand (LINZ) for re-use under the Creative Commons Attribution 3.0 New Zealand licence.

State Highway Data sourced from the Koordinates Data Service (https://koordinates.com/layer/1331-nz-state-highway-centrelines/) and licensed by the New Zealand Transport Agency (NZTA) for re-use under the Creative Commons Attribution 3.0 New Zealand licence.

Figure 3.25: Sample sites at the Ngatamariki Geothermal Field (Whole Field)

Satellite Imagery sourced from the ArcMap 10.1 Basemap "World Imagery" (http://www.arcgis.com/home/item.html?id=10df2279f9684e4a9f6a7f08febac2a9) and licenced by ESRI under the Esri Master License Agreement.

State Highway Data sourced from the Koordinates Data Service (https://koordinates.com/layer/1331-nz-state-highway-centrelines/) and licensed by the New Zealand Transport Agency (NZTA) for re-use under the Creative Commons Attribution 3.0 New Zealand licence.

Road data sourced from the Koordinates Data Service (https://koordinates.com/layer/40-nz-roads-centrelines/) and licensed by Land Transport New Zealand (LTNZ) for re-use under the Creative Commons Attribution 3.0 New Zealand licence.

River data sourced from the LINZ Data Service (River Polygons: https://data.linz.govt.nz/layer/328-nz-mainland-river-polygons-topo-150k/ and River Polylines: https://data.linz.govt.nz/layer/327-nz-mainland-river-centrelines-topo-150k/) and licensed by the LINZ/National Topographic Office re-use under the Creative Commons Attribution 3.0 New Zealand licence.

Hillshade sourced from the Koordinates Data Service (https://koordinates.com/layer/515-nz-greyscale-hillshade-100m/) and licensed by Geographx for re-use under the Creative Commons Attribution 3.0 New Zealand licence.

Figure 3.26: Sample sites at the Ngatamariki Geothermal Field (Springs Area)

Satellite Imagery sourced from the ArcMap 10.1 Basemap "World Imagery" (http://www.arcgis.com/home/item.html?id=10df2279f9684e4a9f6a7f08febac2a9) and licenced by ESRI under the Esri Master License Agreement.

State Highway Data sourced from the Koordinates Data Service (https://koordinates.com/layer/1331-nz-state-highway-centrelines/) and licensed by the New Zealand Transport Agency (NZTA) for re-use under the Creative Commons Attribution 3.0 New Zealand licence.

Road data sourced from the Koordinates Data Service (https://koordinates.com/layer/40-nz-roads-centrelines/) and licensed by Land Transport New Zealand (LTNZ) for re-use under the Creative Commons Attribution 3.0 New Zealand licence.

River data sourced from the LINZ Data Service (River Polygons: https://data.linz.govt.nz/layer/328-nz-mainland-river-polygons-topo-150k/ and River Polylines: https://data.linz.govt.nz/layer/327-nz-mainland-river-centrelines-topo-150k/) and licensed by the LINZ/National Topographic Office re-use under the Creative Commons Attribution 3.0 New Zealand licence.

Hillshade sourced from the Koordinates Data Service (https://koordinates.com/layer/515-nz-greyscale-hillshade-100m/) and licensed by Geographx for re-use under the Creative Commons Attribution 3.0 New Zealand licence.

6.1.3 Chapter 4: Interpreting Controls on Lichen Isotopes

Figure 4.13: Distribution of land use classes at the Ngatamariki Geothermal Area

State Highway Data sourced from the Koordinates Data Service (https://koordinates.com/layer/1331-nz-state-highway-centrelines/) and licensed by the New Zealand Transport Agency (NZTA) for re-use under the Creative Commons Attribution 3.0 New Zealand licence.

Road data sourced from the Koordinates Data Service (https://koordinates.com/layer/40-nz-roads-centrelines/) and licensed by Land Transport New Zealand (LTNZ) for re-use under the Creative Commons Attribution 3.0 New Zealand licence.

River data sourced from the LINZ Data Service (River Polygons: https://data.linz.govt.nz/layer/328-nz-mainland-river-polygons-topo-150k/ and River Polylines: https://data.linz.govt.nz/layer/327-nz-mainland-river-

centrelines-topo-150k/) and licensed by the LINZ/National Topographic Office re-use under the Creative Commons Attribution 3.0 New Zealand licence.

Hillshade sourced from the Koordinates Data Service (https://koordinates.com/layer/515-nz-greyscale-hillshade-100m/) and licensed by Geographx for re-use under the Creative Commons Attribution 3.0 New Zealand licence.

Land Use classes digitised based on satellite imagery sourced from the ArcMap 10.1 Basemap "World Imagery" (http://www.arcgis.com/home/item.html?id=10df2279f9684e4a9f6a7f08febac2a9) and licenced by ESRI under the Esri Master License Agreement.

Figure 4.16: Field scale isoscape of the $\delta^{13}C$ ratios in lichen thalli (*Usnea sp.*) at the Ngatamariki Geothermal Field

Satellite Imagery sourced from the ArcMap 10.1 Basemap "World Imagery" (http://www.arcgis.com/home/item.html?id=10df2279f9684e4a9f6a7f08febac2a9) and licenced by ESRI under the Esri Master License Agreement.

State Highway Data sourced from the Koordinates Data Service (https://koordinates.com/layer/1331-nz-state-highway-centrelines/) and licensed by the New Zealand Transport Agency (NZTA) for re-use under the Creative Commons Attribution 3.0 New Zealand licence.

Road data sourced from the Koordinates Data Service (https://koordinates.com/layer/40-nz-roads-centrelines/) and licensed by Land Transport New Zealand (LTNZ) for re-use under the Creative Commons Attribution 3.0 New Zealand licence.

River data sourced from the LINZ Data Service (River Polygons: https://data.linz.govt.nz/layer/328-nz-mainland-river-polygons-topo-150k/ and River Polylines: https://data.linz.govt.nz/layer/327-nz-mainland-river-centrelines-topo-150k/) and licensed by the LINZ/National Topographic Office re-use under the Creative Commons Attribution 3.0 New Zealand licence.

Hillshade sourced from the Koordinates Data Service (https://koordinates.com/layer/515-nz-greyscale-hillshade-100m/) and licensed by Geographx for re-use under the Creative Commons Attribution 3.0 New Zealand licence.

Figure 4.17: Outcrop scale isoscape of the $\delta^{13}C$ ratios in lichen thalli (*Usnea sp.*) at the Ngatamariki Geothermal Field

Satellite Imagery sourced from the ArcMap 10.1 Basemap "World Imagery" (http://www.arcgis.com/home/item.html?id=10df2279f9684e4a9f6a7f08febac2a9) and licenced by ESRI under the Esri Master License Agreement.

State Highway Data sourced from the Koordinates Data Service (https://koordinates.com/layer/1331-nz-state-highway-centrelines/) and licensed by the New Zealand Transport Agency (NZTA) for re-use under the Creative Commons Attribution 3.0 New Zealand licence.

Road data sourced from the Koordinates Data Service (https://koordinates.com/layer/40-nz-roads-centrelines/) and licensed by Land Transport New Zealand (LTNZ) for re-use under the Creative Commons Attribution 3.0 New Zealand licence.

River data sourced from the LINZ Data Service (River Polygons: https://data.linz.govt.nz/layer/328-nz-mainland-river-polygons-topo-150k/ and River Polylines: https://data.linz.govt.nz/layer/327-nz-mainland-river-

centrelines-topo-150k/) and licensed by the LINZ/National Topographic Office re-use under the Creative Commons Attribution 3.0 New Zealand licence.

Hillshade sourced from the Koordinates Data Service (https://koordinates.com/layer/515-nz-greyscale-hillshade-100m/) and licensed by Geographx for re-use under the Creative Commons Attribution 3.0 New Zealand licence.

Figure 4.18: Field scale isoscape of the $\delta^{15}N$ ratios in lichen thalli (*Usnea sp.* and *Ramalina sp.*) at the Ngatamariki Geothermal Field

Satellite Imagery sourced from the ArcMap 10.1 Basemap "World Imagery" (http://www.arcgis.com/home/item.html?id=10df2279f9684e4a9f6a7f08febac2a9) and licenced by ESRI under the Esri Master License Agreement.

State Highway Data sourced from the Koordinates Data Service (https://koordinates.com/layer/1331-nz-state-highway-centrelines/) and licensed by the New Zealand Transport Agency (NZTA) for re-use under the Creative Commons Attribution 3.0 New Zealand licence.

Road data sourced from the Koordinates Data Service (https://koordinates.com/layer/40-nz-roads-centrelines/) and licensed by Land Transport New Zealand (LTNZ) for re-use under the Creative Commons Attribution 3.0 New Zealand licence.

River data sourced from the LINZ Data Service (River Polygons: https://data.linz.govt.nz/layer/328-nz-mainland-river-polygons-topo-150k/ and River Polylines: https://data.linz.govt.nz/layer/327-nz-mainland-river-centrelines-topo-150k/) and licensed by the LINZ/National Topographic Office re-use under the Creative Commons Attribution 3.0 New Zealand licence.

Hillshade sourced from the Koordinates Data Service (https://koordinates.com/layer/515-nz-greyscale-hillshade-100m/) and licensed by Geographx for re-use under the Creative Commons Attribution 3.0 New Zealand licence.

Figure 4.19: Outcrop scale isoscape of the $\delta^{15}N$ ratios in lichen thalli (*Usnea sp.* and *Ramalina sp.*) at the Ngatamariki Geothermal Field

Satellite Imagery sourced from the ArcMap 10.1 Basemap "World Imagery" (http://www.arcgis.com/home/item.html?id=10df2279f9684e4a9f6a7f08febac2a9) and licenced by ESRI under the Esri Master License Agreement.

State Highway Data sourced from the Koordinates Data Service (https://koordinates.com/layer/1331-nz-state-highway-centrelines/) and licensed by the New Zealand Transport Agency (NZTA) for re-use under the Creative Commons Attribution 3.0 New Zealand licence.

Road data sourced from the Koordinates Data Service (https://koordinates.com/layer/40-nz-roads-centrelines/) and licensed by Land Transport New Zealand (LTNZ) for re-use under the Creative Commons Attribution 3.0 New Zealand licence.

River data sourced from the LINZ Data Service (River Polygons: https://data.linz.govt.nz/layer/328-nz-mainland-river-polygons-topo-150k/ and River Polylines: https://data.linz.govt.nz/layer/327-nz-mainland-river-centrelines-topo-150k/) and licensed by the LINZ/National Topographic Office re-use under the Creative Commons Attribution 3.0 New Zealand licence.

Hillshade sourced from the Koordinates Data Service (https://koordinates.com/layer/515-nz-greyscale-hillshade-100m/) and licensed by Geographx for re-use under the Creative Commons Attribution 3.0 New Zealand licence.

7 Appendices

All data generated from this thesis is available either on the CD inside the back cover (hard-copy), or as an excel file in the location this copy was downloaded from (electronic copy).